UNIVERSITÀ
DEGLI STUDI
FIRENZE

DOCTORAL PROGRAMME IN INDUSTRIAL ENGINEERING
DOTTORATO DI RICERCA IN INGEGNERIA INDUSTRIALE

XXIX

Definition of a FEA based approach to predict the frictional behavior of wearing surfaces

ING/IND-14

Doctoral Candidate
Amedeo Tesi

Supervisors
Prof. Renzo Capitani
Ph. D. Eng. Claudio Annicchiarico

External Referees
Prof. Francesco Ciardelli
Prof. Cecilia Bartuli

Head of the Doctoral Programme
Prof. Maurizio De Lucia

Years 2013/2016

ISBN XXX–XX–XXXX–XXX–X
D/XXXX/XXXX/XX

A Martina

Summary

The work described in this Ph. D. Thesis is developed in the context of tribology research and it is aimed to represent a support to engineers and researchers to estimate the tribological conditions and properties of the mechanical components in reciprocal contact.

The main target of this research is to define a predictive wear model based on a mixed approach, obtained through the union of experimental results and numerical outcomes.

The wear model is defined by implementing two tribological laws, in order to evaluate the wear depth progression occurring in a contact interface. Experimental results obtained from experimental tests define the main tribological characteristics to be used during the wear model definition process, giving the possibility to obtain a matching procedure between the experimental and numerical analyses.

The first part of the work defines the tribologic domain and its main characteristics. An historic review of tribology is described in Chapter 1 and its development in surfaces study is depicted. Friction coefficient and wear definition and overview are described and their main features are outlined in order to characterize as better as possible the contact process occurring between surfaces. A literature review is collected and reported in order to support the assumptions made in the first section of this work.

Chapter 2 is characterized by a description of the experimental tests usually performed to obtain the tribological characteristics of materials in reciprocal contact and an initial definition of test benches used to perform the analyses. The second part of Chapter 2 is addressed to a description of several preliminary tests performed in order to evaluate the Block-on-Ring test bench characteristics and to optimize the working conditions of the test bench itself. A comparison between the preliminary tests results and the evaluations on the tribological results obtained from literature is defined in the final part of chapter, outlining a good accuracy of the test bench.

The central part of this work is characterized by three different experimental analyses performed with the main aim of defining tribological properties of different materials in contact. Chapter 3 is addressed to a description of nanomaterials coatings used with the aim of obtaining a reduction of friction coefficient in the relative contact of automotive components. The experimental campaign is performed using a Block-on-Ring test bench in order to obtain tribological characteristics of nano-coatings.

Following the same approach and objective, in Chapter 4 a discussion on experimental tests performed on reinforced epoxy resins is presented. The resins, reinforced with different graphene nanopowders, are applied on the external surface of the ring during a Block-on-Ring contact configuration. The evaluation of tribological characteristics during a camshaft working

conditions replications, defines the possibility of an epoxy resin implementation in the internal combustion engine components.

Chapter 5 illustrates a study on the molybdenum treatment usually used in clutch pack assemblies. The aim of this research concerns the evaluation of the friction coefficient and of the wear rate generated during the contact between a treated ring and an untreated block. The tribological evaluation leads to a deeper understanding of the behavior of the materials in contact, to define the design of the clutch pack composed by molybdenum-treated disks. The experimental research takes into account the evolution of tribological properties as a function of time to estimate wear progression during components lifetime.

After an experimental characterization of several external treatments, a numerical approach is followed in order to define a predictive wear model based on experimental results. Chapter 6 illustrates the Block-on-Ring characterization in a finite element domain with the aim to represent the contact configuration defined in experimental tests. The target of this part of the dissertation concerns the definition of a wear model based on fundamental tribological laws and their implementation in a custom algorithm. The iterative process defined in the procedure allows the definition of wear depth increments with time, defining consequently the lifetime of components in contact.

The final chapter describes an application of numerical wear model in the clutch pack of a Limited Slip Differential. The aim of this section is the evaluation of wear evolution on disks contact surfaces and the consequent performance decay highlighted in the clutch pack in terms of transmissible torque.

The results are critically discussed in Conclusions sections, defining strengths and weaknesses of predictive wear model. An outlook of future applications and possible implementation of the model are described in the same section, highlighting the possibility of a prediction process during design phase of mechanical components.

Table of contents

List of figures

List of tables

Acronyms List and Nomenclature

FEA: Finite Element Analysis
UK: United Kingdom
GNP: gross national product
HCP: Hexagonal Close-Packed
FCC: Face-Centered Cubic
ASTM: American Society for Testing and Materials International
PVD: Physical Vapor Deposition
CVD: Chemical Vapor Deposition
HVOF: High-Velocity Oxy-Fuel Thermal Spraying
PECVD: Plasma-Enhanced Chemical Vapor Deposition
ICE: internal combustion engine
CNC: computer numerical control
DLC: Diamond Like Carbon
CNTs: carbon nanotubes
CFs: carbon fibers
GSs: graphene sheets
EP: epoxy resin
LSD: Limited Slip Differential
EDS: Energy Dispersive X-ray Analysis
APS: Air Plasma Spray
FEM: Finite Element Method
CAE: Computer-Aided Engineering
CAD: Computer-Aided Drafting
e-LSD: Electronic-Limited Slip Differential
ECU: Electronic Control Unit

μ: friction coefficient
F: tangential friction force
W: normal load force
μ_s: coefficient of static friction
μ_k: coefficient of kinetic friction
A: real area of contact
A_a: apparent area of contact
S_v: sliding velocity
θ: asperity of roughness slope
R_a: average roughness

K: specific wear rate
V: volume loss of removed material
s: sliding distance
m_0: mass of the flexure hinge
m_1: mass of the block support
m_2: mass of the oscillating arm
k_{arm}: stiffness of oscillating arm
m: total mass of support arm
ω_o: natural frequency in vertical direction of the original configuration
m_{lc}: load cell mass
k_{lc}: load cell stiffness
k_{rod}: threaded rod stiffness
ω_{lc}: natural frequency in vertical direction of the load cell configuration
k_{tot}: total stiffness value
m_{tot}: total mass acting on the block-ring components
$R_{S,RING}$: ring's rotational speed
ω_{CAM}: camshaft's rotating speed
ω_{CRANK}: crankshaft's rotating speed
D_{CAM}: external diameter of the cam
r_{CAM}: external radius of the round part of the cam
C_{CAM}: cam circumference
$R_{S,CAM}$: camshaft's rotating speed
D_{RING}: ring's external diameter
F_{CAM}: normal load acting between the cam and the follower
t_e: average thickness of epoxy resin
P_{clutch}: pressure generated on the clutch pack
$D_{e,disk}$: disk external diameter
$D_{i,disk}$: disk internal diameter
W_{disk}: normal load on disks
A_{br}: contact area occurred in the experimental configuration
$R_{S,DISK}$: disks' reciprocating rotational speed
r_{disk}: external radius of the disk
r_{ring}: external radius of the ring
T_{oil}: lubricating oil temperature
Theta: contact surface angle defined at the end of the test
b: block thickness
V_{BLOCK}: worn volume occurred on the block
a: thickness of the worn track
t: block width.
δ: wear depth
p: applied pressure
H: hardness
V_{wear}: volume of material lost for wear effects
L_p: passive work
P_{Reye}: pressure obtained from Reye's theory application
R_c: mean radius of the considered circular crown
C: constant definable for the vertical translation equilibrium

Preface

The tribology field is being paid much interest due to the importance of energy dissipation is such components where friction, lubrication and wear have an important contribution to the whole system behavior.

The development of such systems able to define and evaluate tribological characteristics in particular contacts allowed to intensify researches in surfaces engineering domain during last years.

Researches and studies focused the attention on surface treatments behavior analyses in particular working conditions, aimed to develop surface coatings able to enhance the performance of treated components.

Surface characterization permitted the implementation of tribological studies in engineering domain, outlining the principal features of materials in contact. This innovation guaranteed the definition of several evaluations in the design process of such components in relative contact, inducing an improvement in the design procedure itself.

The introduction of experimental analysis in tribological domain allowed, during last decades, to determine the fundamental features of materials in contact, trying to replicate working conditions of components used in engineering environments.

Simultaneously to the development of experimental techniques, the progress noticed in numerical tests domain allowed the definition of instruments able to recreate and to predict the behavior of particular contact configurations.

In numerical analysis domain, the introduction of Finite Element Analysis (FEA) permitted the replication of conditions difficult to study using only experimental approach, defining the possibility to examine complex processes as wear and, hence, to evaluate principal parameters of processes themselves.

The implementation of experimental characterization in numerical domain allowed the accurate evaluation of physical processes and phenomena as wear generated during the contact of mechanical components. A predictive wear model definition obtained with a combination of experimental and numerical approaches permitted to achieve the target of the work described in this dissertation, giving the possibility of its use during engineering design.

The model described and defined in this study is based on fundamental tribological laws implemented in a custom algorithm and applied in a generalized Block-on-Ring contact configuration. The aim of the numerical model is to define wear depth evolution with time. Wear evolution implementation in actual mechanical systems allows the possibility to estimate their performance evolution according to time and, hence, respect to wear depth increments.

An *a priori* lifetime evaluation and a definition of features decay of the components in reciprocal contact could facilitate the design process of the elements themselves. The creation of a dedicated tool could help engineers and designers during the initial process of a project, defining the parameters characterizing the materials in contact and outlining the best solution in terms of component dimensions, materials surface hardness and lubricating characteristics.

1. Tribology

1.1. History

Tribology is an interdisciplinary science in which materials science, chemistry, physics, fluid dynamics, solid mechanics, etc., are important components. In 1966 the "Jost Report" published by the UK's Department of Education and Science used for the first time the word "tribology" [1]. The word tribology derives from the Greek *tribos* which means "to rub". The birth of this new science was based on the pressing demands of the industry and from the interest expressed by researchers and scientists.

The investigation of the economic and technological potential of this new interdisciplinary concept was studied in the Jost Report, defining tribology as the "science and technology of interacting surfaces in relative motion and of the practices related thereto".

Although the name of the science is quite new, the first practical applications of tribology date back to around 6000 B.C. indicating bitumen as the first lubricant used [2]. In Egypt (around 2500 B.C.) wheels, primitive bearings and lubrication were used when building temples and pyramids. Around 1500 A.D. Leonardo da Vinci conducted the first scientific studies on tribology, defining the coefficient of friction as a ratio between the friction farce and normal force but the studies remained unpublished for several centuries. Guillaume Amontons rediscovered the laws of friction in 1699 and only in 1750 Leonard Euler derived and analytical definition of friction introducing the symbol μ [3]. In 1785 Charles Augustin Coulomb confirmed the results of the previous investigations, but in addition found that friction is independent from sliding velocity, highlighting also a clear distinction between static and dynamic friction.

This oversimplification actually persisted until the mid-20th century when researchers such as Dokos (1946) and Rabinowicz (1951) cast new light on the phenomenon of friction. These researchers showed that the static coefficient of friction is time dependent and that the dynamic coefficient of friction is dependent on the sliding velocity [4].

Nowadays the importance of tribology can be illustrated by the fact that friction losses assume about the 5% of GNP [5] as several surveys in many industrialized countries have indicated, highlighting that even small advances in tribology can lead to very large savings if applied around the world.

Even though in most applications reduction of friction is the primary objective, in some fields friction is necessary and instead of reducing friction a high and well defined level of friction is required.

1.2. Surfaces

As indicated in "Jost Report", tribology is the science and technology of interacting surfaces in relative motion. The importance of a knowledge of the surface structure during a contact is very important to outline the relative interactions between two or more solid touch each other. In addition, surface structures may change during interaction, causing a material transfer phenomenon from one surface to another or a break away process of some bits of matter falling out from the contact region.

The surface of a solid body is the geometrical boundary between the solid and the environment. In addition to surface deviations, the solid surface itself consists of several zones with properties entirely different from the bulk material properties [6]. Tribology studies the interactions and the phenomena occurring on the surface and the near surface regions. As illustrated in Figure 1 the surface layers can be divided in physisorbed layer, chemisorbed layer, chemically reacted layer, Beilby layer, heavily deformed layer, lightly deformed layer, and the base material.

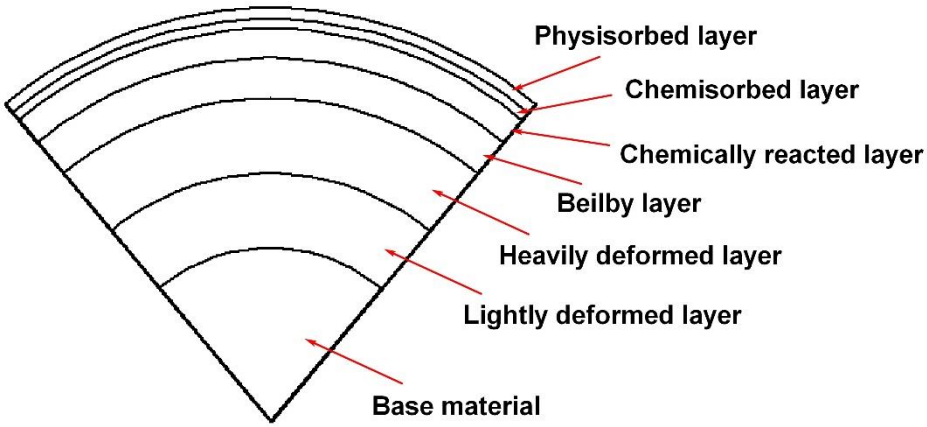

Figure 1 - Surface layers

Physisorbed layer may be formed from the environment on both metallic and nonmetallic surfaces. The adsorbate layers can be composed of molecules of oxygen, water vapor and other substances from the environment that may be condensed and adsorbed by the surface. This layer can have a thickness of about 0.3nm. During the physisorption process the molecules of the adsorbate and those of the adsorbent interact using van der Waals forces, so it takes very little energy to remove physisorbed substances from a solid surface.

Respect to the first layer, in the chemisorption level there is an actual sharing of electrons between the chemisorbed molecules and the solid surface, realizing covalent bonds among the species involved. As the first layer, the chemisorbed level is limited to a monolayer layout with a thickness of about few nanometers.

In all the metals and alloy (other than noble metals) a chemically reacted layer takes place when the solid is in contact with oxygen or other substances, creating layers according to the environments. The thickness of the oxide and other chemically reacted layer depends on the reactivity of the materials to the environment, reaction temperature, and reaction time.

Typical thickness of these layers ranges from 10 to 100nm. Oxide layers can also be produced during the machining process. The presence of lubricant and additives causes the formation of reaction layers that are important in surface protection of the materials.

The Beilby layer is a typical layer presents in metals and alloys. It is produced by melting and surface flow during machining of molecular layers that are subsequently hardened by quenching as they are deposited on the cool underlying material. The thickness typically ranges from 1 to 100nm. This layer is present even in super finished components. The thickness of the Beilby layer can be easily reduced using lapping or wet polishing procedures.

Deformed layer concerns the level of the bulk material where surface preparation operations (grinding, polishing, machining) plastically deformed the solid. The surface layers after the deformation process become highly strained, outlining also residual stresses. The strained layer is called the deformed (work-hardened) layer and is an integral part of the material itself in the surface region. The thickness of the lightly deformed layer ranges from 10 to 100μm. The thickness of the heavily deformed layer ranges from 1 to 10μm.

1.3. Friction and wear

Friction is one of the most important phenomena in the everyday life. Without friction it would be possible to make some usual activities as to walk, use automobiles on a roadway or pick up objects. Depends on the situation, a low or a high value of friction may be desirable. In some automotive applications as brakes or clutches a high value of friction is needed to guarantee a right working principle of the apparatus. However, in most other sliding and rolling components such as bearings and seals, friction is undesirable. Furthermore, friction causes energy loss and the wear of materials that are in contact and so in these cases friction should be minimized.

1.3.1.**Friction**

Friction is the resistance to relative motion of two bodies that are in contact. Friction is a property of the tribological system and it is not a material property. A tribological system consists of at least two bodies in contact, the surrounding environment and the interface. Friction can be divided in dry friction and fluid friction. Dry friction, also called "Coulomb friction" occurs during dry conditions while fluid friction occurs when the contact is a lubricated domain. Surfaces' finishing influences friction characteristics due to the presence of adsorbated molecules or contaminants in the external surface layers. Friction can be described by a parameter called friction coefficient and usually indicated with the Greek letter μ. Friction coefficient is a scalar value defined as the ratio between tangential friction force (F) (called also friction force) and the normal load force (W), as indicated in the following equation.

$$\mu = \frac{F}{W} \tag{1}$$

In technical terms, friction force is the resisting force which acts in a direction directly opposite to the direction of motion. The normal load is defined as the net force compressing two parallel surfaces together and the direction of this force is parallel to the surfaces.

Friction coefficient is not a function of mass or volume and it depends only on the mating materials and the test conditions. However, the magnitude of friction force depends on the normal force and hence the mass of the solid under exam.

The only way to define the friction coefficient of a tribological system is performing experimental tests. Indeed, friction coefficient is an empirical parameter and can be vary over a wide range: from 0.001 in a lightly loaded rolling bearing to greater than 10 for clean metals sliding against themselves in vacuum. For most common tribological systems during a contact in air, the value of friction coefficient can be found in a range from 0.01 to 1.

In a tribological system the friction phenomenon usually described two different behaviors: a static friction process and a kinetic friction process. Static friction is the friction between two solid objects that are not moving relative to each other. The coefficient of static friction, typically denoted as μ_s, is usually higher than the coefficient of kinetic friction, μ_k. This happens because when no sliding occurs between two objects, the surfaces tend to "stick" to each other due to adhesive bonds between them. According to this, the phenomenon described is sometimes called "stiction". To guarantee the movement of an object from a stable condition, the static friction force must be overcome by an applied force. The instant of sliding occurs, static friction is no longer applicable, and kinetic friction becomes applicable. On the other hand, kinetic (or dynamic) friction process occurs during a relative motion between two bodies. The coefficient of kinetic friction is typically denoted as μ_k and, for the same material, it has a lower magnitude respect to static friction coefficient. In Figure 2 static and kinetic friction are illustrated related with time.

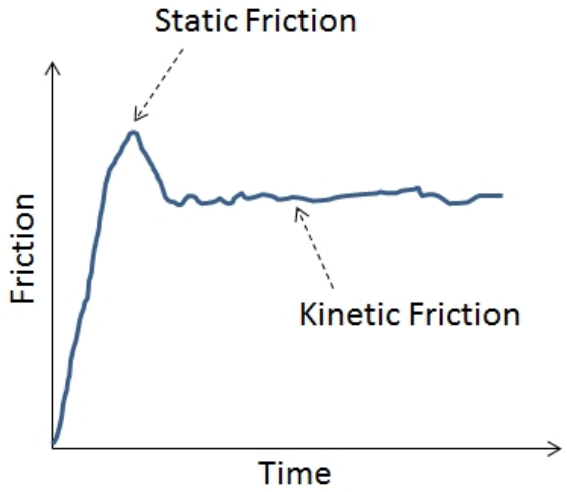

Figure 2 - Static and kinetic friction

As illustrated in the first paragraph, the first systematic experimental investigation of friction was conducted by Leonardo da Vinci in the 1500s and later by Amontons in 1699 and verified by Euler and Coulomb in the 1700s. The most important results obtained from those researches concerned the definition of the empirical laws of friction, presented as follow:

- The friction force is directly proportional to the normal load
- The friction force is independent of the apparent area of contact

- The friction force is almost independent of the sliding velocity

These laws are easy to explain if some assumptions are made:

- The friction force is proportional to the real area of contact, A
- The real area of contact is proportional to the normal load, W

According to these assumptions, the friction force depends upon the real area of contact and also it is independent of the apparent area of contact (A_a) and thus is proportional to the normal load. In practical terms, these three laws state that the friction coefficient is a constant and it does not change with changing A_a, normal load (W) or sliding velocity (S_v) [7].

Friction laws, called also Amontons-Coulomb's empirical laws of friction, are not fundamentals rules of nature and they are not satisfied in many cases, especially at micro-/nanoscale. Indeed, experimental analyses outlined that friction has a dependency from the size of interacted surfaces and the coefficient of friction at micro-/nanoscale is different from that at the macro-scale; load and velocity dependence of the coefficient of friction is also well established [8], [9]. Some studies have been performed in order to suggest several approaches to deal with the laws of friction at micro-/nanoscale, including a formulation of "scaling laws of friction" [8], [10], [11], [12] and specific nanofriction laws, defined with the aim to substitute the Amontons-Coulomb's laws at the nanoscale [9], [12].

Even though Amontons-Coulomb's laws are only approximations, Equation 1 is valid for a wide range of material combinations including metals, ceramics, composite, polymers and so on. Furthermore, friction phenomena are complex processes that involve various physical mechanisms, such as covalent and van der Waals adhesion, elastic and plastic deformation and "third-body" mechanism.

Friction phenomenon is usually dependent to many factors, including surface characteristics, temperature and environment surrounding components during a contact. To better understand how many parameters can affect friction process, a description of each of them is presented as follow.

- Surface roughness: due to the presence of asperities and waviness on the surface of every solid component, one of the early idea to explain friction was to relate it to surface roughness. As described in [13], roughness theory assumed that frictional force is equal to the force required to climb up the asperity of slope θ and, furthermore, the friction coefficient is proportional to $tan\theta$. The dependency to the real contact area is also explained considering an increase in the friction force with an increase of the real area of contact. In the surfaces normally used in the engineering practice, the roughness is at an intermediate range and the friction is at minimum and almost independent of the roughness [14].
- Surface topography: the dependency of the friction phenomena to the surface topography is not well defined yet. In [15], some aspects were focused with the aim to describe a correlation between real contact area, surface topography and lubricant trapped among the asperities. Some other detailed researches on the effects of surface topography in friction was carried out from the 1970s [16]–[26]. From the beginning of 2000s, a wide range of studies were performed in order to quantify surface topography using several well-known roughness parameters [27]–[36]. One of the parameters used in these researches was R_a, the average roughness. Nevertheless, it is possible that that two surfaces can have the same R_a but their

frictional characteristics could be different; therefore, a single roughness parameter cannot describe a characteristic like friction [22], [37], [38]. To better evaluate the correlation between friction and surface topography, new roughness parameters were formulated [31], [35], [37], [38]. The correlation between friction coefficient and surface roughness is, in general, system dependent.

- Strain hardening and harness: during a contact between metal and a harder surface, severe plastic deformation occurs in the surface regions. This process leads to a progressively hardening of the metal and the contact surface reaches a maximum hardness that depends on the method by which it has been deformed [39], [40]. The absence of plastic deformability of hard metals, and the subsequent decrease in the ability of metals to adhere, define the effect of hardness on friction coefficient [34], [41], [42]. For what concerns harder metals, the strong atomic bonds define an enhancement of the resistance to adhesion, providing low frictional characteristics. However, hardness cannot be used such as the only criterion for a prediction of friction coefficient and, furthermore, coefficient of friction is not necessarily lower for harder materials [43].
- Grain size: attempts on a combination of grain size effects and wear behavior of several materials have been studied in order to define a correlation with the friction characteristics of the materials themselves. It was stated that friction coefficient decreases with a decrease in grain size [44]–[47], and one of the most important consequences is an improvement of mechanical and chemical properties of nanomaterials.
- Surface energy: during a contact in dry clean domain, adhesion and friction are strictly in a relation with surface energy of the materials [14]. As illustrated in Paragraph 1.2, the presence of adsorbed layer reduces surface energy of metals and hence decreases coefficient of friction. On the contrary, in a vacuum domain higher values of the ratio of surface energy to hardness of materials lead to higher friction coefficient, 10 times higher than values measured in air [48].
- Sliding velocity: high sliding velocities can cause a surface frictional heating and a consequent formation of a molten layer on the contact surface. This thin molten layer can acts as lubricant between surfaces, resulting in a low friction coefficient [49]. Furthermore, oxide layers' formation at high temperature induced by sliding speed generally leads to a decrease of friction coefficient. However, an increase of surface temperature can define a softening process of the metal surface and a consequent increase of the friction coefficient.
- Temperature: an increase of the temperature in a sliding contact generally induces modifications of mechanical properties of the contact metals, an increase of the rate of oxidation and a phase transformation may take place. All these factors could influence the frictional behavior. Generally, as described in [50], a temperature increase induces a reduction of the material hardness and, hence, an increase of friction coefficient. However, different materials have a different response to temperature increase. In [50] an analysis of different materials was performed with the aim to highlight different behaviors among a steel alloy, a polymer, a copper alloy and a ceramic. The interesting result is that at high temperature, the formation

of external oxide in steel alloy and copper alloy induces a limitation of contact between the surfaces and, hence, a reduction of the friction coefficient.

During last decades, lots of studies were performed with the aim to define a generalization of friction characteristics of such materials classes typically used in engineering practices. As discuss in the previous Paragraph, clean metal surfaces in a vacuum domain show strong adhesion and high friction coefficient, typically 2-10. If the domain is the air, as in practical applications, friction coefficient decrease in the range from 0.2 to 1.0. Some metals oxidize in air to form oxide films on the external surfaces; these layers are between 1 and 10nm thick within a few minutes of exposure. At low normal load, the oxide can create a separation film between the contact surfaces, leading to a low value of friction coefficient. An increment of the normal load induces a transition to a higher value of the coefficient of friction; this phenomenon could be due to the breakdown of oxide layer due to higher loads imposed during sliding.

Ceramic materials are very different from metals or alloys. The main difference is the nature of interatomic forces, with covalent or ionic bonding in ceramics compared to that of metallic bonding in metals or alloys. During a contact between two ceramics surfaces, a very low real contact area is induced, resulting in relatively low values of friction coefficient comparable to metallic couples. The coefficient of friction in ceramic-ceramic contacts keeps typically in the range from 0.2 to 0.8. these values are similar to those seen for a metallic contact in air with the presence of intact oxide on the contact surfaces.

A friction characterization of polymers is generally more complicated than metals or ceramics. The predominant behavior of a contact between polymers or between polymers and a metal is generally elastic and this phenomenon can lead to a layers' transfer, mainly if the counterface is harder than the polymers [34], [38], [51]. Due to this phenomenon, friction coefficient between polymers sliding against themselves or against metals generally is about 0.1-0.5.

1.3.2. **Wear**

Wear is a phenomenon described as a progressive loss of substance from the surface of a body due to surfaces interaction. During the contact between asperities, material on the interaction surfaces may be altered, resulting in a transfer to the mating surface or break lose as a wear particle. Wear is not a material property and, as for friction, it is a system characteristic and working conditions and domain characteristics affect the wear process. This phenomenon is quantified by the term "specific wear rate", usually indicated with *K*. It is defined as the volume loss of material removed (*V*) per unit of sliding distance (*s*) per unit of normal force applied in the contact (*W*). The equation of specific wear rate is illustrated as follow:

$$K = \frac{V}{W \cdot s} \tag{2}$$

Wear phenomenon is usually induced by several mechanisms, such as adhesive wear, abrasive wear, erosive wear, fretting wear, fatigue wear, and corrosive/oxidative wear. A brief description of features and definitions of different wear mechanisms is described in Table 1. Generally, in industrial applications the most common wear mechanisms are adhesive and abrasive wear. In many cases, wear is initiated by one mechanism, and it may proceed by other

wear mechanisms. The examination process of worn components is generally performed to determine the type of wear mechanism by using microscopy or surface analytical techniques.

Table 1 - Wear mechanisms

Mechanism	Definition	Characteristics
Adhesion	Wear due to transfer of material from one surface to another surface by shearing of solid welded junctions of asperities	Adhesive bonding, shearing, and material transfer
Abrasion	Wear due to hard particles or protuberances sliding along a soft solid surface	Plowing, wedging, and cutting
Erosion	Wear due to mechanical interaction between solid surface and a fluid, or impinging liquid or solid particles	Angle of incidence, large-scale sub-surface deformation, crack initiation, and propagation
Fatigue	Wear caused by fracture arising from surface fatigue	Cyclic loading and fatigue crack propagation
Fretting	Wear due to small amplitude oscillatory tangential movement between two surfaces	Relative displacement amplitude and entrapment of wear particles
Corrosive/oxidative	Wear occurs when sliding takes place in corrosive/oxidative environment	Formation of weak, mechanically incompatible corrosive/oxide layer

To better understand wear phenomenon, a brief description of wear mechanisms is fixed as follow:

- Adhesive wear: as stated in [50], adhesive wear is a wear mechanism occurring between two sliding solids where adhesion and plastic deformation between asperities in contact are the main process of debris production. In this wear mechanism, junction forces between asperities can create strong adhesive junctions at the real area of contact. During a relative motion between the contact surfaces, the adhered junctions are sheared and softer material is transferred to harder surface. Soft material may adhere to hard surface or may produce a loose wear debris.
- Abrasive wear: this wear mechanism can be observed in such those contact pairs in which a hard material is kept in contact with a softer surface. The asperities of hard material are pressed into the soft surface with plastic flow of the soft surface. During a movement among the contact surfaces, the hard material will slide and remove the soft material by plowing. Abrasive wear is categorized according to the type of contact as two-body and three-body abrasion. While in two-body contact a hard material slides upon the soft surface, in the three-body abrasion wear debris created during the contact are caught between two surfaces, causing one or both of them to be abraded.

- Erosion wear: when liquid or solid particles impact a solid body, an erosion process occurs and the surface undergoes a damage. Erosion is categorized as solid erosion and liquid erosion. Solid erosion is similar to abrasive wear and it is dependent to kinetic energy of particles impinging the surface, in terms of particle velocity, impact angle and the size of abrasive particles. As for abrasive wear, erosion process occurs by brittle fracture and/or by plastic deformation, depending on material type and environment conditions. Fluid erosion can be divided in two different types - liquid impact erosion and cavitation erosion. The first process occurs when tiny liquid drops impact the solid surface at high speed, inducing a plastic deformation or brittle fracture of the surface. A repetition of impacts against solid surface leads to pitting and, consequently, erosive wear. In cavitation processes, bubbles trapped in a liquid become unstable and implode against the surface of a solid, creating a micro-jet of liquid towards the solid surface. The energy emitted during the implosion of the bubbles is absorbed by the solid material as elastic or plastic deformation or fracture. The repletion of this process induces an erosion of the component.
- Fatigue wear: this wear mechanism is an important phenomenon both in macroscopic and microscopic scale. Macroscopic wear occurs in such those nonconforming contact as rolling contacts, while microscopic wear process is mainly described between sliding asperities. These phenomena could be described as subsurface and surface fatigues occurring during repeated rolling and sliding processes. Loading and unloading cycles repetition induce the formation of cracks on the subsurface or in the surface and, after a critical number of cycles, these cracks will result in the formation of large worn pieces of materials, creating a pitting process in the contact surface.
- Fretting wear: this kind of wear mechanism is commonly in such contact subjected to vibration and low-amplitude oscillatory. During fretting process, a combination of wear mechanisms occurs, mainly adhesion wear due to normal load applied and abrasive wear due to oscillatory movement. If fretting wear occurs in a corrosive domain a fretting corrosion process is induced, forming wear particles harder than their parent metals, inducing abrasion processes. The repetition of oscillation can cause unexpected vibrations, causing fretting fatigue wear processes.
- Corrosive/oxidative wear: corrosive wear is a wear mechanism inducing in contact which take place in a corrosive medium. Corrosion takes place on the external surfaces of metals in corrosive environment when sliding is absent and an oxide film is created. Relative motion between solids in contact wears the oxide layer away and the corrosion process can continue. As illustrated in Paragraph 2.1, oxidation on the sliding surfaces is generally beneficial thanks to the lubrication behave of oxide film. Furthermore, the presence of oxide layer can reduce wear rate in metallic contacts by two order of magnitude, respect to the same pair in a vacuum environment. Oxidation effects depend mainly on the oxidation rate, mechanical properties of base materials and domain temperature.

Even if each wear mechanism were described in the previous Paragraph, during a contact not only a single wear mechanism occurs. A change in operating conditions induces a

transition in dominant wear mechanisms. In 1987, a wear mechanism map was defined by Ashby and Lim [52] with the aim to show different regimes of wear at wide operating conditions. Factors that affects wear can concern the contact working conditions and the material characteristics. The most common factors are normal load, temperature, sliding velocity, environment, hardness, elastic modulus and crystal structure.

- Normal load: an increase in the normal load induces an increase in the real contact area, increasing consequently the number of adhesive junctions. Rabinowicz asserted that wear loss is proportional to normal load applied during a contact [14]. Earlier, Archard [53] highlighted a transition from mild to severe wear when the contact pressure is one-third of surface hardness. An increase of normal load induces also an increase of the interface temperature, reducing yield stress of materials. Therefore, normal load affects directly specific wear rate, as illustrated in Equation 2.
- Temperature: as illustrated in previous point, temperature influences wear response of metals altering their mechanical properties and changing the microstructural characteristics of the metals themselves. In [14] was observed that a phase transformation from HCP to FCC structure induced by a 100K increase, defined a wear rate 100 times higher in the warmer surface.
- Sliding velocity: in an unlubricated contact, an increase of sliding speed induces the generation of heat at the interfaces and a consequent formation of oxide film on the contact surfaces. The oxide layer acts as a lubricant, reducing the wear rate of the contact pair. On the other hand, in lubricated domain, the high sliding velocity induces the formation of hydrodynamic lubricant film, minimizing the specific wear rate. Hence, both in dry and lubricated conditions, an increase of the sliding speed induces a reduction of the wear rate, as confirmed in [54].
- Environment: the environment factor is strictly related to the formation of surface oxide described in the previous point. Indeed, in ambient conditions the contact between air and metals induces oxide formation, preventing the direct contact between metal-metal surfaces. If the oxide layer results strong enough to reduce direct contact between metals, wear rate in air is less than in vacuum atmosphere.
- Hardness: Archard's law defines the wear rate as an inverse function of the hardness of the considered material [53]. Indeed, materials with high hardness resist better to cutting and penetration processes, as it is to demonstrate in abrasive wear.
- Elastic modulus: this factor is directly related to wear resistance in accordance with adhesive wear mechanisms, as illustrated in [55]. For such those materials with high value of elastic modulus, a decrease of real contact area induces a low adhesion and, hence, a low wear among the surfaces. Furthermore, the abrasive wear resistance of a material can be varied increasing the ratio between hardness and elastic modulus (i.e., H/E ratio).
- Crystal structure: in 1970s an experimental campaign performed by Buckley [56] showed that wear rate in cubic crystal microstructure is about twice the wear rate in hexagonal crystals. This phenomenon could be due to the plastic deformation produced by sliding of metals. This process induces dislocation cell structures near the surface region, serving as pathway for subsurface cracks. This is the reason why materials with limited slip systems (HCP – Hexagonal Close-Packed) highlight a

lower wear rate respect to materials with large number of slip system (FCC – Face-Centered Cubic).

2. Experimental tests and tribometers

The main aim of tribological experimental tests concerns the definition of friction coefficient trend and wear rate during a contact of two or more components. A dedicated apparatus, called tribometer, can measure both the friction and the wear evolution between the materials. Experimental tests need an accurate preparation in order to replicate the same tribologic behavior of the real contact. Indeed, it is necessary to choose the right test procedure and the right input test parameters in order to induce the same wear process and the same wear mechanism of the real contact. Due to the wide range of wear processes, different tribometers can be used to replicate the exact contact behavior. A brief list of the principal tribometers and the relative wear processes and wear mechanisms is described in the Table 2 [50].

Table 2 - Tribometers type

Tribometers type	Wear process	Induced wear mechanisms
Pin-on-Disk	Sliding wear	Adhesive wear Oxidative wear
Block-on-Ring	Sliding wear	Adhesive wear Oxidative wear
Disk-on-Disk	Rotating-sliding wear	Surface fatigue wear
Four-Ball wear test	Rotating wear	Surface fatigue wear
Pin Abrasion Test (PAT)	Abrasive wear	Abrasive wear
Dry-Sand, Rubber Wheel Wear Test (DSRW)	Abrasive wear	Abrasive wear

2.1. Test configurations

Tribometers used for testing material can be commercially acquired or built to suit a specific application. In a lot of cases, commercially-based machine can be modified in order to guarantee various environmental conditions, as the possibility to replicate a particular lubricated condition. In each type of tribometer, two or more partners are in contact each other; generally, one is static and the other(s) is sliding or rotating. The normal load applied to the components during the contact is provided by dead weights or by some form of load actuation, as a piston or a load cell. Both these systems have advantages or disadvantages, according to the test type is performing.

2.1.1.**Pin-on-Disk test**

Pin-on-Disk tribometer is the most used test configuration. Experimental tests can be conducted in either linear-reciprocating or rotating modes and the respectively ASTM standards are [57] and [58]. Pin-on-Disk test allows the definition of friction coefficient and wear rate both for the sample and the static component. A schematic image of the test configuration is illustrated in Figure 3. The dynamic partner is mounted in a chuck and kept in rotation by a motor, while the static component is placed in contact with the other sample by an elastic arm. Normal load is provided by dead weights or using a load cell. The relative motion between the samples generates a tangential force (friction force) which is recorded by a sensor installed on the elastic arm. ASTM standards specify the shapes of the static partner; generally, a flat-ended pin or a 6mm diameter ball are used, depending on the contact configuration desired. As illustrated in Table 2, the wear process replicated using this test configuration is a sliding wear process, inducing an adhesive wear mechanism. The wear trend is recorded directly by a transducer, measuring the pin height variation. However, a wear occurring on the disk could influence also the pin weight; in this case disk wear is measured using a profilometer. Thanks to the wide range of conductible tests, Pin-on-Disk apparatus has been used for nearly 50 years in the tribologic measurement of friction coefficient and wear trend [4], [6], [59]–[62].

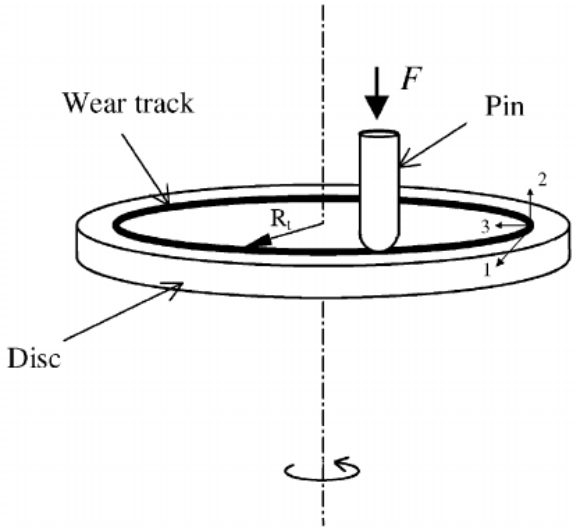

Figure 3 - Pin-on-disk test configuration

2.1.2.**Block-on-Ring test**

Block-on-Ring configuration is similar to the Pin-on-Disk test apparatus. According to Table 2, this kind of tribometer is generally used to replicate a sliding wear process, inducing an adhesive wear mechanism. The test configuration is composed by a prismatic block pressed against the external surface of a rotating ring, as illustrated in Figure 4. One important advantage of the Block-on-Ring apparatus is its flexibility; indeed, the block or the ring can be easily fabricated with the material choose for the experimental test. Furthermore, this test

configuration is widely used to perform lubricated contact conditions and, mainly, to study scuffing process under high pressure conditions [50]. According to ASTM G77 standard [63], wear measurement is quantified weighting the block and the ring before and after each test. To provide an accurate weight definition, the samples need a cleaning process before putting them on a precision scale. A high difference of surface hardness of the material in contact permits an evaluation of the wear measuring the worn track on the block or on the ring. Tribometers are commercially available for this test, with some differences in apparatus configurations, parameters setting possibilities and method of friction coefficient measuring.

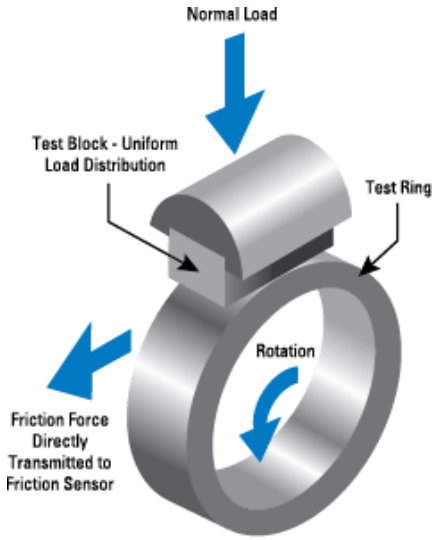

Figure 4 - Block-on-ring test configuration

2.1.3. **Disk-on-Disk test**

The configuration of this kind of test is realized using two disk with an external diameter of 50[mm], put in contact on the lateral surface inducing an on-A-line contact. The Disk-on-Disk test bench is usually used to characterize a tribologic contact affected by fatigue wear mechanism. Experimental tests can be conducted both in dry conditions or in lubricated domain and input parameters could be varied in order to modify Hertzian contact pressure. Surface fatigue wear is identified when a change occurs in friction coefficient trend or some vibrations occur on the contact pair. A scheme of this test configuration is illustrated in Figure 5.

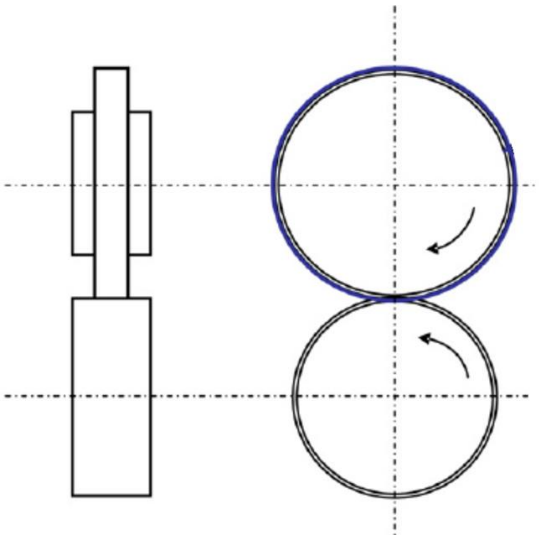

Figure 5 - Disk-on-Disk test configuration

2.1.4.**Four-Ball wear test**

The Four-Ball tribometer is composed by three steel balls clamped together and a fourth ball pushed and rotating against the other. The four ball are immersed in the lubricated oil at specified temperature and the upper sphere rotates at fixed speed. During the test, the normal load is increase every 10 minutes and the friction coefficient is acquired at the end of each load increase interval by a specific sensor indicated in [64]. This test configuration was ideated to outline anti-wear properties of a wide range of lubricant under boundary lubrication, due to the very high contact pressure. The end of each experimental test occurs when the rotating ball "welds" the static balls due to the high normal load. The test procedures are illustrated in ASTM D4172 [65] and ASTM D2266 [66] standards. Figure 6 illustrates the scheme of the tribometer described.

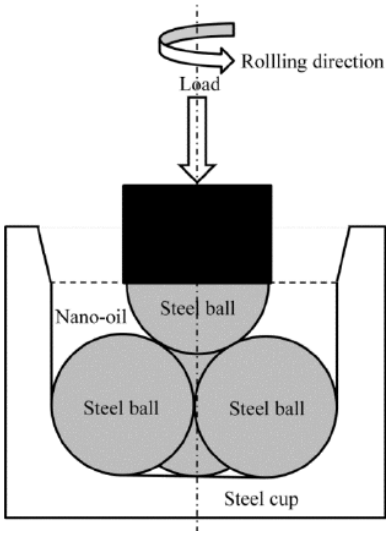

Figure 6 - Four-Ball Wear test configuration

2.1.5.**Pin Abrasion Test (PAT)**

This tribologic test is designed in order to highlight materials behavior under abrasion wear mechanism. A cylindrical pin is put in a rototraslation movement against a sandpaper made of ceramic particles, allowing a uniformly wearing on the contact surface of the sample. The test procedure is indicated in ASTM G132-96 standard [67].

2.1.6.**Dry Sand, Rubber-Wheel Wear Test (DSRW)**

The DSRW test configuration is usually used to identify abrasive resistance of solid materials, such as metals, minerals, polymers, composites, ceramics and thick coating. The tribologic test is conducted with a prismatic sample pushed against a rotating rubber wheel. A sand deposition between the counterparts generates the tribologic system and induces an abrasive wear between the surfaces. The sand composition, grain size and flow rate are controlled parameters. A schematic view of the system is illustrated in Figure 7. In the ASTM G65 standard [68] the synthetic wheel rotates in the same direction of the flow of sand. The value of the mass loss during the experimental test is defined as the weight difference of the sample before and after the test.

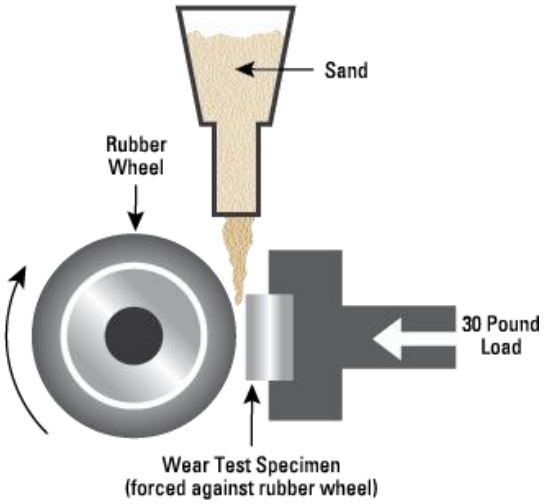

Figure 7 - DSRW test configuration

2.2. Metrocom "PIN RING" 640 test bench

The experimental campaign described in this Ph. D. Thesis was performed using a Block-on-Ring tribometer. This test bench is a commercial apparatus called METROCOM "PIN RING" 640 and it was designed to replicate the ASTM G77 standard procedure [63].

The Technical Manual [69] illustrates the possibility for this test bench to perform both dry and lubricated tests. The apparatus is composed by a basement where is installed the electric engine, the supports for the block and for the ring and the linear transducers. The block is mounted on an oscillating arm, as illustrated in Figure 8; on the right end of the arm a specific number of dead weights are installed in order to provide the normal load on the contact between the block and the ring, while on the left end of the arm is fixed the vertical linear transducer aimed to guarantee the measurement of the wear increase. The ring is mounted on a rotating shaft, connected with the engine by a transmission belt. The test bench is equipped with two linear transducers, one installed vertically on the left side of the arm with the aim to measure the vertical movements of the contact pair, and the other mounted horizontally connecting the block support and the main structure of the apparatus. This transducer has the purpose to guarantee the measure of the friction force induced during the contact.

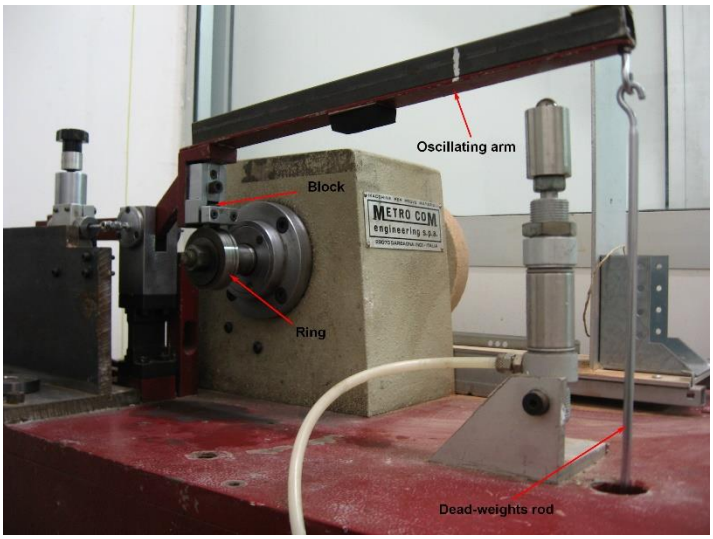

Figure 8 - METROCOM "Pin Ring" test bench

Friction force and vertical movement variations are acquired by an external data acquisition system directly connected with the two transducers described before. The data acquisition system used in the experimental campaign is a PicoLog Datalogger ADC 24 [70] which, connecting to a computer, provides the digital acquisition of friction force and vertical movement signals. Furthermore, the Datalogger has the possibility to acquire temperature signals and so on.

The test bench is equipped with a rotating speed regulator that allows a speed variation from 0.39m/s to 2m/s corresponding to 149rpm and 771rpm respectively. Furthermore, the apparatus is provided with a rpm counter in order to evaluate the cycles carried out at the end of each test.

Following the ASTM G77 standard and the data illustrated in the test bench Technical Manual, the samples used for the whole test campaign have imposed measures. Technical drawings of the samples are depicted in Figure 9 and Figure 10.

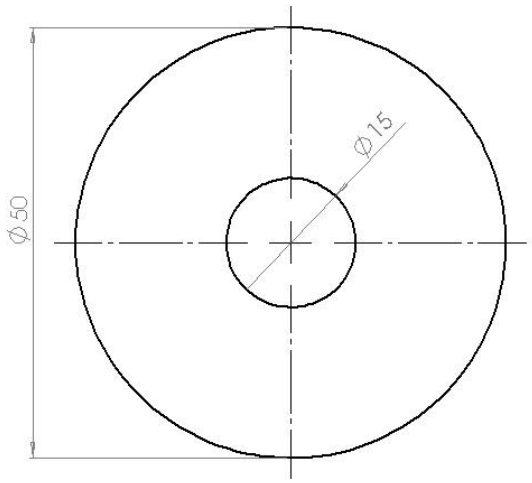

Figure 9 - Ring technical drawing

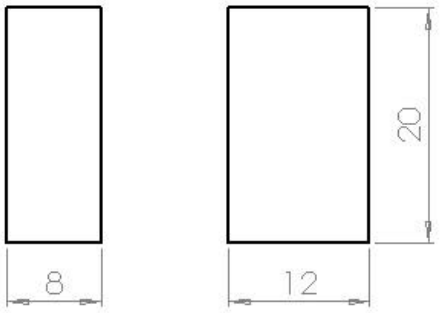

Figure 10 - Block technical drawing

2.2.1. **Preliminary tests**

Before starting with the experimental campaign, a calibration phase was performed on the test bench with the aim to highlight and to correct possible measuring issues of friction coefficient value. In order to achieve this goal, some preliminary tests were performed on a lubricated steel-steel contact. The decision to perform this kind of contact allowed the possibility to correlate the results with those available in literature, evaluating the test bench response.

The contact was configured using mild steel samples both for the block and for the ring. The preliminary tests were carried out in a lubricated domain, using mineral oil and filling a bin positioned under the components. The ring, during the rotation, guarantees contact lubrication, as illustrated in Figure 11.

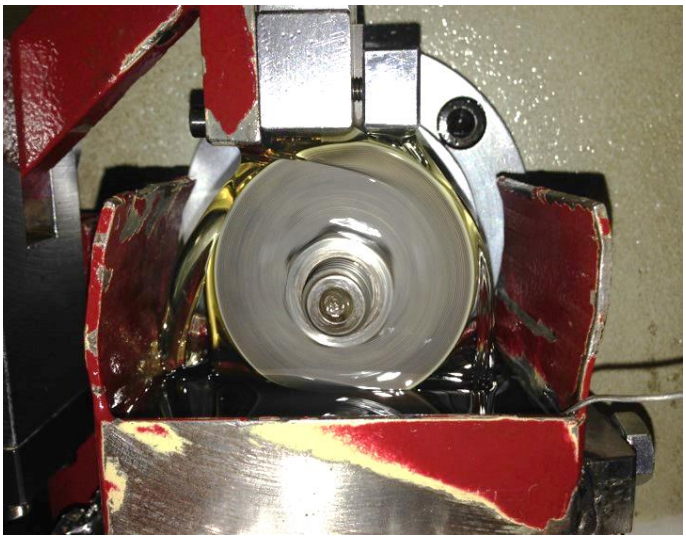

Figure 11 - Lubrication during a Block-on-ring contact

Following ASTM G77 [63] a load of 130N was installed on the right end of the arm inducing the normal load acting on the contact. The rotation speed was set at 180rpm as indicated in the ASTM standard. The preliminary test campaign was performed using 5 different pair of samples with the aim to guarantee a good repeatability of the results. Each test had a duration of about 3500s, an adequate time to verify coefficient trend and wear evolution.

During the execution of each test, tangential force and vertical displacement were measured using the transducers installed on the test bench and the tension signals were acquired on a computer by the Datalogger. A correlation formula defines the relationship between milliVolt of the signals and, respectively, Newton for the friction force and millimeters for the wear increase. Following the Equation 1, the evolution of the friction coefficient respect to time was defined as illustrated in Figure 12. In these preliminary tests, only the friction coefficient trend was taken in account considering an easier and faster verification of its value respect to the wear value.

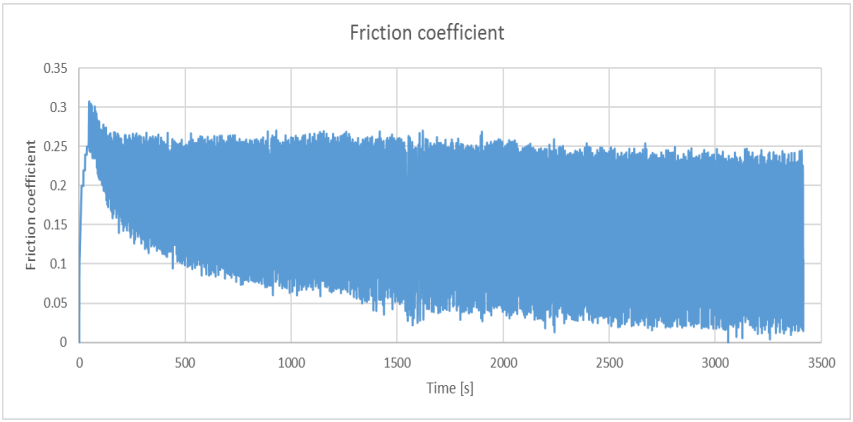

Figure 12 - Mild steel-steel friction coefficient trend - original test bench configuration

As one can see from the Figures above, the acquired signals have a high oscillation mainly due to the low stiffness of the test bench configuration. Indeed, the installation of dead weights at the end of the free arm induces an oscillation of the arm itself during the rotation of the ring. This phenomenon induces an incorrect definition of the average value of the friction coefficient and the wear.

To overcome this issue, a customization of the normal load application method was implemented, in order to achieve a higher stiffness of the structure. As illustrated in Figure 13 a load cell was installed at the right end of the oscillating arm and at the basement of the test bench.

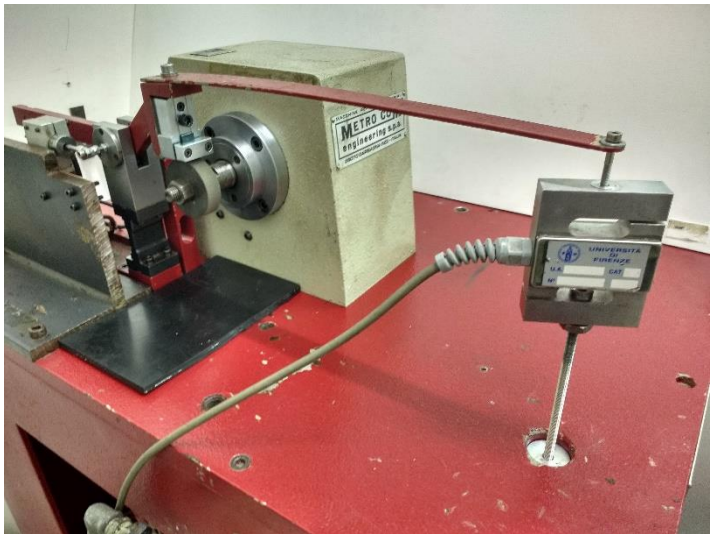

Figure 13 - Load cell implementation

The connection between the basement, the load cell and the oscillating arm is provided by a screw and a threaded rod installed at the load cell ends, as shown in the Figure 14.

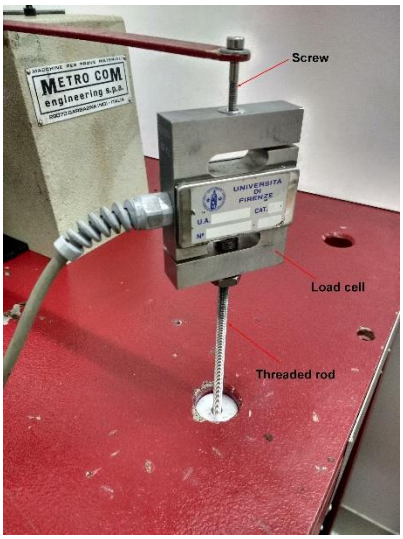

Figure 14 - Load cell connection system

The threaded rod and the screw guarantee a high stiffness of the whole system and allow the regulation of the normal contact load, replacing the dead weights mounted on the original test bench. Furthermore, the use of a load cell instead of a simple threaded rod allows a direct acquisition of the normal load acting on the contact pair during the execution of each experimental test. Indeed, the load cell is connected to the Datalogger and hence the normal load is acquired by the computer.

In order to evaluate the oscillating frequency of the whole system and to verify the choice made, a dynamic characterization of the test bench was performed.

The principal components of the test bench were schematized as illustrated in Figure 15, where m_0 represents the mass of the flexure hinge, m_1 is the mass of the block support, m_2 represents the mass of the oscillating arm and W is the normal load represented by dead weights.

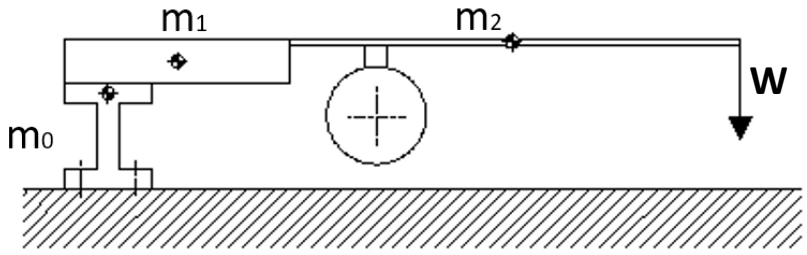

Figure 15 - Test bench schematization

Considering original test bench configuration (without load cell), it was possible to schematize the apparatus as a mass-spring system, assuming damper as negligible. Figure 16

shows the schematization, considering m as the total mass acting on the block-ring contact and k_{arm} the stiffness of oscillating arm.

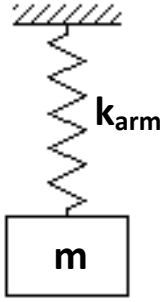

Figure 16 - Original configuration mass-spring system

Considering approximatively m=4kg and k_{arm}=1·10^{3}N/m, the natural frequency in vertical direction of the original configuration is defined with ω_o, as indicated in the following equation:

$$\omega_o = \sqrt{\frac{k_{arm}}{m}} \tag{3}$$

and it has a value of ω_o=16rad/s.

On the other hand, a schematization of the whole system was made also following the load cell configuration. As for the original set up, a mass-spring system was defined, illustrated in Figure 17:

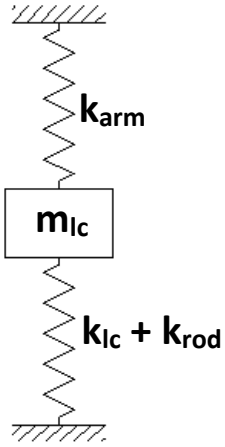

Figure 17 - Load cell configuration mass-spring system

In figure above, m_{lc} defines the load cell mass, k_{arm} is the oscillating arm stiffness, k_{lc} is the load cell stiffness while k_{rod} is the threaded rod stiffness. These parameters were measured as m_{lc}=0.54kg, k_{arm}=1·10^{3}N/m, k_{lc}=2.4·10^{6}N/m and k_{rod}=20.6·10^{6}N/m. As before, natural frequency ω_{lc} was obtained substituting the parameters above in the following equation:

$$\omega_{lc} = \sqrt{\frac{k_{tot}}{m_{tot}}} \tag{4}$$

Where k_{tot} is the sum between each stiffness values while m_{tot} is the total mass acting on the block-ring components. In this case the natural frequency of the configuration was ω_{lc}=6526rad/s.

As illustrated before, during preliminary tests ring's rotational speed was fixed at $R_{S,RING}$=180rpm, corresponding to $R_{S,RING}$=18.85rad/s. According to this, one can easily see how the load cell implementation defined a higher distance between natural frequency compared to the original configuration, avoiding oscillation issues.

After the installation of the load cell, new preliminary experimental tests were performed using the same contact configuration of the previous tests and maintaining the input parameters set on the test bench. As illustrated in Figure 18, friction coefficient has a lower oscillation compared to the first array of tests, highlighting an accurate installation of the load cell.

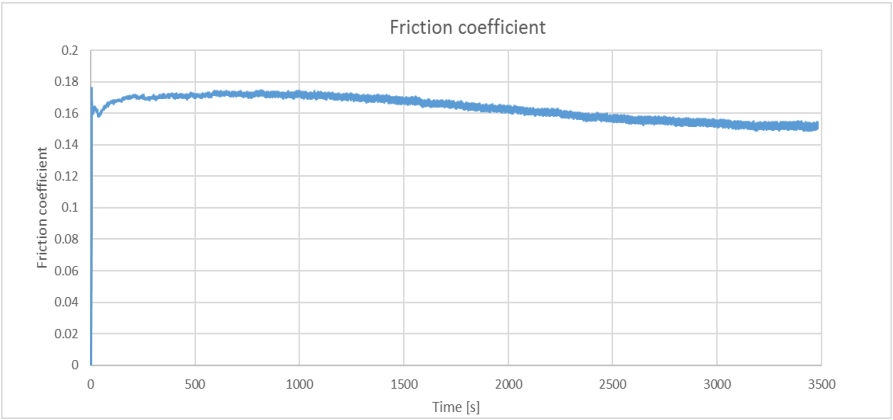

Figure 18 - Mild steel-steel friction coefficient trend - load cell test bench configuration

As earlier described in this Paragraph, the preliminary test had the aim to verify the test bench functionality and to highlight eventually measurement issues. Friction coefficient trend defined from the second array of preliminary tests has an average value of μ=0.16÷0.17, value verifiable in literature for a lubricated mild steel-steel contact [71].

The load cell implementation allowed a reduction in the oscillation magnitude and the noise in the acquired signals. Thanks to this feature, this configuration was chosen for the fulfilment of the entire test campaign object of this thesis.

3. Nanomaterials

3.1. A new materials approach

Materials and their knowledge are fundamental for our culture and to defining historical periods. Since prehistory, materials characterized human behaviors, giving the opportunity to develop knowledge about materials' characteristics and uses. This reflects how important materials are to us and the continuous battle among human and the world around him in order to understand and modify the stuff of which it is made.

Since last years of 21st century, it became more interesting the study of materials combinations instead of a focusing on a better knowledge of a particular material. Following this approach, it is possible to take advantage of the properties of combined materials, enhancing synergistic functions and using new materials in such innovative applications.

It is not so easy to find a single technology with the capability to influence a wide range of industries, imposing new frontiers on materials' study. Nanotechnology falls into this category and allows the creation of a wide range of combined materials, composites and structures on a molecular scale. Nano-scale technology has the possibility to redefine the methods used for developing high-performance structures highlighting unique and non-traditional properties [72].

Nanotechnology could be defined as any kind of technology that manages with elements or materials characterized by dimensions between 1 and 100 nanometers.

European Commission adopted the following definition for a nanomaterial [73]:

"A natural, incidental or manufactured material containing particles, in an unbound state or as an aggregate or as an agglomerate and where, for 50 % or more of the particles in the number size distribution, one or more external dimensions is in the size range 1 nm - 100 nm. In specific cases and where warranted by concerns for the environment, health, safety or competitiveness the number size distribution threshold of 50 % may be replaced by a threshold between 1 and 50 %. By derogation from the above, fullerenes, graphene flakes and single wall carbon nanotubes with one or more external dimensions below 1 nm should be considered as nanomaterials."

Nano-scale technology is not limited to just one, but it includes many technical disciplines as biology, chemistry, material science, electronics and so on. The union of these different technologies allows nanomaterials to generate new features more efficient than larger structures of the same materials. Conventional materials properties can be improved thanks to a modification of physical and chemical properties of nano-materials. Indeed, at nanometer

scale, the surface properties start becoming more dominant than the bulk material properties, generating new material characteristics and chemical reactions. These features allow the materials to change their characteristics, including optical properties, light absorption and emission behavior.

This new class of materials allows to overcome the limits imposed by classic material characteristics, enabling the development of new synergisms between different materials that only occur when element dimensions are reduced to nano-scale.

3.2. Applications

It should be noted that even though nanotechnology applications started its development only since the end of 21st century, nano-scale-based technologies are already being used in some industrial applications. Nanostructures used in industrial applications are mainly composed by a matrix and a nanomaterial that acts as a reinforcement, defining nano-composites.

Generally, nano-composites are realized using a matrix of standard material such as polymers, reinforced with nano-sized particles. Nanoparticles additions to the matrix allow an enhancement of the properties of the base material, including mechanical strength, toughness and thermal or electrical conductivity [72]. One of the advantages of nanoparticles is such that the amount of reinforcement added to the matrix is usually only 0.5-5.0% by weight. Furthermore, industries developed simple and quite cheap techniques to synthesize these innovative materials, increasing future applications.

Thanks to their characteristics and features, nano-composites are used in a wide range of industrial applications, such as biomedical field and automotive industries, passing through the modification of material structure in order to obtain custom properties.

An important progress was made in order to enhance the manufacture process of useful structures and coatings using custom Physical Vapor Deposition (PVD) and Chemical Vapor Deposition (CVD) processes modified for special applications. In biomedical field, nanocrystalline coatings were applied using High-Velocity Oxy-Fuel Thermal Spraying (HVOF), obtaining improvements in environmental impact and a reduction in toxic solvents during the use in biomedical implants [74].

The fast growing of the worldwide interest in nanotechnologies and nanomaterials observed during last years [75] interested not only the study and research of surface treatments but also the development of material structure modifications in order to achieve particular properties. Recently, lots of studies were performed with the aim to discover the effects of bainite nano-structure on wear resistance. One of the most important research performed on nano-scaled bainitic steels outlined a decrease of the wear rate proportionally with the austempering temperature [76]. Other studies were directed toward the investigation of carbide-free bainitic steels; results indicate that it is possible to obtain excellent wear performance using steel with a bainitic ferrite microstructure without carbides [77], [78]. All these research topics were developed and studied with the aim to investigate the wear resistance of nano-scaled bainitic steels in different conditions, highlighting their potential use in engineering applications.

Automotive industry also benefits of the nanomaterial revolution occurred in macrosystems, supporting the large diffusion of the emerging nanotechnology. The possibility of nanostructure to combine different materials properties allowed the use of new materials' concepts into a wide range of applications, including but not limiting to lightweight construction, energy conversion, pollution sensing and reduction, interior climate and wear

reduction. In this direction, the research of powertrain improvement concerned friction and wear reduction of translating and rotating components. In internal combustion engines, the largest amount of mechanical losses come from piston, piston rings, crankshaft gear and valvetrain [79]. Innovative nanocomposites with SiC, SiO_2, TiO_2, BN_3 or Teflon particles mixed in polymeric matrix reduce the friction losses and, consequently, enhance the wear resistance of contact pairs. These features allow a reduction in lubricants used in internal combustion engine, outlining longer service intervals and a pronounced fuel saving.

The evolution of nanomaterials imposed a consequent development of innovative application methods and techniques able to manage with nano-scale elements. Following the object of this thesis, a brief description of the application technologies used for thin layer coating is illustrated:

- Mechano-made: the mechano-made process involves both mechanical and chemical actions, allowing the possibility to combine solids at the nano-scale performing in-situ reactions. The advantages obtained using this technique concern a design of treatment (in terms of composition and industrial realization process), a definition of material's features and fewer production limitations respect to usual technologies. One of the most interesting applications involved the use of tungsten and cobalt carbides as wear resistance treatments of mechanical components [81].
- CVD: in the Chemical Vapor Deposition process a chemical reaction takes place between treatment material in a volatile phase and a gas inflated near the surface to be covered. When the reaction occurs, the surface treatment covers the surface, creating a compact layer. The main advantages of this technique concern a high layers' density, a low porosity of the layers and high thickness uniformity and material adherence. The chemical process involved in this deposition technique allows the possibility to use a wide range of materials taking advantage of their reaction capabilities.
- PVD: with the Physical Vapor Deposition technique it is possible to deposit a nanostructured film without preparing ultrathin powder, as for CVD processes. This process describes a variety of vacuum deposition methods which can be used to produce thin films. PVD uses physical process (such as heating or sputtering) to produce a vapor of material, which is then deposited on the object which requires coating. The most used physical process can be listed as:
    - Cathodic Arc Deposition
    - Electron beam physical vapor deposition
    - Evaporative deposition
    - Pulsed laser deposition
    - Sputter deposition
    - Sublimation sandwich method

  Cathodic arc deposition and sputter deposition allow the deposition of nanolayers, defining tribologic properties among the layers deposed on a surface. Thanks to this, a custom design of the treatment could be made, achieving the characteristics desired.

- PECVD: in the Plasma-Enhanced Chemical Vapor Deposition technique the component is treated with the coating using a plasma source. With this technique it is possible to treat the external surface of the piece with thin nano-layers, obtaining a

surface with low porosity and high adherence. Studies were carried out on SiO_2 nano-layers with the aim to obtain a high value of surface passivation in solar cells application [80].

3.3. Experimental analyses

Since the beginning of 21st century, the increasingly more restrictive anti-pollution laws stimulated automotive industry in a more in-depth research about new materials and new production processes in order to obtain a reduction of lubricants in anti-wear applications. Anti-wear features are very important during the normal working conditions of an internal combustion engine (ICE), mainly because only 12% of the available energy in the fuel is transformed into driving force, while 15% is dissipated as mechanical and friction losses [82]. Based on the data obtained in [82], a 10% reduction in mechanical losses would lead to a 1.5% reduction in fuel consumption. Considering the energy consumption within an ICE, friction loss is about 48%, defining the major portion of energy dissipated [82], as illustrated in Figure 19. Friction losses could be also divided in piston skirt friction, piston rings friction and bearings concerning the 66% of the total amount, while valvetrain assembly, crankshaft, transmission and gears are approximately 34% [83].

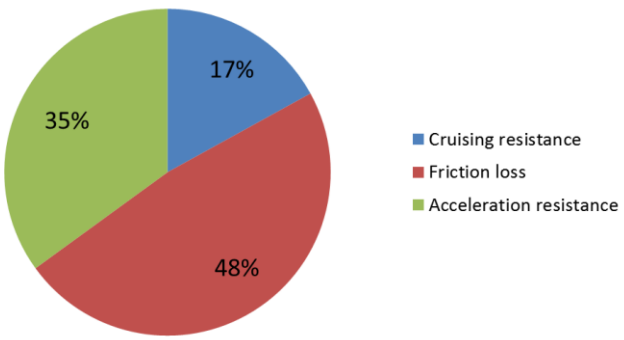

Figure 19 - Energy consumption developed in an ICE

Considering the aspects described, application of tribologic principles in ICE design and development is necessary in order to increase reliability, giving lots of advantages:

- Reduced fuel consumption
- Increased engine power output
- Reduced oil consumption
- A reduction in harmful exhaust emissions
- Improved durability, reliability and engine life
- Reduced maintenance requirements and longer service intervals

Following this approach, automotive industries started since 90s using and developing innovative nanostructures with the aim to define surface treatments and oil additive to reduce friction losses in ICE. Lots of studies were carried out mainly on the piston skirt and piston rings, outlining good results for ceramic-based coating [84]–[87], while the study of valvetrain assembly tribology concerned mainly the development of steels with high surface hardness [88], limiting surface treatments applications due to the high contact pressure achieved during the contact between valvetrain assembly components.

3.3.1. **Block-On-Ring experimental campaign**

Following what described in the previous paragraph, an experimental campaign was carried out in order to analyze two coatings with the aim to define a possible application on ICE components.

The possibility to use a Block-on-Ring test bench allowed to perform experimental tests on the nanostructured treatments replicating the working conditions of a valve train assembly, focusing the attention on the cam-follower contact pair.

The main aim of the experimental campaign was to analyze two different nanostructured treatments trying to replicate the characteristics generated during a contact between a cam and a follower, in terms of contact load, rotating speed and lubrication process.

In order to obtain a good replication of valve train working conditions, fundamental features of a cam-follower contact were analyzed, defining the real normal load acting between these two components, the average rotating speed of a camshaft and the oil temperature achieved inside an ICE. These evaluations allowed the test bench's input parameters definition, taking into account that the dimensions of real components (cam and follower) are different compared with those of samples used on the Block-on-Ring test bench.

In an internal combustion engine, the rotating speed of the camshaft and the rotating speed of the crankshaft are related with the following equation:

$$\omega_{CAM} = \frac{1}{2}\omega_{CRANK} \tag{5}$$

where ω_{CAM} is the camshaft rotating speed and ω_{CRANK} is the crankshaft rotating speed.

The average engine speed of a light-duty vehicle during its normal use is about ω_{CRANK}=3000rpm; consequently, the average value of camshaft rotating speed achieves ω_{CAM}=1500rpm. With the assumption to consider only the round part of the cam profile, it was possible to fix the external diameter of the cam at about D_{CAM}=30mm. Following the same assumption made before, it was possible to obtain the cam circumference thanks to the following equation:

$$C_{CAM} = 2\pi r_{CAM} \tag{6}$$

where r_{CAM} is the external radius of the round part of the cam. Substituting the values in the Equation 6, cam circumference can be defined as C_{CAM}=94.2mm=0.0942m. As illustrated in Paragraph 2.2, the test bench used in the experimental campaign defines the ring rotating speed using [m/s] as units of measure. Hence, it was necessary to define camshaft rotating speed with the same units of measure used in the test bench in order to correlate the velocities.

The following equation specifies the camshaft rotating speed using [m/s]:

$$R_{S,CAM} = \frac{\omega_{CAM} C_{CAM}}{60} \tag{7}$$

Substituting the values in the equation above, the camshaft rotating speed was defined as $R_{S,CAM}$=2.35m/s. This value is associated with a cam's external diameter of 30mm.

In order to determine the rotating speed to be fixed on the test bench, it was necessary to correlate the camshaft rotating speed and its diameter with the external dimension of the ring. The following equations helped us in the definition process:

$$D_{CAM} : R_{S,CAM} = D_{RING} : R_{S,RING} \tag{8}$$

where D_{RING} is the ring external diameter and $R_{S,RING}$ is the ring rotating speed. The resulting rotating speed is $R_{S,RING}$=3.9m/s.

As indicated in [88], [89], the normal load between the cam and the follower can reach the average value of F_{CAM}=800÷1000N. The contact surface generated between the cam and the follower is a line-type contact surface and this kind of contact surface can be defined also in the Block-on-Ring configuration. Hence, the specific pressure defined should have the same value.

During working conditions, an ICE generates a large amount of heat; consequently, the lubricating oil reaches an average temperature of about 100÷120°C.

Table 3 makes a recap of the input parameters that should be set on the test bench.

Table 3 - Test bench input parameters

Rotating speed [m/s]	**Normal load [N]**	**Oil temperature [°C]**
3.9	800÷1000	100÷120

Paragraph 2.2 illustrates test bench technical characteristics; due to technical limits it was not possible to set the input parameters resumed in Table 3. According to this, rotating speed and normal load were fixed at $R_{S,RING}$=2m/s and W=180N respectively, maximum values achievable by the test bench. The lubricating oil temperature was the only parameter that could be reached also in the experimental campaign. The difference between hypothesized and real values set on the test bench could lead to a difference of results, defining a reduction of wear process occurred on the specimens.

In order to replicate camshaft characteristics, both the blocks and the rings used in the experimental campaign were machined using 18NiCrMo hardened steel alloy, a material commonly used for camshaft fabrication. Samples were CNC machined to obtain the same surface finishing achieved in a cam-follower contact. Both the rings and the blocks were submitted to surface hardness tests using a Knoop micro-hardness testing machine. Hardness tests were performed on three blocks and three rings casually chosen from the whole array of samples. Table 4 recaps values obtained as an average of 5 measurements performed on each specimen.

Table 4 - Samples' surface hardness

Rings surface hardness [HK]	Blocks surface hardness [HK]
803.6	820.2
850.8	817.1
810.9	803.5

As illustrated in Paragraph 3.2, one of the main characteristics of nanostructured materials concerns the wide range of possible composites. To facilitate the choice of materials suitable for a friction coefficient reduction purpose, experimental campaign was carried out thanks to the support of an industry leader in nanomaterials fabrication. Thanks to their support, it was possible to define two different thin coatings, both of them composed by polymeric matrix and nanomaterials as reinforcements. Unfortunately, it was not possible to know the reinforcements typology because the composites were under patent approval.

Coatings were deposited on the external surface of the rings, maintaining unaltered the contact surface of the blocks. Thanks to this feature, it could be possible to hypothesize an application of the treatments on the external surface of the cam.

After coatings deposition process, blocks and rings were put in ethanol, cleaned using an ultrasonic device and weighted using a high-precision scale. Samples were installed on the test bench and the experimental campaign started. Since the beginning of the test, ring rotation guaranteed a continuous lubrication of the contact, replicating the lubricating process occurring in a cam-follower assembly. The oil was placed in a custom container and its temperature achieved slowly an average value of 100[°C], as defined before.

Both for Treatment 1 and for Treatment 2 test duration was not fixed, defining it as a characterizing output of treatments experimental analyses. Indeed, test duration was defined evaluating the wear process occurring on the ring external surface and verifying friction coefficient and wear value trend. This process was possible thanks to a direct visualization of output parameters in terms of tangential force generated on the contact, normal load acting by the load cell and the wear value generated during ring rotation.

3.3.2. **Results**

In order to guarantee the statistical significance and to evaluate the repeatability of the obtained results five tests were performed both for Treatment 1 and for Treatment 2. Friction coefficient and specific wear rate values obtained from experimental campaigns are listed in Table 5 and in Table 6 for Treatment 1 and Treatment 2 respectively. As indicated in Chapter 1, friction coefficient was defined following Equation 1 while specific wear rate was obtained using Equation 2. Since tests were performed using a Block-on-Ring configuration, worn volume amount was obtained following ASTM G77 standard procedure [63].

Table 5 - Treatment 1 tribologic characteristics

Friction coefficient	Specific wear rate $[\frac{m^3}{Nm}]$
0.15	$4.54 \cdot 10^{-14}$
0.16	$5.38 \cdot 10^{-14}$
0.14	$6.34 \cdot 10^{-14}$
0.14	$4.29 \cdot 10^{-14}$
0.15	$3.97 \cdot 10^{-14}$

Table 6 - Treatment 2 tribologic characteristics

Friction coefficient	**Specific wear rate** $[\frac{m^3}{Nm}]$
0.10	$7.35 \cdot 10^{-13}$
0.12	$6.89 \cdot 10^{-13}$
0.11	$8.11 \cdot 10^{-13}$
0.11	$6.84 \cdot 10^{-13}$
0.14	$6.91 \cdot 10^{-13}$

To facilitate discussion of data obtained, a graph for each treatment was chosen in order to define friction coefficient and wear value trends, highlighting potential differences among tests on same treatment.

Figure 20 illustrates friction coefficient trend of Treatment 1. It is easy to see an initial trend increment due to the first contact phase between block and ring, displaying a running-in phenomenon. Progressively, friction coefficient value shows a constant trend, maintaining its measure at about 0.15÷0.16 for approximately 17 hours, defining the end of the test. This phenomenon occurred when ring external surface was no longer covered by treatment's layer, showing a steel-steel contact process.

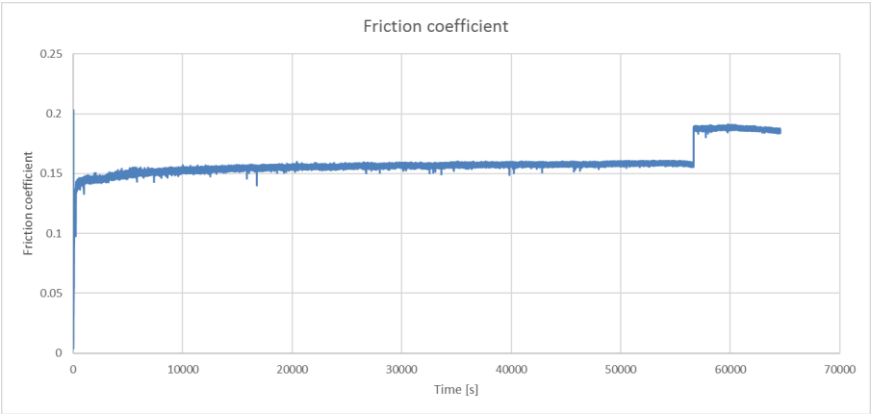

Figure 20 - Treatment 1 friction coefficient trend

The evaluation described above was confirmed by the wear depth value evolution with time. As it possible to see in Figure 21, the initial phase occurred on the wear value was the same described for friction coefficient trend, defining a running-in process between contact surfaces. Consecutive constant increment of wear trend illustrates typical evolution occurring during a contact between materials characterized by different surface hardness.

Proving analysis carried out on wear graph, it is easy to see the trend variation occurred after about 17 hours on the wear value evolution. Indeed, variation shown in that moment coincides with the completely treatment wear, highlighting the steel-steel contact process. This evaluation was performed compared the friction coefficient value described at the end of the analysis with the steel-steel contact results described in the previous chapters.

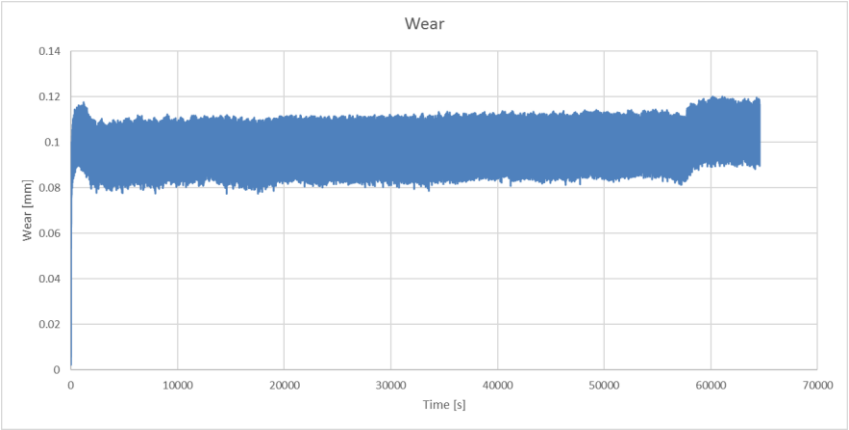

Figure 21 - Treatment 1 wear value trend

The other tests performed on Treatment 1 highlighted similar trends, comparable with those illustrated in Figures above.

At the end of each test, rings showed a wear track with a uniform distribution on the external surface, highlighting a completely wear of the treatment (Figure 22). On the other hand, blocks didn't display a significant wear on the contact surface due to the high value of the hardness; the wear track visible in Figure 23 could be due to the steel-steel contact occurred at the end of the test.

Figure 22 - Treatment 1 worn ring

Figure 23 - Treatment 1 worn block

The evaluation of tribologic characteristics was conducted also on the Treatment 2. As for Treatment 1, also in this case the graphs that best characterize the behavior of Treatment 2 were chosen. As shown in Figure 24, friction coefficient trend is comparable with the first treatment trend, outlining the initial increment due to the running-in process and the consequent decrease till a constant value of the friction coefficient itself. The main difference between the two treatments concerns the lower value reached by Treatment 2 compared with Treatment 1, key factor in order to reduce friction in components in contact.

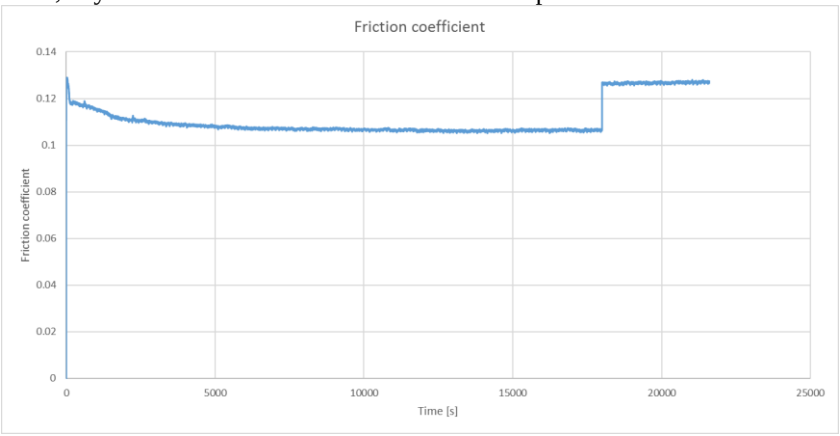

Figure 24 - Treatment 2 friction coefficient trend

However, Treatment 2 shows a low wear resistance. Indeed, as highlighted in Figure 24 and in Figure 25, treatment was completely worn after only 5 hours of work, outlining a duration a third smaller compared to first treatment. The graphs illustrate a clear trend variation, pointing out the end of the surface treatment on the external area of the ring.

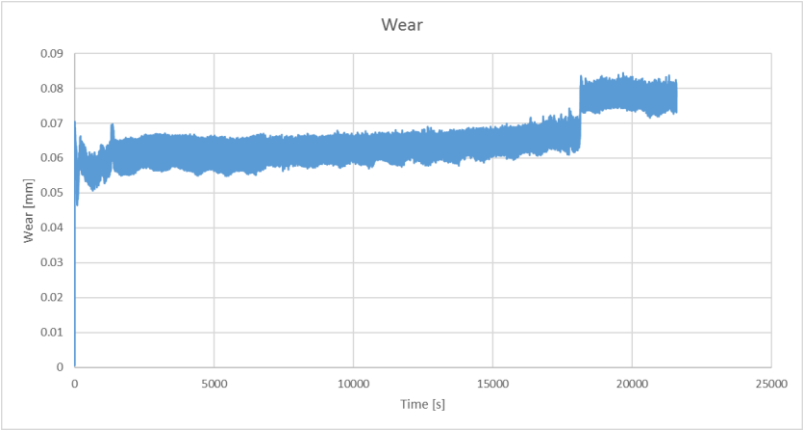

Figure 25 - Treatment 2 wear value trend

Also in this case, rings external surface showed a wear track at the end of each test (Figure 26), while blocks contact surface outlined a thick wear track due to the final steel-steel contact, as visible in Figure 27.

Figure 26 - Treatment 2 worn ring

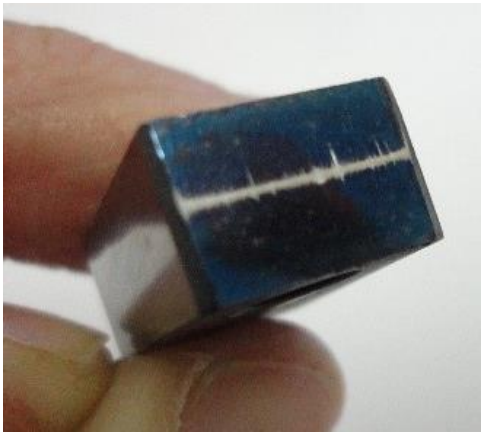

Figure 27 - Treatment 2 worn block

Experimental campaign underlined that both the treatment analyzed are characterized by a good friction coefficient value and a low wear resistance. Indeed, friction coefficient outlined in both treatments are comparable with those verifiable in literature for Diamond Like Carbon (DLC) and Silicon carbide (SiC), treatments usually used in friction reduction field [90]–[92]. On the other hand, the specific wear rate evaluation outlined a high treatments wear, displaying a lower duration of the nanostructured coating compared to verifiable in literature [90]–[92].

In view of the above, a treatment application on such components with high reciprocating contact force and consequent specific pressure (as in a cam-follower contact) is not desirable and favorable. Indeed, in these cases contact typology and working conditions would cause surface treatments removal in few camshaft rotations, eliminating the benefits of the treatment itself.

4. Reinforced epoxy resin

4.1. Epoxy resins

Epoxy resins are a class of thermoset materials usually used in a wide range of applications, mainly structural and specialty composite implementations thanks to their unique combination of features impracticable with other thermoset polymers.

The first industrial production of epoxy resins was carried out in Switzerland at the end of 1930s by Pierre Castan who first investigated the reaction between bisphenol-A and epichlorohydrin. The initial commercialization of epoxy resins concerned their applications as coatings and casting compound, but the same composites sold by Castan are nowadays commodity materials that provides the basis for most epoxy formulations [93]–[95].

In general, epoxy resins are a class of polymers and pre-polymers which contains epoxide group. The epoxide group can be thought as a molecule containing one oxygen atom and two carbon atoms, as illustrated in Figure 28.

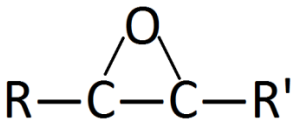

Figure 28 - Epoxide group

Epoxies may be reacted with other epoxy resins, making a homopolymerization, or with a wide range of co-reactants including acids, phenols, thiols and amines. The chemical reaction occurring between resins and co-reactants is commonly referred as curing. Curing process generates a thermosetting polymer with high mechanical properties, temperature and chemical resistance. Indeed, this class of polymers offers a high strength, low shrinkage, good adhesion to different substrates, electrical insulation, chemical resistance and low cost. Epoxy resins guarantees a good wettability of substrates, making them a good suited product for composite applications.

From the initial commercialization of epoxy resins, lots of possible applications were studied with the main aim to guarantee high mechanical properties, low cost and low weight. According to this, their most interesting implementations are found in aerospace and automotive industries where resins are applied in order to produce complex composites and structures, including flooring panel, wings and also fuselage. To satisfy a wide variety of nonmetallic designs, epoxies are formulated to generate specific composites with custom

characteristics and structural properties. Following this approach, chemical engineers have to combine the limitations of raw material in complex recipes including other different resins, modifiers for a specific desired property and curative that drives specific reactions at specified times.

The innovation brought by nanomaterials influenced also epoxy resins, extending the application field to a lot of surface treatments. As described in Chapter 3, nanostructured materials guarantee a wide range of properties and their applications achieve nowadays lots of mechanical components, including automotive parts and biomedical implants. The customization of nanomaterial features allowed their implementation in such mixture composed by polymers as epoxy resins, defining high-properties reinforced resins characterized by a low production cost.

Reinforced epoxy resins found their applications in structural devices and also in surface treatments, trying to enhance friction characteristics and wear resistance of treated components.

4.1.1. **Tribology of epoxy resins**

The tribology field is being paid much interest due to the importance of energy dissipation is such components where friction, lubrication and wear have an important contribution to the whole system behavior. Within this field, polymer materials have been applied as an important material category. During last decades, the study of polymer tribology has been treated both in a macroscopic scale assumption [96]–[98] and in a nanoscale point of view [99], [100].

Nanomaterial's revolution imposed a reorganization of design ideas trying to define custom mixtures of elements with specific properties. These materials found large application in tribological field, trying to outline surface treatments with the aim to improve friction and wear features. Polymer composites are widely used for tribologic implementations because their properties can be easily tailored using carbon nanotubes (CNTs), carbon fibers (CFs) and graphene sheets (GSs), as indicated in [101]–[104]. While CNTs reinforced composites did not found large application due to their high cost and difficult dispersion in epoxy-based matrix [101], [105], graphene became during last years one of the most suitable candidates for the development of structural and functional epoxy-based mixtures [104], [106].

A large number of studies were carried out during last decades on the implementation of graphene nanopowder in tribologic applications. In [107], graphene modified polyamide coatings were tribologically studied in order to evaluate wear resistance compared to neat polyamide coatings. Furthermore, in [104], [106] studies on lubricating effect of graphite particles in polymers contact were performed while in [104], [106], [108] graphite was studied as solid lubricant during a contact between polymers composite, outlining reduction of wear.

The enhancement of tribological performance of polymer materials concerns the modification of polymer surface, as described in [109]. In particular, taking in account a regulation of the surface energy dissipation, the low friction efficient [110], [111] was achieved using varieties of carbonaceous reinforcements, such as carbon nanotube, graphite and graphene. The effect of carbon-based reinforcements on tribological properties of polymers materials will become an interesting research field, as outlined in the study on metal-on-metal tribology described in [112].

As indicate in [113]–[117], graphene reinforcements are being studied in recent years thanks to their properties, such as high flexibility, good thermal conductivity and large surface area. Furthermore, the study of how graphene can influence the properties of bulk polymer

materials is being of large interest, mainly for practical applications. As illustrated in [118], [119], graphene was used as reinforcement in a large field of polymer materials, such as epoxy resins (EP), polypropylene, Nylon and silicone rubber. The study carried out in [120] described that using graphene oxide instead of pristine graphene should also have an evident improvement on tribological property of polymer mixture. The confirmation of this has been evaluated in [121] outlined a wear resistance enhancement by the addiction of graphene oxide into epoxy with a reduction of wear rate of about 90.0 – 94.1%.

The following Paragraphs will describe the experimental analysis performed on three different graphene reinforcements mixed within a commercial epoxy resin in order to evaluate the tribological characteristics of the composites. The experimental analysis was performed using a block-on-ring test bench with the aim to obtain a direct evaluation of friction coefficient and specific wear rate between the epoxy mixtures and a steel-made counterpart. The results analysis outlined some interesting outcomes usable in the definition of a surface treatment able to guarantee a long duration and a low friction coefficient.

4.2. Experimental analysis

The work proposed in this Doctoral Thesis concerns the study of some epoxy based surface treatments for application in mechanic field. Following the aim outlined in Chapter 3, experimental tests were performed in order to reproduce the contact characteristics of a camshaft commonly used in the automotive field; hence, the specimens used in the experimental campaign were made using the same material of a camshaft.

Both the rings and the blocks were machined from the same 18NiCrMo5 steel alloy raw bar. The epoxy resin used as matrix has the commercial name of EP-506 H17. To guarantee the properties resumed in Table 7, the resin needs a melamine catalyst added during the curing process.

Table 7 - Epoxy resin characteristics

	Value	**Unit**
Material	Epoxy resin	
Aspect	Liquid	
Color	Yellow	
Density	1.10	g/ml
Viscosity	1100	mPas
Hardness	82	Shore D
Flexural Modulus	3260	MPa
Tensile strength	74.9	MPa
Compression strength	61.5	MPa
Linear shrinkage	1.5	%
Tg (glass temperature)	77	°C

In the present test campaign three different commercial carbon-based reinforcements were used, distinguished by the average grain size:

- AO-2 with an average flakes thickness of 8nm
- AO-3 with an average flakes thickness of 12nm
- AO-4 with an average flakes thickness of 60nm

The mixture composed by epoxy resin, melamine catalyst and carbon based reinforcement was spread on the outer surface of each ring using a common brush. Due to a manual application, coating thickness can't be homogeneous among the samples. Furthermore, a measurement on 5 different rings outlined an average thickness of about t_e=0.5 +/- 0.07mm. The curing process was made on the treated samples and it took part in an oven. This process was carried out starting from a temperature of 80°C till a final temperature of 200°C after a 2-hour period.

Following these steps the final result was a surface treatment with a quite high hardness able to put in contrast the ring and the untreated block.

4.2.1. **Testing methods**

The main aim of the experimental campaign was the evaluation of the tribologic properties of some epoxy based mixtures in order to apply them in some critical lubricated contact pairs.

Following this objective, the tests were made using a METROCOM "PIN RING" 640 block-on-ring test bench, the same apparatus used in the tests described previously. The main input parameters (ring rotational speed, normal load and oil temperature) were set trying to replicate the working conditions usually present in an internal combustion engine during its use, illustrated in Table 8.

Table 8 - Test bench input parameters

Rotating speed [m/s]	**Normal load [N]**	**Oil temperature [°C]**
3.9	800÷1000	100÷120

During each test, friction load and the wear value were acquired using two linear position transducers: friction load is acquired measuring the deformation of a flexure hinge rigidly connected to the block, while wear value is obtained measuring the vertical displacement of the block. In addition, oil temperature was acquired using a thermostat and two thermocouples: one to measure the oil temperature in the tank and the other the temperature upon the heating plate. A continuous and simultaneous monitoring permitted to keep both the temperatures at a constant value of about 100÷120°C during the tests. The campaign was carried out following ASTM G77 standard while test duration was not fixed, defining it as a characterizing output of treatments themselves. Indeed, test duration was defined evaluating the wear process occurring on the ring external surface and verifying friction coefficient and wear value trend. This process was possible thanks to a direct visualization of output parameters in terms of friction force generated on the contact, normal load acting by the load cell and the wear value generated during ring rotation.

It is important to highlight that before test campaign, other two steps were required to prepare the specimens: a cleaning process using an ultrasonic apparatus and a weighing phase using a scale with a resolution of $1 \cdot 10^{-7}$kg. The cleaning process is repeated at the end of each test in order to remove all the oily residue attached to the specimens' surfaces and, in turn, to facilitate the following weighing, with the main purpose to evaluate the weight loss.

Following the idea of a friction coefficient reduction and with the main aim to obtain a good reproducibility of each test, 3 tests for each graphene reinforcement were performed. Two preliminary tests were carried out in order to evaluate the contact behavior between a steel ring – steel block pair and a ring covered only with epoxy resin (without any reinforcement) and a steel block. These two tests were performed with the main purpose to set

the initial characteristics of the steel-steel contact pair and the steel-epoxy resin contact pair, evaluating the friction coefficient and the wear rate.

4.3. Results and discussion

The complicated process of homogenization between epoxy resin and each carbon based reinforcement suggested to organize the test campaign performing three tests of each kind of treatment. Following this approach, a good repeatability of the results carried out from the block-on-ring test bench was guarantee.

4.3.1. **Test A: Steel - Steel contact pair**

The first test performed in this experimental campaign was carried out using an untreated block and an untreated ring. The main purpose of this study was the evaluation of the friction coefficient and the wear rate this kind of contact pair in order to verify the value that can be found in literature.

The test was performed using the same input parameters set for the other tests.

As one can see from the Figures 29 and 30, both friction coefficient and wear evolution have the typical trends of a lubricated steel-steel contact pair.

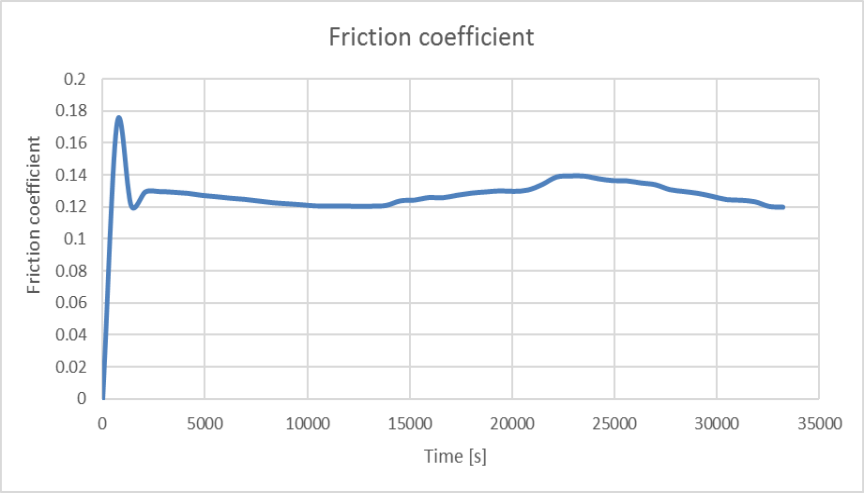

Figure 29 - Friction coefficient trend - Steel-Steel contact

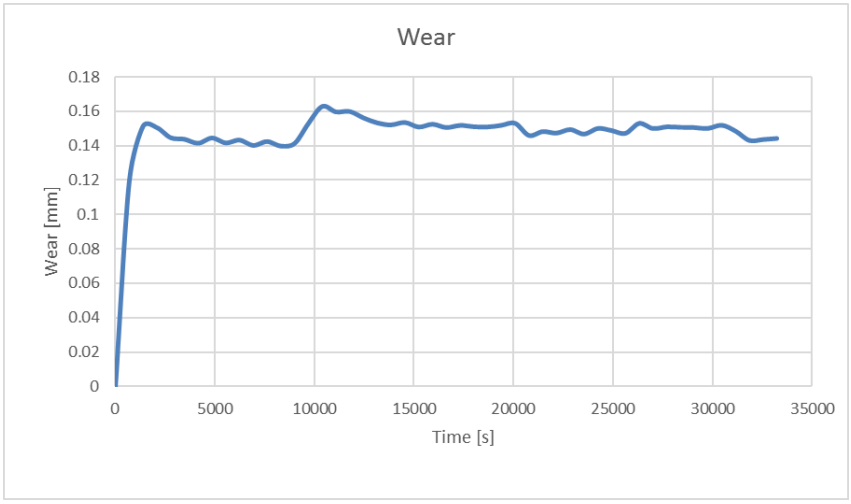

Figure 30 - Wear trend - Steel-Steel contact

It is possible to highlight an average value of the friction coefficient of about μ=0.13 and a final value of wear of about 0.15mm. From these results it was possible to define the specific wear rate using Equation 2. The average specific wear rate obtained for this contact was K=9.01·10^{-11}m^3/N·m.

4.3.2. **Test B: Steel - Epoxy resin contact pair**

After a first test conducted on a Steel-Steel contact pair, the attention was focused on a Steel – Epoxy resin contact pair. The block was maintained untreated while the outer surface of the ring was covered with the epoxy resin without reinforcement. This second preliminary test was performed with the main aim to obtain an evaluation of the tribologic properties of the epoxy resin itself.

The parameters set on the Block-on-ring test bench were the same as for the whole test campaign. As for Test A described before, results obtained from this test concern the average friction coefficient trend and the average wear trend.

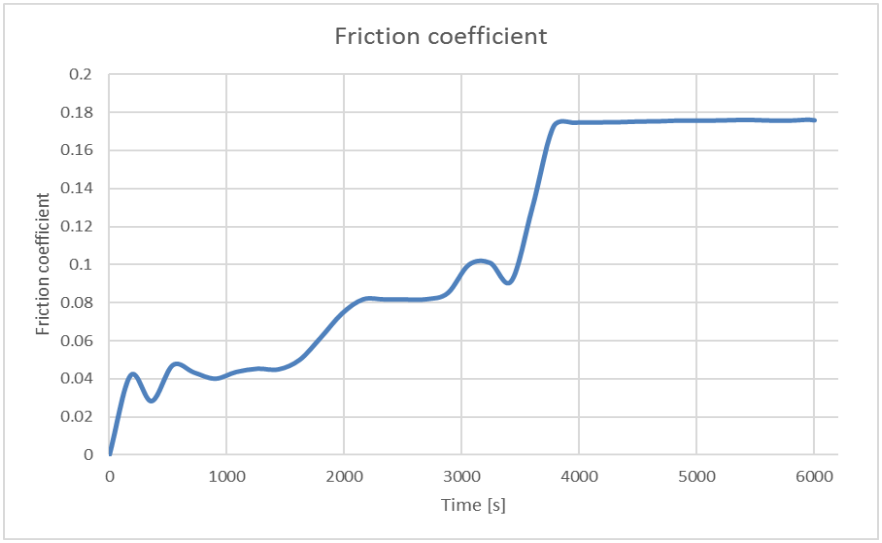

Figure 31 - Friction coefficient trend - Steel-Epoxy resin contact

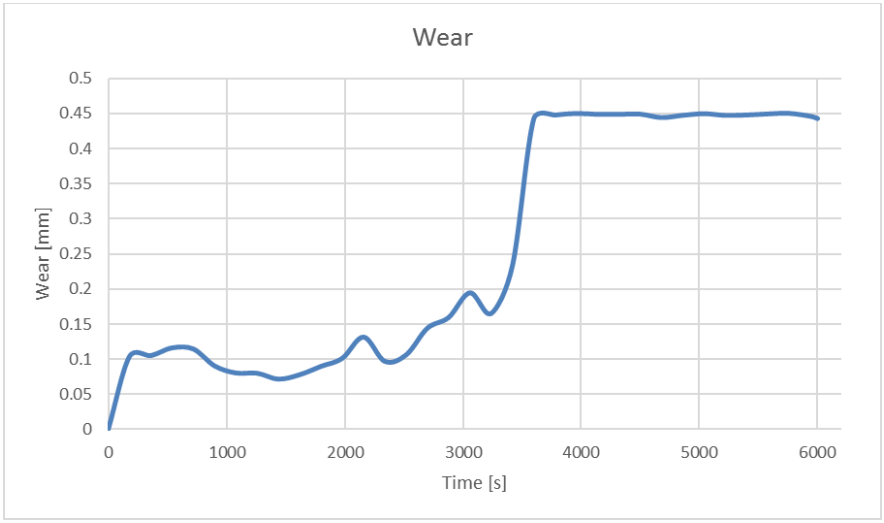

Figure 32 - Wear trend - Steel-Epoxy resin contact

Figure 31 shows an average value for the friction coefficient of about μ=0.06 but a reduction in the life-time of the coating compared to the steel-steel contact discussed in the previous paragraph. Indeed, the specific wear rate of the Steel-Epoxy resin contact pair is higher than the value obtained in Test A, reaching a value of K=3.62·10^{-7} m^3/N·m obtained from the value shown in the Figure 32.

4.3.3. **Test C: Steel - Epoxy resin + AO-2 reinforcement contact pair**

The reinforcement used in the Test C has the commercial name of AO-2 and it is characterized by an average flake thickness of 8nm.

The low dimension allowed a high homogenization of the graphene within the epoxy resin, as shown in the Figure 33. Furthermore, this characteristic allowed a distributed contact between the block surface and the coating, highlighting graphene's tribologic properties.

Figure 33 - AO-2 reinforcement distribution

As it is possible to observe in Figure 34, wear trend has an unusual evolution, showing an initial increase and a consequent reduction. This unusual wear trend is a characteristic behavior of such materials with a low value of surface hardness. The high value of lubrication oil temperature achieved during the contact led to a melting process of the epoxy resin and a consequent solidification of the resin itself on the block contact surface. The specimens were relatively pushed away due this process, producing the unusual trend of the wear value. This phenomenon could be due to the low capacity of the resin to create solid links among itself and the graphene grains, limiting the relative cohesion and producing the resin detachment during the tests.

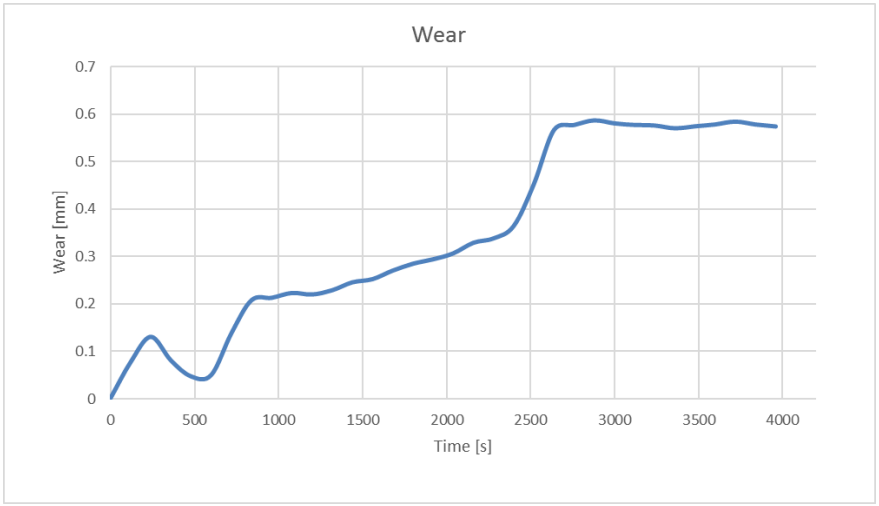

Figure 34 - Wear trend - AO-2 reinforcement

The contact occurred between steel and resin mixture produced a high value of specific wear rate and, therefore, a limited resin life-time. The average value of the friction coefficient is about μ=0.05 during the contact between the epoxy resin and the block, as shown in Figure 35, highlighting an improvement compared to the Test B.

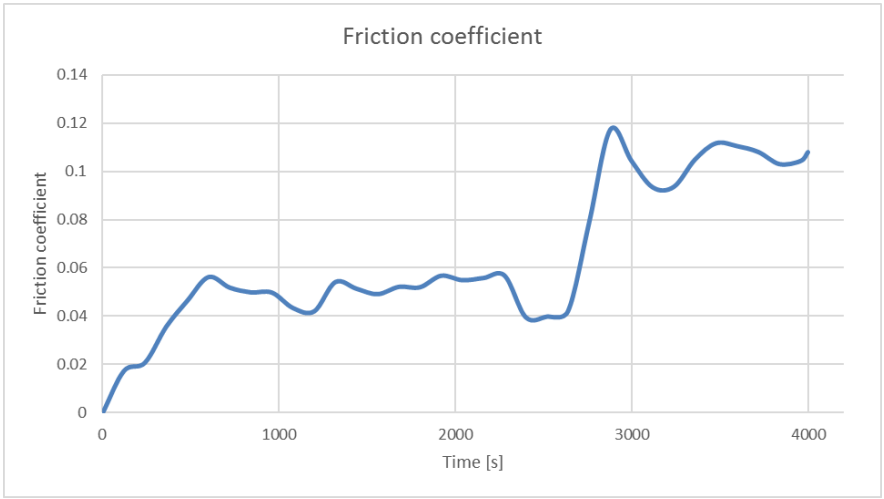

Figure 35 - Friction coefficient trend - AO-2 reinforcement

4.3.4. **Test D: Steel - Epoxy resin + AO-3 reinforcement contact pair**

The second test was performed using the AO-3 graphene commercial powder mixed with the epoxy resin. This reinforcement is characterized by an average flakes thickness of about 12nm. The powder homogenization level within the epoxy matrix is quite high, producing a uniform and compact layer of the reinforcement.

Thanks to these characteristics the behavior of the contact during the test underlined a particular trend in the friction coefficient evolution.

Indeed, Figure 36 shows an initial increase of friction coefficient trend due to the starting running-in phase between the steel of the block and the coating on the ring.

After the first phase is easily recognizable a decrease in the friction coefficient value due to the direct contact occurred between the steel and the graphene reinforcement. This kind of contact was guaranteed only for a short period due to a low magnitude of resin under the graphene layer. Indeed, graphene powder layer was completely worn in few seconds, defining the end of surface treatment.

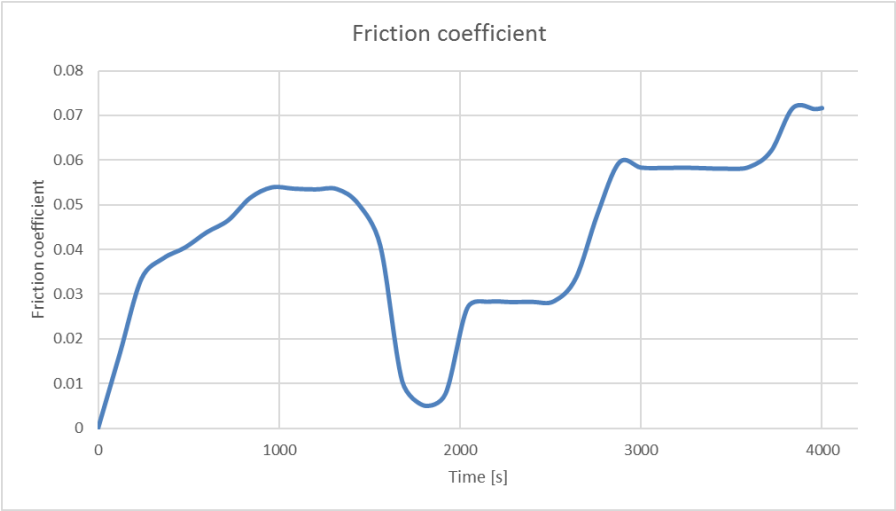

Figure 36 - Friction coefficient trend - AO-3 reinforcement

For what concerns wear trend, Figure 37 outlines a slow decrease of the value mainly due to the resin transfer process between the outer surface of the ring and the block. The phenomenon has a less pronounced decrement compared to the previous test thanks to the contribution of the graphene during the direct contact between the block and the reinforcement.

As for the previous experiment, resin was completely worn after 1 hour of work, defining a low wear resistance of the epoxy resin+AO-3 mixture.

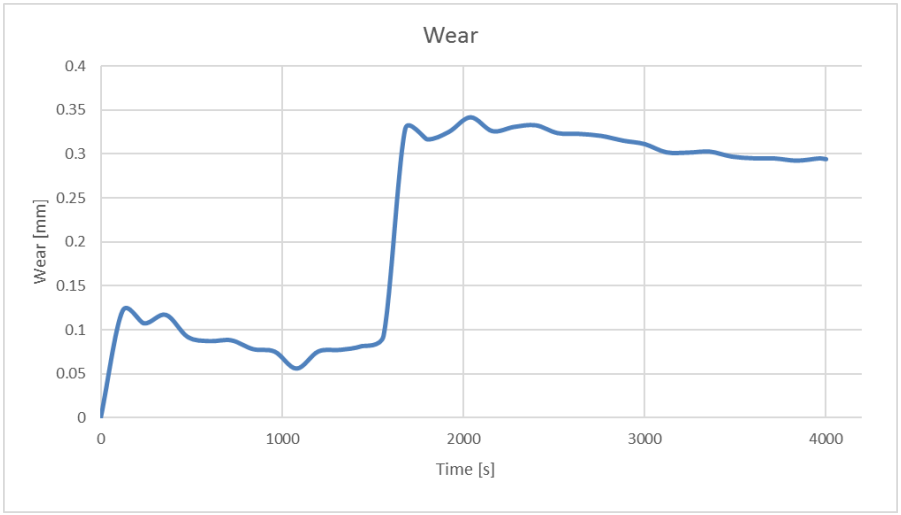

Figure 37 - Wear trend - AO-3 reinforcement

4.3.5. **Test E: Steel - Epoxy resin + AO-4 reinforcement contact pair**

Last test performed was carried out using a mixture composed by the epoxy resin and a reinforcement with an average flakes thickness of about 60nm.

The homogenization capability of the graphene powder within the resin matrix was verified also in this kind of mixture, producing a large contact zone and a constant distribution of the powder on the outer ring surface (Figure 38).

Figure 38 - AO-4 reinforcement distribution

Compared to previous tests, results obtained from Test E outlined an interesting trend for friction coefficient and for wear evolution.

Figure 39 shows the typical initial running-in period and a consequent decrease of friction coefficient value. This process has a continuous decrease trend mainly due to the

constant wear process occurred on the outer resin surface and to the following contact between steel and the graphene reinforcement.

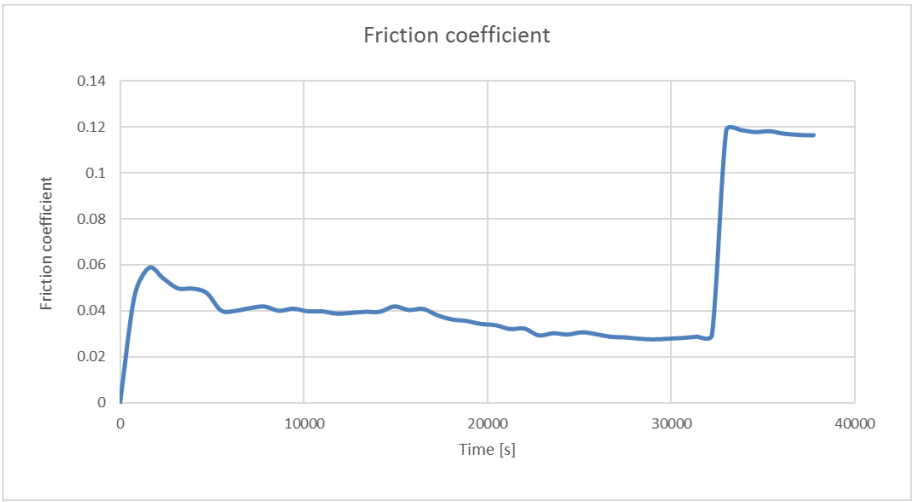

Figure 39 - Friction coefficient trend - AO-4 reinforcement

This event continued till the graphene was completely worn, highlighting the end of the external coating, as shown in the Figure 40. Wear trend outlined the typical evolution with an initial increase due to a running-in phase and a consequently constant growth of the value.

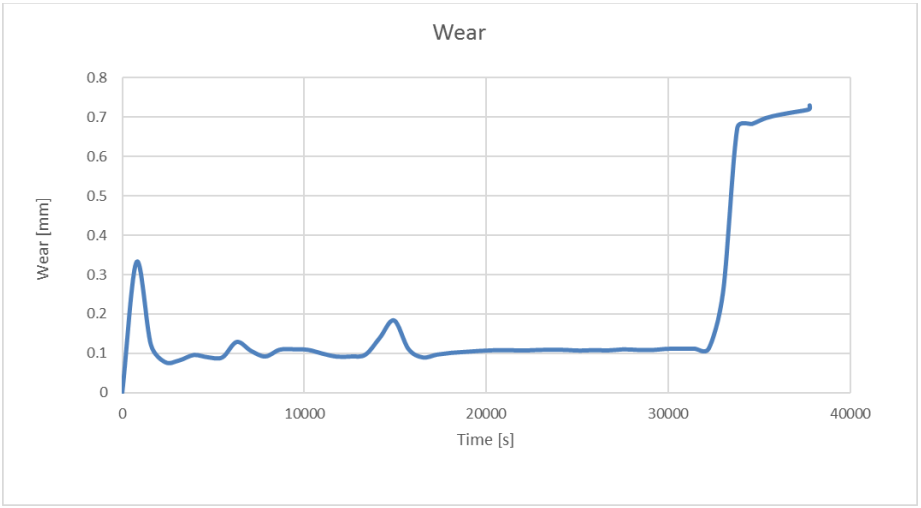

Figure 40 - Wear trend - AO-4 reinforcement

In this test, wear trend obtained at the end of the experiment has a central phase characterized by a constant trend, defining the life-time of the surface coating in about 10 hours, much higher compared to the values achieved from other reinforcements.

4.4. Results

The tests performed during the experimental campaign outlined some interesting behaviors concerning the contact between a steel block and an epoxy resin reinforced with three different graphene powders.

Following the main purpose of the study, it was possible to define the tribologic characteristics of different mixtures, evaluating the friction coefficient and wear trends.

Table 9 shows a resume of friction coefficient and specific wear rate average values for each test performed.

Table 9 - Experimental campaign results

Test ID	**Test type**	**μ**	**K** $\left[\frac{m^3}{N\,m}\right]$
Test A	Steel – steel	0.13	$9.01 \cdot 10^{-11}$
Test B	Steel – resin	0.06	$3.62 \cdot 10^{-7}$
Test C	EP-506 + AO-2	0.05	$2.75 \cdot 10^{-7}$
Test D	EP-506 + AO-3	0.03	$3.17 \cdot 10^{-7}$
Test E	EP-506 + AO-4	0.04	$3.03 \cdot 10^{-8}$

It is easy to highlight the high level of wear resistance shown by the mixture composed by epoxy resin and AO-4 reinforcement and the good value of friction coefficient, halving the measure obtained from the steel-steel contact in Test A.

The reason because epoxy resin + AO-4 compound results the most suitable solution for mechanical applications could be found in the reinforcement grain average dimension.

The AO-4 powder has an average flakes thickness of about 60nm; this characteristic allows, compared to the other solutions, a larger particle lateral size among the epoxy resin and the reinforcement itself.

As one can see from Figure 41, the EP-506 + AO-4 mixtures guarantees a good value of friction coefficient, comparable with the other composites studied, but outlines a specific wear rate one order of magnitude lower compared to the other.

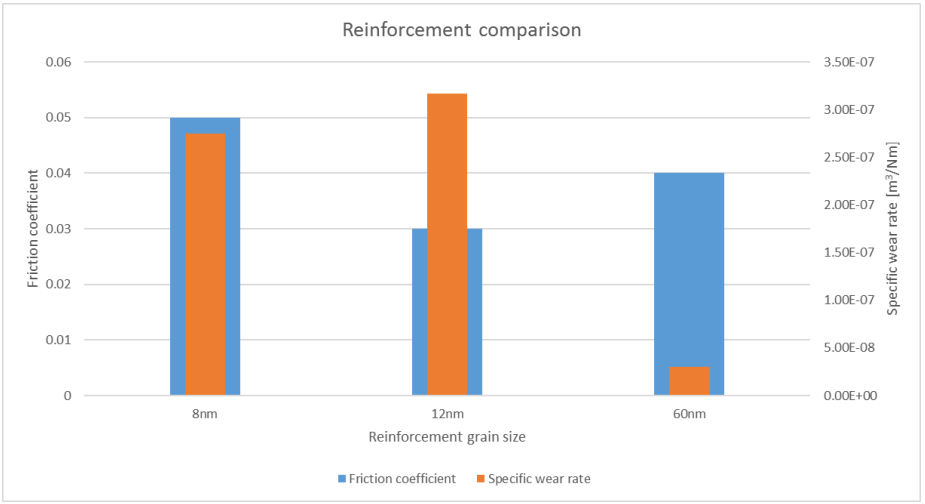

Figure 41 - Reinforcement comparison

The larger area respect to the other powders guarantees a higher cohesion within the mixture and a higher wear resistance. This feature guarantees a long life-time of the surface coating and a low value of the friction coefficient.

By the way, as for nanostructured surface treatments described in Chapter 3, also reinforced epoxies highlighted important issues for an application on the external surface of camshafts. Indeed, even if the specific wear rate and consequently the treatment duration outlined in Test E were remarkable, an implementation of such treatment directly on a cam external surface would define a quickly and completely wear of the treatment itself. This phenomenon is due to the low surface hardness of epoxies and to the extreme working conditions achieved in a cam-follower contact.

5. Molybdenum

Molybdenum is a chemical element with symbol Mo and atomic number 42. The name derives from Latin word *molybdaenum* and it means "like lead" due to its ore were confused with lead ores [122]. Molybdenum does not occur naturally as a free metal but it is found only in different oxidation states in minerals. It forms hard and stables carbides in alloys and for this reason it is usually used in high-strength steel alloys.

Molybdenum is usually extracted as molybdenite, the principal ore easily findable on Earth. Due to its exterior aspect, molybdenite was usually used and confused as it were graphite and lead sulfide. By 1778 Swedish chemist Carl Wilhelm Scheele stated that molybdenite was neither lead sulfide nor graphite [123], [124]. Furthermore, Scheele proposed that molybdenite was the ore of a completely new element, named molybdenum. He tried to isolated molybdenum by its ore, but this process was achieved only in 1781 by Peter Jacop Hjelm using carbon and linseed oil [125].

In 1800 molybdenum has no industrial diffusion due to the difficult in the extraction of the pure metal and to the immature metallurgy techniques [126]–[128]. During the first decades of 1800, early molybdenum steel alloys were manufactured, showing great promise of increased hardness. However, efforts to manufacture the alloys on a large scale were hampered with inconsistent results, highlighting brittleness and recrystallization. In 1913, Frank E. Elmore developed a froth flotation process to recover molybdenite from ores; flotation remains the primary isolation process [129].

A large diffusion of molybdenum was achieved during World Wars, using this element both in armor plating and as a substitute for tungsten in high speed steels. British and German tanks were equipped with molybdenum steel plates instead of manganese steel plates, achieving a whole weight reduction of the tank itself [125], [130].

After the wars, demand of molybdenum plummeted until metallurgical advances allowed extensive development of peacetime applications. Nowadays, molybdenum is usually used as metallurgic element in alloys production and as compounds in particular applications. About 86% of molybdenum produced is used in metallurgy, with the rest used in chemical applications. The estimated global use is structural steel, stainless steel, tool and high-speed steels, cat iron, molybdenum elemental metal and super alloys [131]. One of the most important feature of molybdenum is the capability to withstand extreme temperatures without significantly modify its shape. This characteristic makes it useful in environments with intense heat as military armor, aircraft components, electrical contact and industrial motors [125].

Molybdenum is also used as compound and one of the most used is the molybdenum disulfide (MoS_2). This chemical compound is used as a solid lubricant and anti-wear agent. It forms strong films on metallic surfaces and it is common added to greases, making a thin layer on contact surfaces in case of catastrophic grease failure during mechanical contacts [132].

Molybdenum disulfide is also used in electronics applications thanks to its semiconducting properties [133] and as catalyst in hydrocracking of petroleum [134].

5.1. Molybdenum tribology

As illustrated above, molybdenum in its principal compound state (MoS_2) is usually used in lubricating applications, added to base oil or grease and sometimes as solid lubricant. Indeed, in such applications involving high temperature and pressures and particular environments, organic-based lubricants are precluded and hence a development of solid lubricants was carried out. Graphite and molybdenum disulfide are the most frequently used inorganic solid lubricants. Since the beginning of 21st century lots of studies were carried out with the aim to develop and apply solid lubricants in mechanical components; in Winer literature review on MoS_2 used as solid lubricant [132], an early patent was cited concerning the use of molybdenite in friction reduction domain [135]. In [136] MoS_2 was described as lubricant for vacuum applications, highlighting its use in particular domain. Indeed, molybdenum disulfide is intrinsic solid lubricant in that it does not required adsorbed materials or additives to develop lubricating capabilities.

MoS_2 is usually applied to surfaces by a large number of methods, including rubbing, air spraying and PVD techniques such as sputtering. Application method defines surface finishing and wear life of molybdenum disulfide treatment, highlighting coating thickness and tribologic features. Early research on sputtered MoS_2 [137] reported treatment characteristics in terms of layer thickness and friction coefficient, outlining a better behavior of the coating in a vacuum environment compared to atmospheric domain.

Recent studies concerned other applications of molybdenum disulfide as solid lubricant, focused the attention on particular implementations domain. In [138]–[140], MoS_2 was implemented in different material bases in a nano-structure state in order to obtain a better mixture and performance of the additive itself. Other recent researches outlined MoS_2 tribologic characteristics in such uses as surface coating [141]–[143].

As illustrated in literature, one of the most used Mo compound is the molybdenum disulfide. Tribologic applications and implementations of this compound were defined mainly in order to obtain a reduction of the friction coefficient, using it as a solid lubricant. Thanks to its high surface hardness, molybdenum in its pure form could be used as a wear resistance material, avoiding a friction coefficient reduction. This approach was followed in this part of the dissertation, focused the attention on an application of the molybdenum powder in a different way compared to the typical use. Indeed, pure molybdenum-based coating was obtained and implemented on clutch disks with the aim to increase friction coefficient and to reduce wear.

As described above, molybdenum is characterized by a good wear resistance when it is applied as surface treatment. Following this feature, an experimental campaign on molybdenum coating was scheduled in order to define friction coefficient and specific wear rate trends according to time. Contrary to what described in Chapters 3 and 4, in this case the main aim of the experimental tests was to define the tribologic characteristics of Mo based coating sprayed on a Limited Slip Differential (LSD) internal clutch pack in order to obtain a good value of friction coefficient and an excellent wear resistance. Indeed, the behavior of a clutch pack during its working condition is influenced by the friction coefficient value and the wear progression achieved during its lifetime.

5.2. Experimental analysis

The LSD clutch pack object of this analysis is composed by 12 steel-based disks, 6 of them with molybdenum coating and the other uncoated. Experimental campaign was carried out replicating this contact material configuration in order to have the same conditions occurred in the clutch pack.

5.2.1.**Materials**

The first step of experimental analysis concerned the evaluation of metallurgical properties of the materials used in the LSD clutch pack. Metallurgical samples from spare parts components and test samples have been obtained by abrasive wet cutting, mounting in transparent epoxy resin, grinding with SiC paper and diamond polishing. After chemical etching (Nital 2%) the microstructure of coated and uncoated samples was investigated by light and electron microscopy techniques. Surface and bulk micro-hardness measurements have been made in order to determine the mechanical properties of the samples.

Two commercial coated and uncoated disks installed on the clutch pack were used as reference samples. The structural analysis showed the typical microstructure of quenched and tempered steel. The structure, as shown Figure 42, is very fine and not resolvable by optical microscopy. The composition as determined by EDS (Energy Dispersive X-ray Analysis) is reported in Table 10 and corresponds to low carbon steel alloy. The coating shows the typical lamellar structure of Air Plasma Sprayed coating with a high content of pores and partially or unmelted particles. The measured average thickness is about 50µm, which is a typical value for this kind of application.

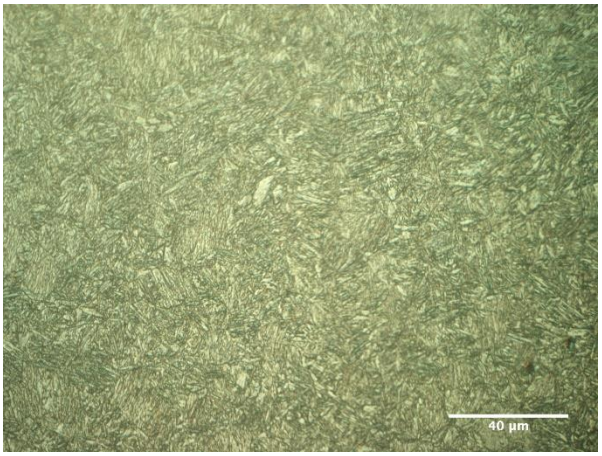

Figure 42 - Base material structure (1000x)

Table 10 - Clutch disk composition

Si weight (%)	Mn weight (%)	Fe weight (%)	Si weight (%)
0.46	0.78	96.66	0.46

The micro-hardness value of the molybdenum coating resulted as high as 1600 +/- 200HK_{25} while the substrate measured about 390 +/- 40HK_{25}. The microhardness of uncoated disk resulted a bit higher with an average value of 530 +/- 40HK_{25}.

In order to have a statistical validation of the results the experimental tests were conducted on 15 couples of samples.

The five rings and the five blocks used in the test were machined from a commercial AISI 1042 steel alloy round bar following the dimensional characteristics defined in [69]. To have a better evaluation of wear process occurred during the contact, the machining process on the blocks was carried out to have a non-conformal contact between the block and the ring during the friction test.

Before coating the rings, all the sample were heat-treated in order to present the same mechanical and microstructural features as the reference samples just described. All the samples were heated at 900°C for 30 minutes, quenched in calm water and tempered for 2 hours at 370°C. The process was contextually made also on portions of the clutch disk in order to check the right procedure of the treatment by reproducing the original hardness values, as illustrated in [144].

The microhardness values, comparable with the average hardness of the untreated friction disks, are listed in the Table 11 and in Table 12; these were obtained as the result of 5 indentation tests made on the polished lateral surface of the samples.

Table 11 - Block hardness values

Specimens ID	**Knoop hardness [HK_{50}]**	**Standard deviation**
1	389	
2	489	**Indicate average**
3	434	**35.28**
4	464	
5	415	

Table 12 - Ring hardness values

Specimens ID	**Knoop hardness [HK_{50}]**	**Standard deviation**
1	486	
2	480	**Indicate average**
3	457	**44.35**
4	533	
5	581	

The molybdenum treatment application was made by Air Plasma Spray technique (APS) after the removal of the oxide scale achieved after the thermal treatment directly on the specimens' surface, but without a bond-coat operation.

After the wear and friction test, three pairs of samples have been prepared for metallographic examination as previously described in order to compare and check also the microstructure.

Representative micrographs are reported in Figure 43 and in Figure 44.

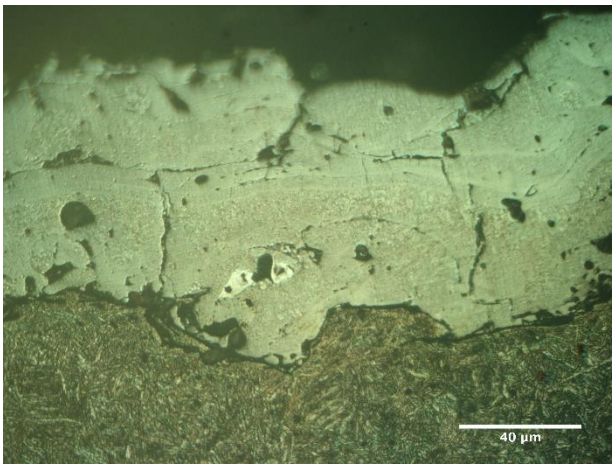

Figure 43 - Molybdenum treatment and base material substrate: clutch disk

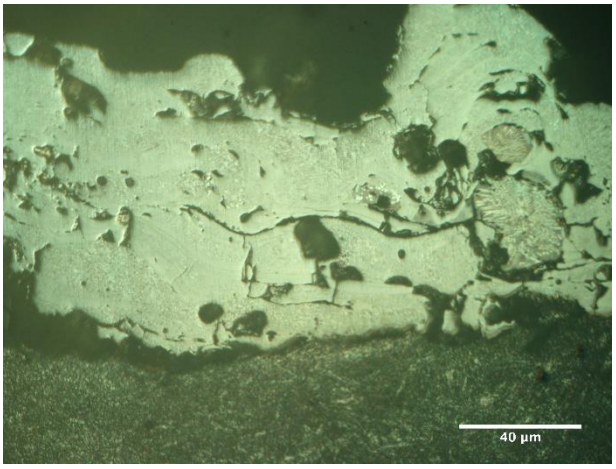

Figure 44 - Molybdenum treatment and base material substrate: test ring

As one can see, the base material in the differential disk and in the ring used in experimental campaign are comparable.

5.2.2. **Testing methods**

Experimental tests were performed using the Block-on-Ring test bench described in Chapter 2 and following ASTM G77 standard [63]. As indicated before, the aim of the experimental campaign was to define tribological characteristics of a molybdenum-steel contact configuration in order to have a better knowledge of LSD clutch pack behavior during its engagement. To achieve this goal, working conditions usually occurred in a Limited Slip Differential were replicated in terms of test bench input parameters.

As for nanomaterials experimental tests, also for LSD clutch pack the input parameters were defined following a comparative between the working conditions and the dimension of

the clutch pack and the technical limits imposed on the test bench in terms of samples dimensions and input parameters.

According to this, some assumptions were made. Table 13 illustrates the main dimensions of clutch disks and the normal load acting during clutch engagement.

Table 13 - Clutch disk dimensions

$D_{e,disk}$, Disk External Diameter [mm]	**$D_{i,disk}$, Disk Internal Diameter [mm]**	**W_{disk}, Normal load on disks [N]**
75	47	3700

Following these values, the pressure generated on the clutch pack surface could be defined thanks to the equation below:

$$P_{clutch} = \frac{W_{disk}}{\frac{\pi}{4}\left(D_{e,disk}^2 - D_{i,disk}^2\right)} \tag{9}$$

and the values obtained is P_{clutch}=1.38MPa. Considering a comparative between pressure acting on clutch pack and pressure generated in the Block-on-Ring contact and assuming the contact area occurred in the experimental configuration with a value of A_{br}=96mm^2, the normal load to be set on the test bench was defined thanks to the following equation:

$$W = P_{clutch} \cdot A_{br} \tag{10}$$

Substituting the values in Equation 10, the value of normal load is W=132N.

In a LSD, disks have an average reciprocating rotational speed of about $R_{S,DISK}$=2rad/s. From Table 13 it is possible to define the external radius of the disk, assuming a value of r_{disk}=37.5mm; consequently, it is easy to define disk rotational speed expressed in [m/s], obtaining a value of $R_{S,DISK}$=0.075m/s. In order to determine the rotating speed to be fixed on the test bench, it was necessary to correlate the clutch disks rotating speed and its external radius with the external radius of the ring. The following equation helped us in the definition process:

$$r_{disk} : R_{S,DISK} = r_{RING} : R_{S,RING} \tag{11}$$

where r_{ring}=25mm. The value obtained after a substitution is $R_{S,RING}$=0.05m/s.

As illustrated in [145], during the working conditions of a LSD differential oil temperature can achieve values of about T_{oil}=90÷100°C.

Table 14 makes a recap of the input parameters that should be set on the test bench.

Table 14 - Input parameters

Rotating speed [m/s]	**Normal load [N]**	**Oil temperature [°C]**
0.05	132	90÷100

Paragraph 2.2 illustrates test bench technical characteristics; due to technical limits it was not possible to set ring rotating speed resumed in Table 14. According to this, rotating speed was fixed at $R_{S,RING}$=0.39m/s, minimum value achievable by the test bench. On the other hand, normal load and lubricating oil temperature were set following measures defined above.

All the test campaign was carried out in a lubricated domain using a synthetic oil. Differential oil characteristics are shown in Table 15.

Table 15 - Mobilube SHC technical characteristics

SAE Grade	75W-90
Viscosity, ASTM D445	
cSt at 40°C	120
cSt at 100°C	15.9
Viscosity index, ASTM D2270	140
Pour Point, °C, ASTM D97	-48
Flash Point, °C, ASTM D92	205
Density at 15°C kg/l, ASTM D4052	0.859

As for experimental tests described in Chapters 3 and 4, the acquisition of tangential load and wear value were guaranteed thanks to a digital Datalogger connected to two linear transducers and to a computer. Furthermore, oil temperature was maintained at a constant value using two thermocouples and a digital thermostat.

In order to achieve the main aim of this experimental campaign, it was necessary to divide the 15 pairs of samples in 3 different groups of test, each of them characterized by different data acquisition period. The first group of samples, called X-Group, was characterized by a data acquisition period of 1 hour. In this case, all the samples performed a 1-hour test and tribologic characteristics were acquired during all the test duration, as resumed in Figure 45.

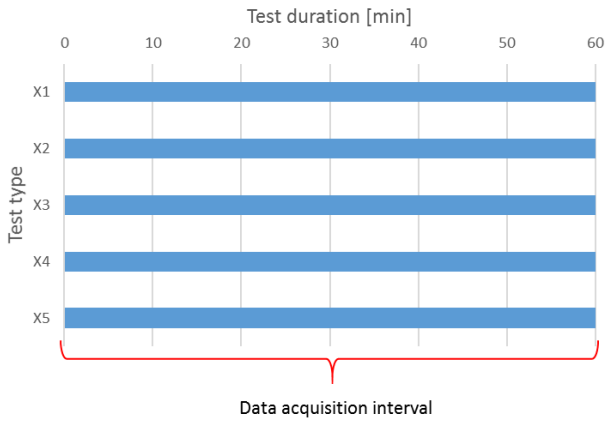

Figure 45 - Data acquisition interval - X-Group

The second and the third groups of samples, called respectively A-Group and F-Group, concerned selective tests performed with the objective of acquired tribologic data at the end of

15-minutes test duration. Both A-Group and F-Group were scheduled in order to perform two different steps of analysis for each pair of samples.

As illustrated in Figures 46 and 47, samples of the A-Group performed a first test phase with a duration of 15 minutes and a data acquisition interval with the same length. At the end of this first step, samples were weighted, cleaned and installed again on the test bench for the second test phase. In this case, total duration of each test was fixed to 30 minutes, while data acquisition period was from minute 30 till minute 45. Data were acquired during last 15 minutes permitting block-ring contact to perform a running-in process, avoiding data acquisition issues.

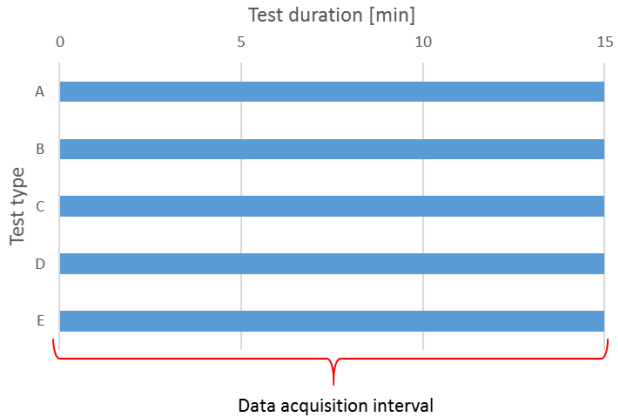

Figure 46 - Data acquisition interval - A-Group, first phase

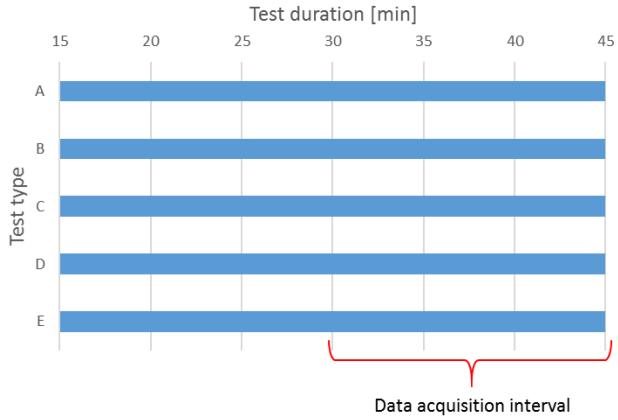

Figure 47 - Data acquisition interval - A-Group, second phase

The F-Group was scheduled following the approach described above, with the difference in data acquisition intervals. Figures 48 and 49 illustrate the first and the second step performed on F-Group samples; in the initial phase data were acquired from minute 15

till minute 30, while in the second phase tribologic values were defined from minute 45 till minute 60.

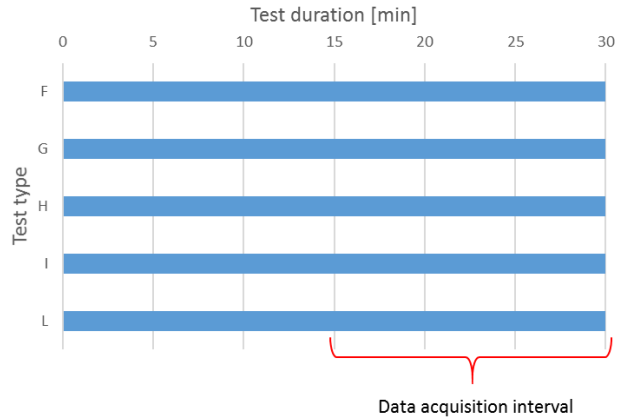

Figure 48 - Data acquisition interval - F-Group, first phase

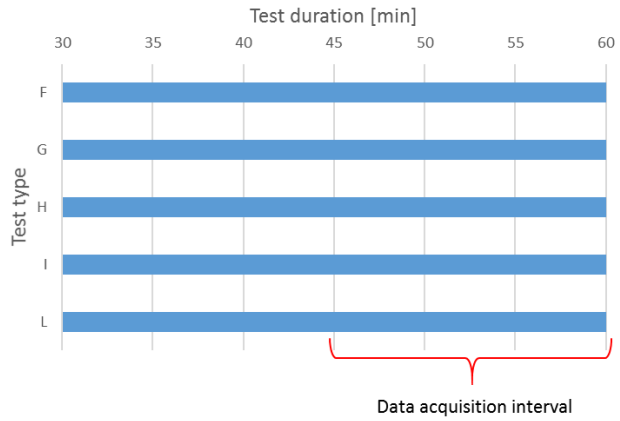

Figure 49 - Data acquisition interval - F-Group, second phase

Before starting each test phase, the specimens were cleaned with acetone, using an ultrasonic apparatus to remove dust and any other particles, which would otherwise modify the tribologic characteristics of the materials.

After the cleaning process, the specimens were weighted using a scale with a resolution of $1 \cdot 10^{-7}$kg; the high resolution of the instrument permitted to analyze accurately the small weight losses recorded in the tests.

At the end of each test phase, the specimens were cleaned again with acetone, in order to remove all the oily residue attached to the specimens' surfaces.

5.3. Results and discussion

5.3.1. X-Group tests

The first test campaign carried out concerned the evaluation of tribological characteristics of X-Group samples. As indicated above, these tests were conducted with the aim to evaluate friction coefficient and specific wear rate at the end of 1-hour test.

Following the procedure illustrated in the previous paragraph and the input parameters defined above, tests were performed using all the 5 pairs of samples. In order to give a better comprehension of the results obtained, only the most significant trends for friction coefficient and for wear were illustrated. Furthermore, a recap table was defined in order to evaluate all the values obtained from the test campaign.

Figure 50 shows the friction coefficient trend obtained from one of the tests conducted on the X-Group of samples.

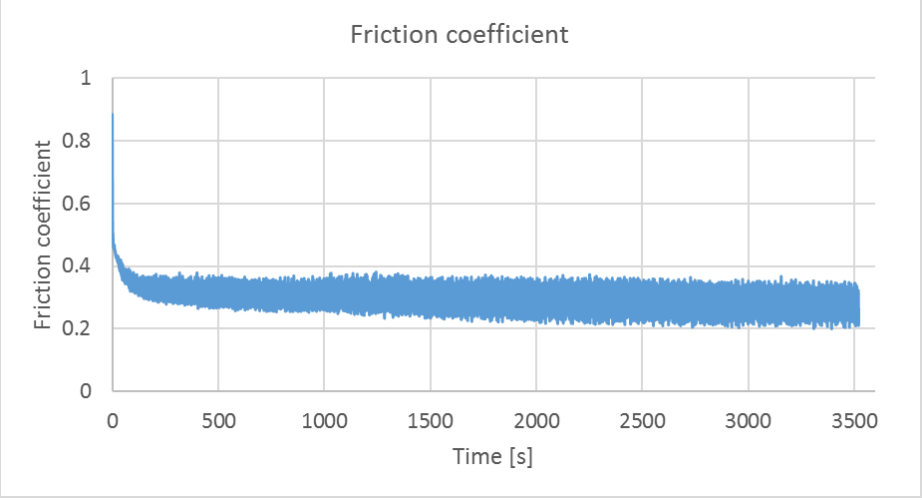

Figure 50 - Friction coefficient trend - X-Group

Indeed, the first phase illustrates a sudden increment of the friction coefficient value due to the initial running-in phase occurred between the block and the ring.

According to time, the value shows a decrease and a final constant value till the end of the test. The average value defined at the end of this test was about μ=0.23. As indicated before, test duration was fixed in 1 hour. This time was confirmed by wear trend and especially by the wear occurred on the block contact area.

Wear value trend is shown in Figure 51. As one can see, also in this case the wear value highlights a typical trend; indeed, the initial phase is characterized by an increase of the value, followed by a constant increase of the trend. The first phase concerned the running-in process occurred between the samples, characterized by a high value of wear. On the other hand, the following phase reflected a constant increase of the wear value till the end of the test.

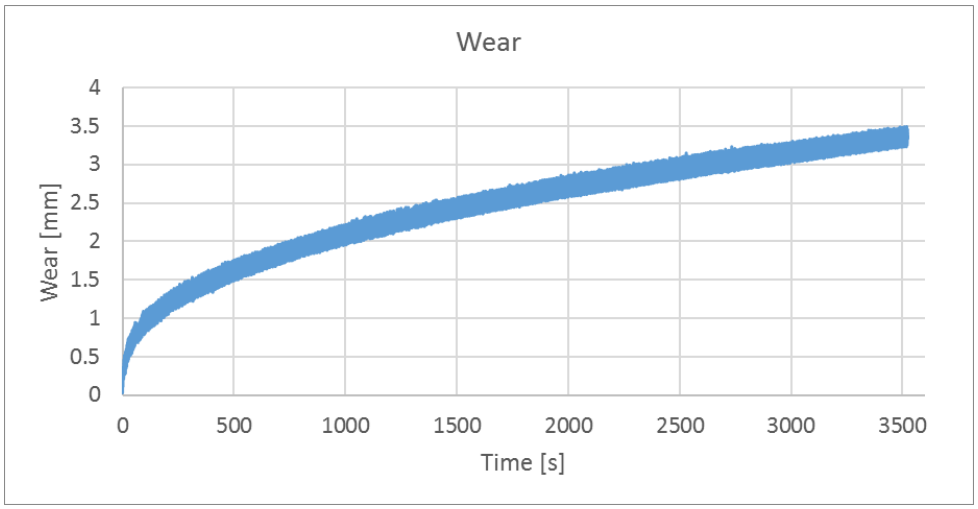

Figure 51 - Wear value trend - X-Group

An evaluation of wear process occurred on the samples can be highlighted from Figures 52, 53 and 54. As one can see, the block shows a high value of wear generated on the contact surface, highlighting a plastic deformation of the material, indicated with the red arrow. On the contrary, the external surface of the disk – the coated one – shows a very little amount of wear mainly due to the higher surface hardness of molybdenum compared to the hardness of the steel used for the block.

Figure 52 - Worn block - isometric view

Figure 53 - Worn block - frontal view

Figure 54 - Worn ring - isometric view

Due to the plastic deformation occurred on the block contact surface, the evaluation of the specific wear rate was conducted following geometrical assumptions instead of defining a weight difference before and after each test. This choice allowed the definition of the real worn volume, considering also possible material transfer from the block to the ring. For this reason, a definition of worn volume generated on the block contact surface was made, following the equation below and Figure 55.

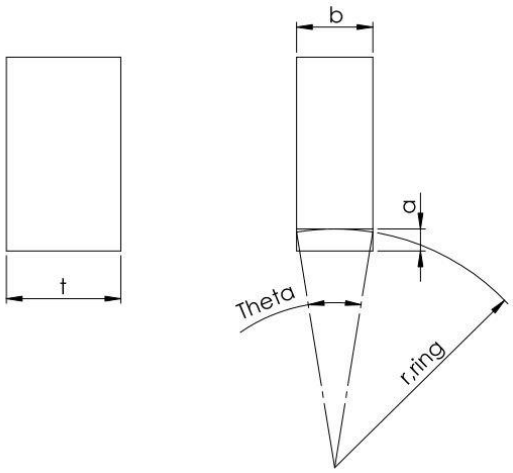

Figure 55 - Ring characteristic dimensions

$$Theta = 2\sin^{-1}\frac{b}{D_{RING}} \tag{12}$$

$$V_{BLOCK} = r_{ring} \cdot Theta \cdot a \cdot t \tag{13}$$

where *Theta* is the contact surface angle defined at the end of the test, *b* is the block thickness, D_{RING} is the ring external diameter, V_{BLOCK} is the worn volume occurred on the block, r_{ring} is the ring external diameter, *a* is the thickness of the worn track and *t* is the block width.

According to equations above, to evaluate specific wear rate on the blocks and on the rings a simple process was followed. The weight difference of the ring before and after each test was evaluated; thank to the molybdenum density it was possible to calculate the volume worn on the block. On the other hand, thanks to a microscope and following Equations 12 and 13, it was possible to evaluate the geometrical difference of the block contact surface and, consequently, the worn volume amount.

Thanks to Equation 2, specific wear rate was defined for each pairs of samples. A recap of average values of friction coefficient and specific wear rates is shown in Table 16.

Table 16 - Tribological characteristics - X-Group

Test ID	**Friction coefficient, μ**	**Standard deviation (μ)**	**Specific wear rate, K $\left[\frac{m^3}{N\,m}\right]$**	**Standard deviation (K)**
X_1	0.23		$1.52\cdot10^{-12}$	
X_2	0.30		$9.52\cdot10^{-13}$	
X_3	0.24	**0.036**	$1.45\cdot10^{-12}$	**$3.71\cdot10^{-13}$**
X_4	0.25		$9.05\cdot10^{-13}$	
X_5	0.20		1.7510^{-12}	

5.3.2. **A-Group tests**

The second group of samples composed the A-Group. As indicated in the previous paragraph this array of specimens performed selective tests in order to evaluate tribologic characteristics during 15-minutes data acquisition interval. These tests were divided in two separated steps with the difference in the starting and finishing point of acquisition time, as described before.

Figure 56 illustrates friction coefficient trend obtained from one of the most characteristic test performed during the first step of analysis. As it possible to see, friction coefficient defines the typical trend that could be found in literature, generating an initial rapid increase due to the first contact between samples. The consequent trend has a decrease till a constant value of about μ=0.32.

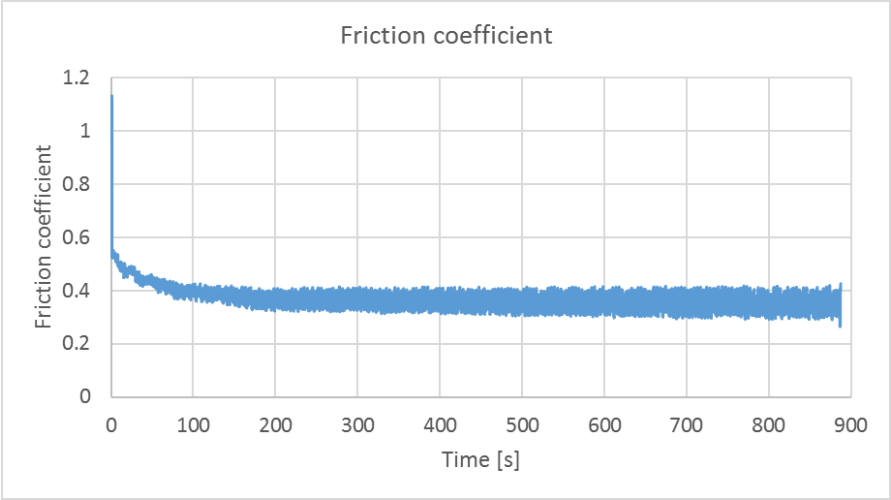

Figure 56 - Friction coefficient trend - A-Group, first phase

Also for wear value trend it is possible to see a typical evolution. Indeed, Figure 57 shows the wear progression according to time obtained from the same test. As one can see, the initial increase due to the first contact between samples is followed by a continuous and regular increase of the wear value till the end of the test.

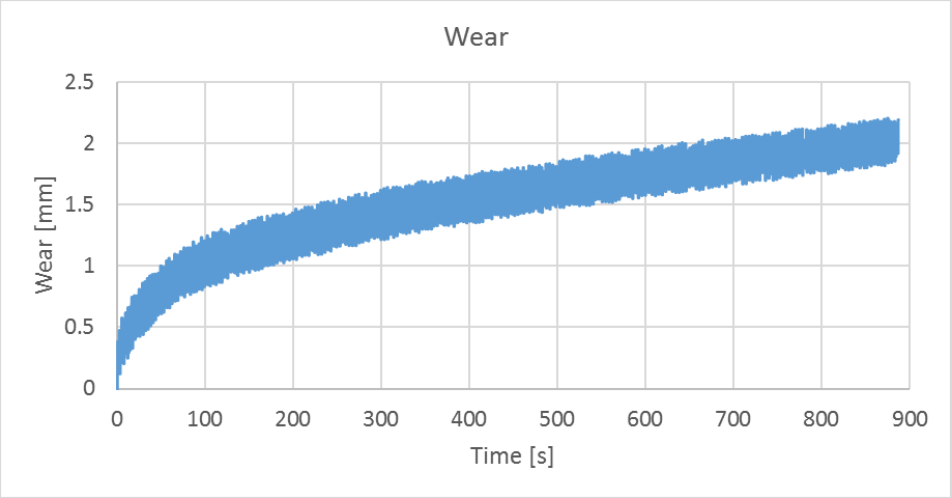

Figure 57 - Wear value trend - A-Group, first phase

As for X-Group tests, specific wear rates were calculated following a geometrical process for the blocks and a weight difference for the ring. A recap of the average values is illustrated in Table 17.

Table 17 - Tribological characteristics - A-Group, first phase

Test ID	**Friction coefficient, μ**	**Standard deviation (μ)**	**Specific wear rate, K** $\left[\frac{m^3}{N\,m}\right]$	**Standard deviation (K)**
A_1	0.30		$2.73 \cdot 10^{-12}$	
B_1	0.35		$1.84 \cdot 10^{-12}$	
C_1	0.33	**0.023**	$2.01 \cdot 10^{-12}$	$\mathbf{3.38 \cdot 10^{-13}}$
D_1	0.34		$2.12 \cdot 10^{-12}$	
E_1	0.30		$2.08 \cdot 10^{-12}$	

The second step of the A-Group of samples were performed following the assumptions described in Paragraph 5.2.2. Figure 58 shows the friction coefficient trend of one of the test performed. As one can see this trend highlights an important difference between the one obtained in the first step of analysis. Indeed, even if there is the initial increase of the friction coefficient value, the following evolution has an increase trend instead of a decline as illustrated before. This unusual trend was reported for all the contact pair and could be due to an irregular installation of the samples on the test bench. Indeed, a misalignment between the samples can generate an imperfect contact surface and an inhomogeneity of the wear process. Furthermore, due to this reason and to the possibility of plastic deformation occurring on block surface, some steel slivers left the deformed zone and took part in the contact, defining a three-element wear process with a friction coefficient increase.

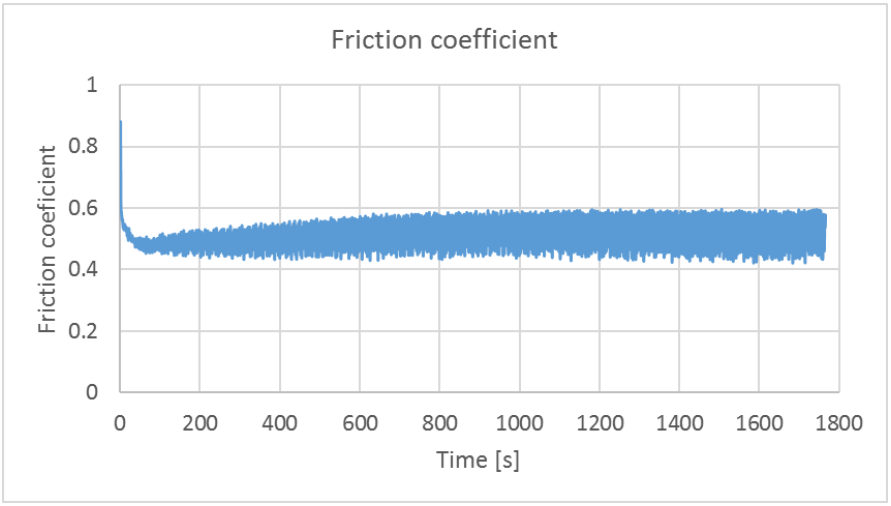

Figure 58 - Friction coefficient trend - A-Group, second phase

Wear value obtained from these test shows the typical trend highlighted before. Figure 59 illustrates the trend obtained from the same test described above. As one can see, wear has the typical initial increase due to the first contact between samples and the consequent constant evolution till the end of the test. Even if friction coefficient trend showed an unusual evolution, this issue could not be highlighted in the wear trend due to the wear value acquisition method. Indeed, the Block-on-Ring test bench acquired wear increment using a linear transducer and the value obtained is a total wear value.

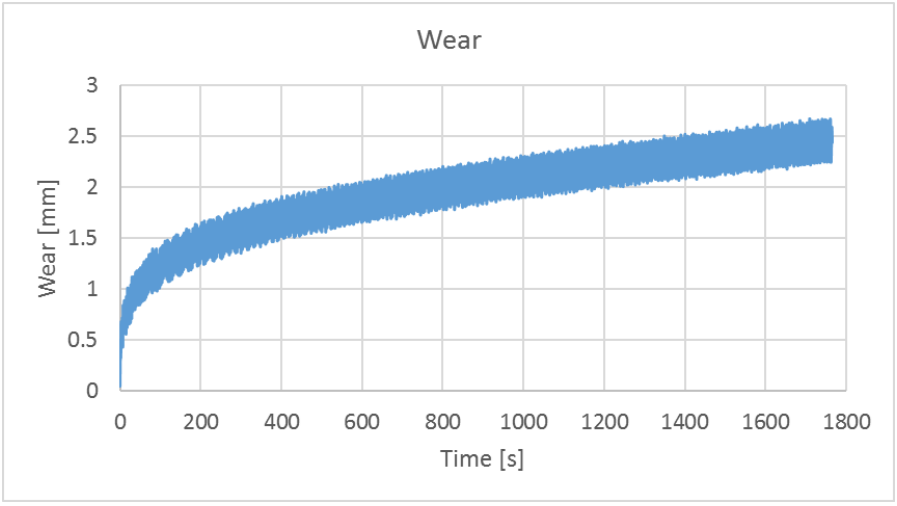

Figure 59 - Wear value trend - A-Group, second phase

As before, a resume of tribologic characteristics obtained from the second step of the analysis is illustrated in Table 18.

Table 18 - Tribological characteristics - A-Group, second phase

Test ID	Friction coefficient, μ	Standard deviation (μ)	Specific wear rate, K $\left[\frac{m^3}{N\,m}\right]$	Standard deviation (K)
A_2	0.55		$1.83 \cdot 10^{-12}$	
B_2	0.48		$1.02 \cdot 10^{-12}$	
C_2	0.45	**0.040**	$8.25 \cdot 10^{-13}$	$\mathbf{3.95 \cdot 10^{-13}}$
D_2	0.52		$1.44 \cdot 10^{-12}$	
E_2	0.53		$1.12 \cdot 10^{-12}$	

5.3.3. F-Group tests

As for the second group of samples, also the F-Group of specimens was implemented in an experimental analysis divided in two different phases, each of them characterized by a 15-minutes data acquisition interval.

In this case, the first step of analysis was conducted from the minute zero till minute 30, recording data during the second half of the test. Figure 60 shows the friction coefficient trend obtained from this analysis. As one can see, also in this case friction coefficient value defined an initial increment due to the first running-in phase occurred between samples. After this starting behavior, friction coefficient had a decrease, achieving a constant value at the end of the test. As one can expect, the value achieved at the end of the test is lower than the values obtained from A-Group tests, defining an average value of μ=0.30.

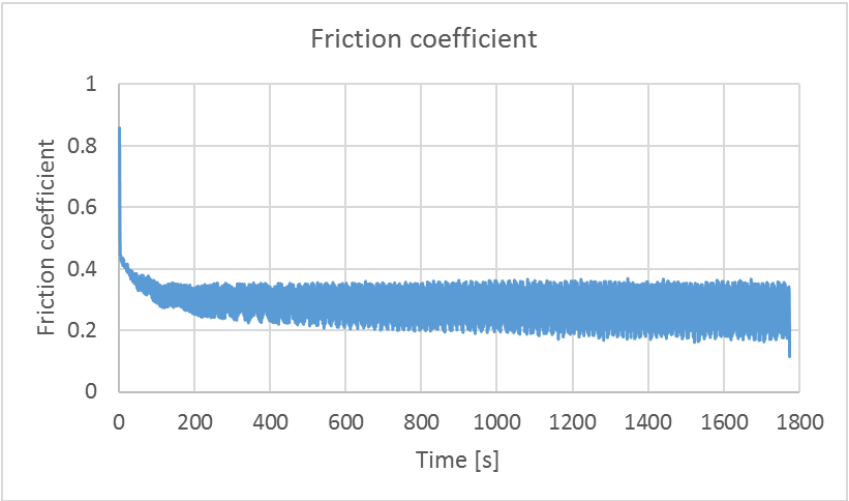

Figure 60 - Friction coefficient trend - F-Group, first phase

The first phase of F-Group tests defined a wear value evolution as described in Figure 61. As one can see, the trend obtained from this analysis corresponds to the typical evolution of the wear value during a contact between two materials with a very difference in surface hardness, as in this case. The initial phase concerned a running-in contact between specimens, characterizing a quick increase of the wear value. After this behavior, a constant increase described the wear trend till the end of the test.

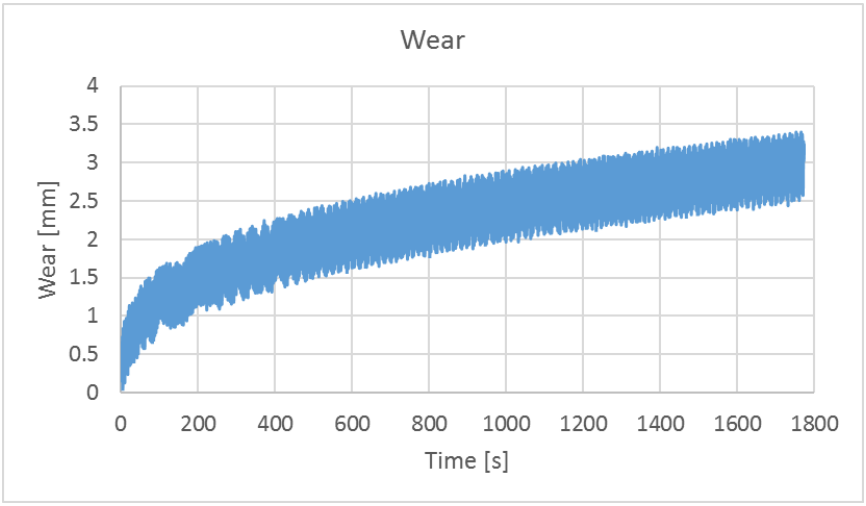

Figure 61 - Wear value trend - F-Group, first phase

As for the A-Group, also in this case a recap of the friction coefficient values and the specific wear rates obtained from the first phase of the test analysis is reported in Table 19.

Table 19 - Tribological characteristics - F-Group, first phase

Test ID	**Friction coefficient, μ**	**Standard deviation (μ)**	**Specific wear rate, K** $\left[\frac{m^3}{N\,m}\right]$	**Standard deviation (K)**
F_1	0.27		$1.04 \cdot 10^{-12}$	
G_1	0.31		$1.31 \cdot 10^{-12}$	
H_1	0.33	**0.025**	$2.09 \cdot 10^{-12}$	**$4.13 \cdot 10^{-13}$**
I_1	0.30		$1.44 \cdot 10^{-12}$	
L_1	0.33		$1.14 \cdot 10^{-12}$	

The second step of F-Group was conducted defining a test duration of 30 minute and acquiring data between minute 45 till minute 60. Friction coefficient trend obtained from this test is shown in Figure 62. As one can see, the trend defined an initial increase due to the first contact between specimens and a consequent constant decrease till achieving an average value of μ=0.21 at the end of the test.

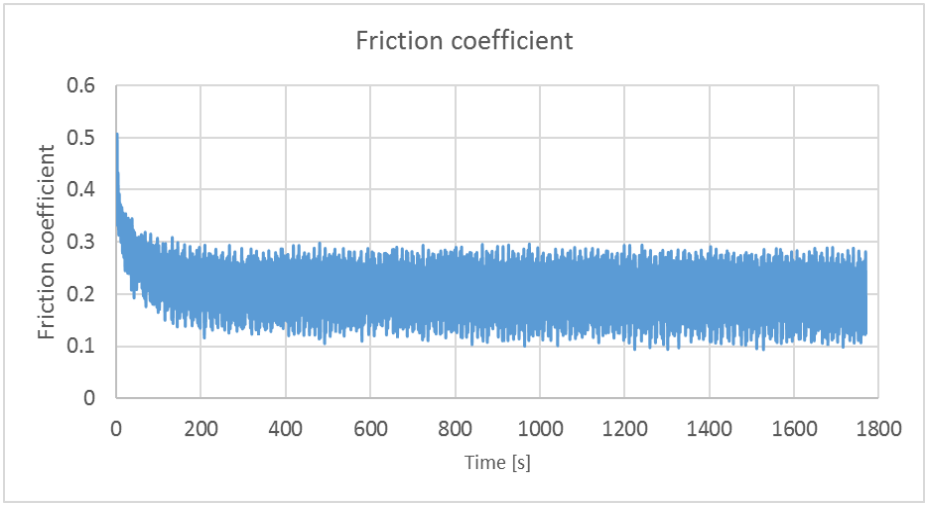

Figure 62 - Friction coefficient trend - F-Group, second phase

For what concerns wear value trend, Figure 63 illustrates the evolution obtained from the analysis performed. As in the other cases, wear progression described an initial increase due to the first contact phase occurred between samples. Consequently, the wear value had a constant growth till the end of the test, defining the total amount of worn material occurred during this analysis.

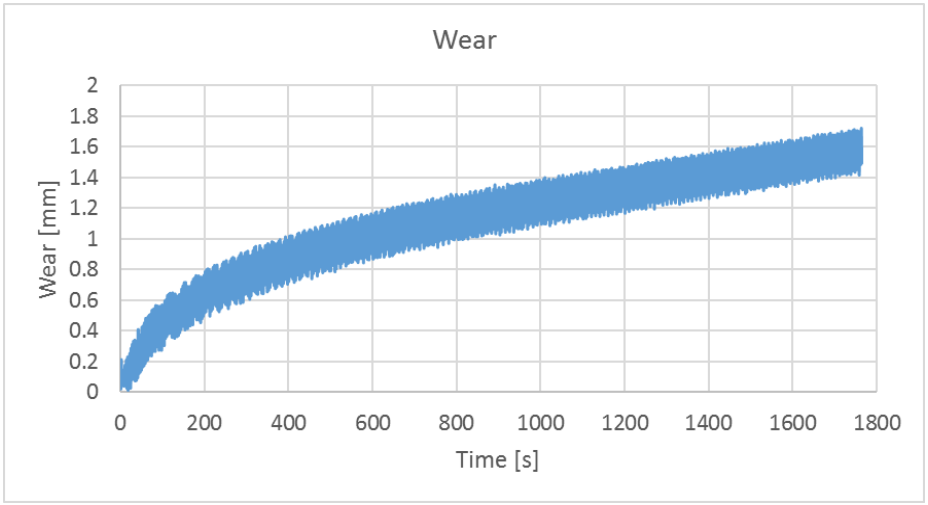

Figure 63 - Wear value trend - F-Group, second phase

A recap of friction coefficient values and specific wear rates obtained from this experimental campaign is illustrated in Table 20.

Table 20 - Tribological characteristics - F-Group, second phase

Test ID	Friction coefficient, μ	Standard deviation (μ)	Specific wear rate, K $\left[\frac{m^3}{N\,m}\right]$	Standard deviation (K)
F_2	0.20		$1.03 \cdot 10^{-12}$	
G_2	0.21		$1.33 \cdot 10^{-12}$	
H_2	0.25	**0.027**	$1.13 \cdot 10^{-12}$	**$1.14 \cdot 10^{-13}$**
I_2	0.18		$1.15 \cdot 10^{-12}$	
L_2	0.23		$1.08 \cdot 10^{-12}$	

5.4. Outcomes

The experimental analysis carried out and described in the previous paragraphs had the main aim to define tribological characteristics of a contact pair composed by a molybdenum surface and a steel surface. The experimental tests were performed scheduling the procedure in accurate time-steps in order to obtain the average value of friction coefficient and wear at the end of each step and, hence, according to time.

According to this, graphs described in Paragraph 5.3 are not so useful to obtain a good evaluation of the tribologic properties evolution according to time. To do this, the average values of friction coefficient and wear obtained at the end of each test phase were reported in two different graphs related to the test time duration.

Figure 64 shows friction coefficient trend. Blue line describes friction coefficient trend obtained by connecting average values defined at the end of each acquisition step. In the same graph the red line identifies the hypothesized friction coefficient trend. This evolution, characterized by a logarithmic law, was hypothesized assuming an average of trends obtained from experimental tests and attempting the mathematical law that best fits results obtained.

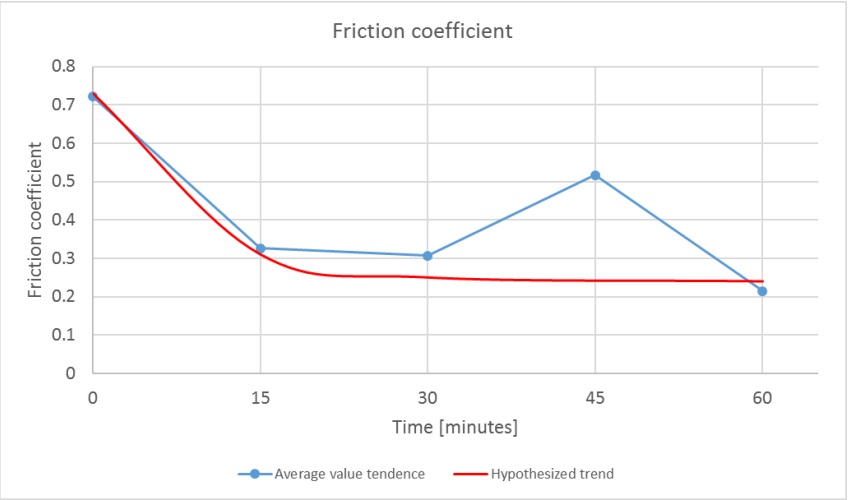

Figure 64 - Friction coefficient average trend

As it is easy to see, the evolution obtained connecting average values of experimental tests could be compared with the hypothesized trend. As explained before, friction coefficient value presented an unusual behavior during the second phase of A-Group tests. Indeed, a considerable variation between friction coefficient value and hypothesized trend could be easily seen, reporting an error among the values. The issues related to this unusual behavior of friction coefficient could be due to an imperfect installation of samples on the test bench and a consequent misleading wear process occurred between samples, as described before.

For what concerns wear trend evolution, Table 21 illustrates the average values obtained at the end of each test phase.

Table 21 - Average wear values – Experimental analysis

Step [minute]	Average wear value [mm]
15	**1.81**
30	**2.27**
45	**2.35**
60	**2.59**

These results were described according to time and reported on a graph, as illustrated in Figure 65 where the experimental values trend and the hypothesized one are defined. The process followed to obtain the lines illustrated in the graph was the same as for friction coefficient, using in this case an exponential law to fit as better as possible the evolution of experimental wear value. The average values obtained at the end of each acquisition intervals were defined as increments, starting from values obtained in the first step of A-Group tests till the last measure made on the pair of samples used in the F-Group tests.

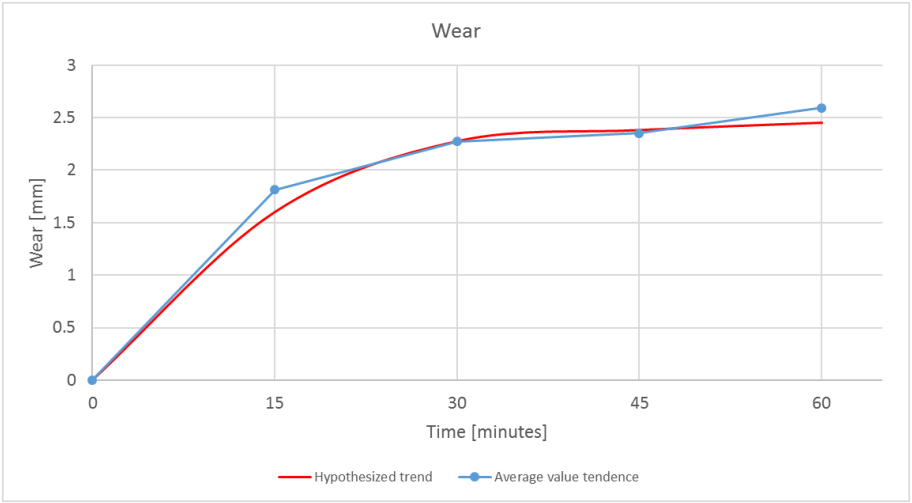

Figure 65 - Wear value average trend

Experimental wear trend shows an evolution comparable with the theoretical one, highlighting few differences between the trends illustrated in the graph. The evaluation of wear trend and the verification of its accuracy against a theoretical trend was a good instrument to

define and calibrate a numerical model of the wear process occurred between block and ring. Indeed, in next Chapters wear evolution and specific wear rates defined during the experimental campaign described in this Chapter will be used with the aim to define a generalized wear model useful to predict wear occurring in contact pairs.

Furthermore, the evaluation of tribological characteristics of molybdenum-steel contact configuration allowed to achieve a better knowledge of this contact pair, defining an initial step for a better design of LSD internal clutch pack.

6. Block-on-Ring numerical analysis

6.1. Finite element method

The finite element method (FEM) is a numerical technique developed with the aim to find approximate solutions to boundary value problems for partial differential equations. This method, called also finite element analysis (FEA), subdivides a large problem into smaller and simpler parts, usually referred as finite elements. Each finite element is governed by simple equations; these equations are assembled into a larger system of correlations that models the whole system.

6.1.1. **History**

As the most important scientific developments, it is not easy to give an exact date of birth of finite element method.

Since early 1900s some studies were conducted trying to approximate solution of problems in the mechanics of deformable solid, as in Ritz's research [146]. This study concerns an approximation of energy functional by the known functions with unknown coefficients. One of the restrictions of this method is that functions used in the model should satisfy to the boundary conditions of the problem.

Later, in 1943, Courant developed an improvement of Ritz's method, introducing special linear functions defined over triangular regions [147]. Ritz's method together with Courant improvement were considered as the starting point for the study carried out by Clough many years later. Clough introduced for the first time in 1960 the term "finite element" in his paper "The finite element method in plane stress analysis" [148]. The wide spreading of FEM in 1960s was due to the possibility to use computers in such computational analyses required by FEM. Important contributions for FEM development were brought by the papers of Turner [149], Martin [149] and Hrennikov [150]. Furthermore, in 1967, Zienkiewicz and Cheung [151] wrote the first textbook on finite element, called "The finite element method in structural and continuum mechanics". This book presents the broad interpretation of the method and its applicability to any general field problems.

In 1970s further impetus was provided by available open source software developed to enhance finite element solutions. In 1973, Strang and Fix [152] defined a rigorous mathematical basis to finite element method. Their approach was generalized for numerical modeling of physical system in a wide range of disciplines, including electromagnetism, heat transfer and fluid dynamics [153].

Since 1980s, development and improvement of finite element software were the main activities performed in order to obtain a better evaluation of the model solution and to reduce error between numerical and analytical analysis.

6.1.2. **Process**

The process of subdivision of the entire system in finite elements outlines lots of advantages [154], defining an accurate representation of complex geometries, the inclusion of dissimilar materials presented in the system and the possibility to represent local effects occurred on the system.

The main characteristic of the finite element method is the discretization achieved on the whole system by creating a grid (called also mesh) made up of finite element in coded form (triangles and quadrangles in 2D domains, hexahedrons and tetrahedrons for 3D domains). On each element characterized by this basic form, the solution of the problem is assumed to be expressed by the linear combination of basis functions and shape functions. Note that sometimes the function is approximated, and not necessarily the exact values of the function will be those calculated in the points, but the values that provide the least error on the entire solution. In its original form, and still more widespread, the finite element method is used to solve problems resting on linear constitutive laws. Typical examples are the stress-deformations problems in the elastic range and the heat diffusion inside a system. More sophisticated solutions allow to explore the behavior of the materials even in highly non-linear range, assuming plastic behavior or visco-plastic solutions.

The finite element method is part of the Galërkin method class [155] based on a weak formulation of a differential problem. The Galërkin type methods are based on the idea of approximating the problem solution in a weak form written by a linear combination of elementary functions (the shape functions). Coefficients of this linear combination (also called "degrees of freedom") become the unknowns of the algebraic problem obtained by discretization.

The process followed to achieve the representation of the whole system in simpler parts involve two main steps, each of them characterized by an implementation of an error in the final solution:

- Modeling: in this phase the physical system is transformed in a mathematical model, focusing the attention on few variables interesting for the model solution and “filtering” the others. In case of a complex physical system, this can be divided in simpler subsystem. Each subsystem is divided in finite elements to whom a mathematical model is applied. The choice of a type of element in a software program is very important and it has to be made with high attention because it is equivalent to an implicit choice of the mathematical model that characterized the element. This choice characterizes the model solution and the computational time spent to achieve the solution.
- Discretization: in a numerical simulation it is necessary to pass from an infinite number of degrees of freedom to a finite number of degrees of freedom. The discretization process has the main aim to define a discrete model characterized by a finite number of degrees of freedom. During this phase an error is implemented in the model; the better is the discretization value (high number of elements per unit area or volume), the smaller will be the error compared to mathematical solution.

Each finite element defined in a numerical model is characterized by dimensions (1D, 2D or 3D), nodes, degrees of freedom, nodal forces, constitutive properties and solution of equations system. All these features characterize the model and a good choice of these characteristics guarantees a high level of accuracy of the solution and a low value of the error generated.

6.1.3. **Applications**

Finite element method is usually used in a wide variety of mechanical engineering disciplines, such as aeronautical, biomechanical and automotive industries. This method is integrated during the design process, helping engineers with the development of their products.

FEM found a wide implementation in structural simulation thanks to the possibility to obtain stiffness and strength visualizations, providing also a help in minimizing the weight and the final cost of the components.

Standard of engineering designs and methodologies connected to design processes were significantly enhanced thanks to the widespread of FE method in many industrial applications [156]. FEM development and diffusion generated a decrease of the time spent from products concept to the production line [156], highlighting some benefits as an accuracy increase, the virtual prototyping approach, fewer hardware prototypes and a faster and less expensive design cycle with a consequent increase of productivity and revenue [156].

According to this, FEA development was clearly due to the possibility to its implementation into Computer Aided Engineering (CAE) software. Indeed, an easily use of finite element program is dependent on the possibility of effective pre- and post-processing tools implemented in software user interface, allow input and output of data. The development of CAD-tools capable of a manipulation of model geometry and capable of defining model characteristics guaranteed a large spread of FE method in a wide variety of industrial disciplines.

During last years, FEA was also implemented in stochastic modeling with the aim to resolve probability models [157], [158].

In summary, FEM is a good tool for analyses of problems over complicated domains and environments (like cars or pipelines), when a change of the domain can occur, when the desired precision varies over the entire domain or when the solution lacks smoothness. For instance, in a frontal crash simulation of a car it is possible to increase the accuracy of system and discretization of those areas considered “important” for the simulation and, hence, reduce the accuracy in the rear part of the car.

6.2. Finite Element Method in tribology

As described in previous paragraphs, FEM is nowadays usually used in a wide variety of disciplines, including structural analyses, fluid studies, thermodynamics and so on.

During last years, lots of researches focalized the attention on the development of finite element models capable to describing complex process occurred during mechanical contact.

One of the most studied processes is wear phenomenon generated during a contact between different components. Finite element method allows the characterization of such contacts difficult to study using only an experimental approach. Furthermore, a numerical analysis based on finite elements method allows to predict the behavior of components in contact in terms of wear evolution on the interfaces and friction coefficient progression.

The most accurate approach to follow in order to obtain a good evaluation and comprehension of wear process using FE method is to conduct the numerical analysis simulating the behavior occurred on a standard test bench. Following this way, numerical analysis results could be compared with experimental tests carried out on the same test configuration and using the same materials.

Podra and Andersson [159] proposed a modeling and simulation procedure using linear wear law and Euler integration scheme. They conducted their research using commercial finite element software ANSYS. The study concerned the evaluation of a spherical Pin-on-Disk unlubricated steel contact behavior in an unlubricated domain; the research was conducted both experimentally and using finite elements method. Thanks to the Lim and Ashby wear map [nota], the researchers identified wear mechanisms and outlined that FEA wear simulation could be used as basis of wear prediction and evaluation.

In 2005, Kim proposed a numerical approach that simulates the wear progression in oscillating metal on metal contacts [160]. He conducted reciprocating Pin-on-Disk analyses to measure the wear rate for the material pair of interest. The wear rate obtained from experimental tests was implemented in a FE model of Block-on-Ring configuration. After the simulations, Block-on-Ring experimental tests were performed using the same materials used in the numerical analysis. Results from FEA outlined a low discrepancy between experimental results.

In 2006, Zhang [161] proposed a linear sliding wear model considering also ratcheting effects to describe wear behavior. a simplified mathematical method was presented in order to simulate the wear occurred on the rotor bushing sliding on the ground surface. He explored the effects of geometry parameters, material properties and applied operating conditions on the wear rates generated on the contact between the rotating rotor busing and the ground plane. Results obtained from numerical tests were analyzed and the effects of wear coefficient, material selections and geometry structures were discussed in detail. From this study it was highlighted that non-linear effects could not be ignored and these results must be evaluated on a relative scale to compare different design options.

Studies performed by Hegadekatte [162]–[165] concerned calculation of wear of micro-mechanical devices based on finite element simulations. These studies outlined a good accordance between experimental and numerical results.

Finite element method was also used in fretting wear simulations as well as the evolution of fretting variables with the number of wear cycles in a cylinder on flat configuration using a Super CMV alloy [166].

In [167], an adopted abrasive-diffusive wear model was proposed and implemented into a 3D Finite Element code to study the tool wear phenomenon. FEM simulations were conducted in order to estimate the tool wear development in turning operations. The adopted wear model gave the possibility of evaluating the tool wear of actual turning operations during the transient phase and the steady-state phase. FEM results were compared with experimental data, highlighting a good comparison.

Pin-on-Disk wear simulations were described in [168] using finite element method and an incremental wear-prediction technique, taking into account the worn material at the end of each iteration.

Telliskivi [169] carried out numerical simulation with the aim to predict wear process in a Disk-on-Disk configuration using Winkler mattress model.

A mixed numerical-experimental approach was followed by Dickrell and Sawyer [170] during their study on wear evolution process occurred on a shaft-bushing assembly.

The study conducted and described in this Ph. D. Thesis concerned the evaluation of wear evolution on a generalized Block-on-Ring contact. Both the block and the ring were modeled in a finite element domain, replicating the same materials characteristics outlined in the experimental analysis described in Chapter 5 and the input parameters set on the test bench.

Thanks to fundamental tribological laws, wear depth evolution was defined, using a custom algorithm, on the contact surfaces and the wear progression was finally defined according to time.

The main aim of this study was to correlate the wear evolution obtained from the experimental analysis (described in Chapter 5) and the wear progression evaluated thanks to finite element approach. The correlation obtained could be used during the design step in order to predict lifetime of the components.

6.2.1. **Block-on-Ring FE model description**

The first step of finite element modeling process concerned the geometrical modeling of Block-on-Ring contact configuration. According to what described in previous paragraph, finite element model was defined in order to replicate the same dimension of the actual samples used in the experimental campaign.

Figure 66 illustrates the components modeled in the finite element domain. Both the block and the ring were defined directly in ANSYS domain thanks to their simple geometries. Due to the symmetry characterizing the ring, only the nearest section to the contact interface was modeled. This assumption guaranteed a low computational effort, maintaining the same accuracy of results.

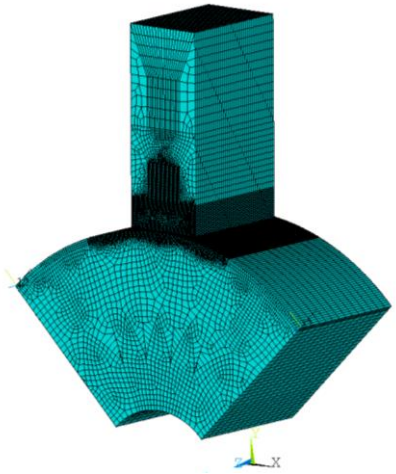

Figure 66 - Finite element Block-on-Ring configuration

Both the block and the ring followed a 3D modeling approach in order to evaluate the wear value on all Cartesian directions. To replicate the materials characteristics concerning the Block-on-Ring experimental analysis described before, some assumptions were fixed. As one can see in Figure 67, the frontal view of the ring was modeled defining a “core section” and an external annulus. The first one (in red) was modeled following the material properties of the steel used in experimental tests, while the external region (in blue) was characterized using

molybdenum features described in Chapter 5. This approach guaranteed a replication of material characteristics defined in the numerical model.

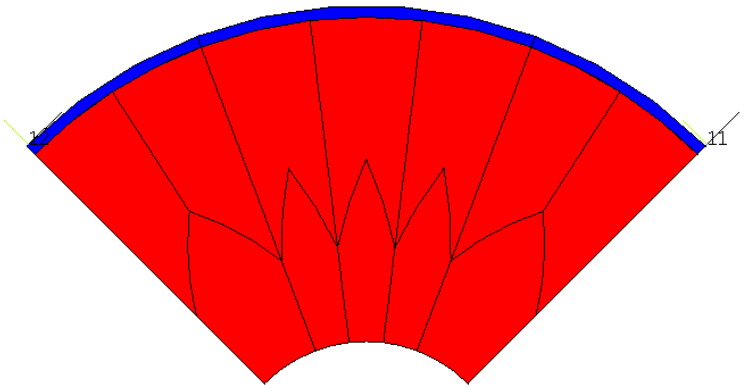

Figure 67 - Ring frontal sections

As for the ring, also the block was modeled defining two main different regions. The necessity to define a region with a higher discretization of finite element compared to the other areas, led to a division process occurred near the contact region of the block. Figure 68 illustrates the different areas, defining in blue the contact region and in red the others.

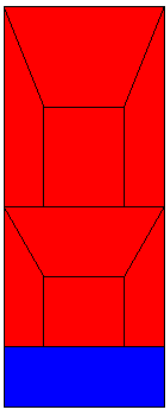

Figure 68 - Block frontal sections

Molybdenum region and contact area defined on the ring and on the block respectively described the contact surfaces. According to this, discretization process on these surfaces was performed with the aim to obtain finite elements dimensions as little as possible. This assumption guaranteed a good evaluation of the wear process thanks to the comparable

dimensions between element sizes and worn particles generated during the contact. Figure 69 shows the molybdenum region and the block contact surface after the meshing process.

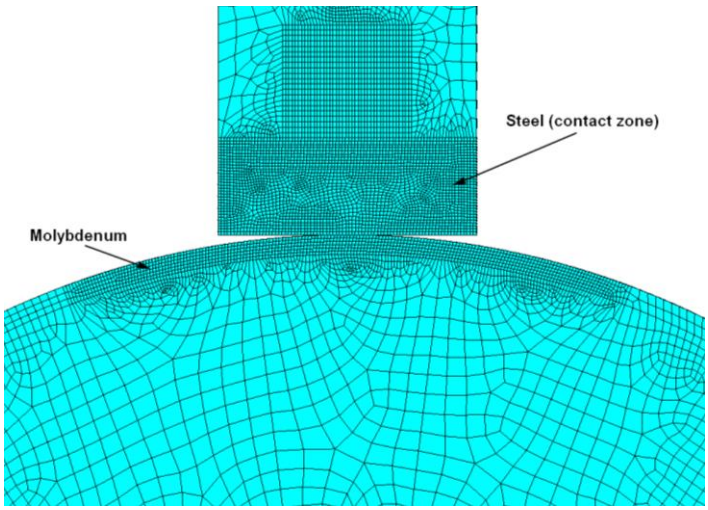

Figure 69 - Discretization zones in Block-on-Ring contact

To replicate the constraints present in the actual Block-on-Ring configuration, the ring modeled in FE domain was fixed in its position linking the nodes of the internal diameter to an infinite mass placed at the center of the ring, as shown in Figure 70. In the model ring was assumed as fixed respect to the block; by the way, ring rotation was considered in wear algorithm, as described in next paragraphs.

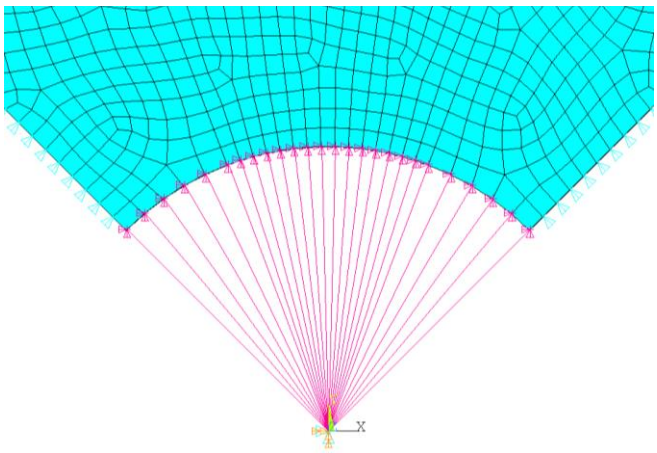

Figure 70 - Ring's constraints

The block was constrained in all directions, except for the vertical displacement. This assumption guaranteed contact process between specimens during the simulations.

The normal load acting on the real test bench was replicated also in the numerical analysis. Indeed, a normal load of W=130[N] was applied to a mass placed on the top of upper block surface. This mass element (defined as MASS21 in ANSYS) was linked to the nodes located in the upper area of the block.

As in the experimental test, contact was defined between the lower surface of the block and the external surface of the ring. These areas were modeled using CONTA173 element type for the block surface and TARGE170 for ring external area. To find the contact regions the simulation was set using a Lagrange-penalty contact algorithm, the model was limited to experience only small deformations and excluding initial penetration or gap between interfaces.

Following this process, it was possible to define the geometric model of Block-on-Ring contact configuration. Thanks to the optimization carried out during meshing phase, simulations were conducted with a low computational effort, providing accurate results in a short time.

6.2.2. **Wear simulation algorithm**

Wear evaluation on Block-on-Ring configuration was performed using two fundamental tribological laws: the Archard's law and the Reye's theory.

Archard's law [53] correlates the wear depth δ, the applied pressure p and the macroscopic displacement occurred during the contact s. Equation 14 described below defines, moreover, a relation between two characteristics of the material in contact: the specific wear rate K and the hardness H of the softer material, both outlined in the experimental tests described in Chapter 5.

$$\delta = s \cdot p \cdot \frac{K}{H} \tag{14}$$

Reye's hypothesis, in its most generalized definition, put in a relationship the worn volume and the work made to wear it [171]. This law could be synthetized as follow: the volume of material lost for wear effects (V_{wear}) is proportional to the passive work L_p done by the friction forces producing that wear, as illustrated in Equation 15.

$$V_{wear} \propto L_p \tag{15}$$

Reye's law gives the possibility to define pressure distribution between two components in relative contact and, hence, the wear occurred during the contact.

In the numerical analysis described in this chapter, Archard's law and Reye's hypothesis were put in a relationship combining pressure distribution on the contact surfaces and the consequent wear depth values.

To achieve this goal, a custom algorithm was defined. The algorithm was divided in 5 different steps:

- Pressure distribution evaluation
- Real contact area definition
- Reye's theory application
- Wear depth evaluation
- FE geometry modification

In the first step, block and ring were put in contact and the normal load defined in previous paragraph was applied. At the end of simulation, an estimation of the pressure distribution generated on the contact surface was made. Figure 71 shows the pressure distribution (described in [MPa]) achieved at the end of the first step of the iterative process carried out. As described in Chapter 5, the block showed a higher value of wear compared to the external surface of the disk. According to this, only the pressure distribution generated on block surface was evaluated.

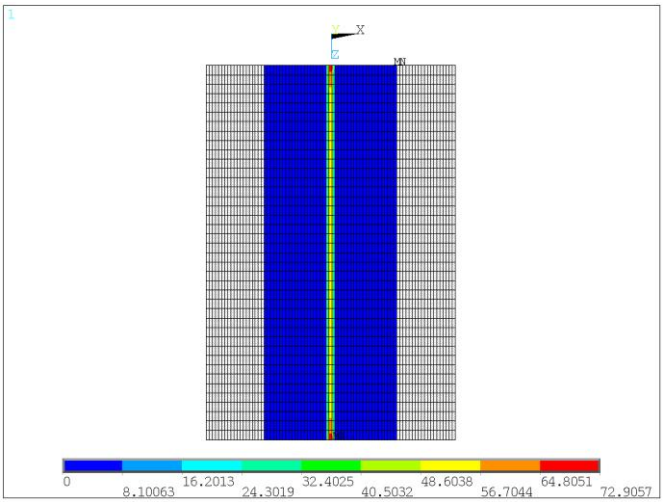

Figure 71 - Pressure distribution on contact surface - first step

The definition of pressure distribution allowed the evaluation of the real contact areas generated during the contact. This step assumed high importance due to the possibility to define the actual interface between block and ring and its evolution according to time, procedure possible only using a FE domain.

Pressure distribution achieved on each element area on real contact surfaces was implemented in the Reye's law, defining a new pressure distribution. This process was carried out defining a vertical translation equilibrium of normal load acting on each element, as described in [171].

The new pressure distribution (called P_{Reye}) was implemented in Archard's law, following Equation 14. According to the process performed in the experimental tests, the simulation was carried out performing 12 sub-steps, each of them with a total duration of 5 minutes. Indeed, the total simulation duration was fixed in 1 hour of work. Considering the ring rotating speed set on the actual test bench (and defined in Chapter 5), 5 minutes of rotation corresponds to a displacement made by the ring of about s=117m. This value was implemented in Equation 14 in order to define the wear depth values occurred on each element of block contact surface. Besides the value of displacement made by the ring, in Equation 14 was inserted the steel surface hardness and the average specific wear rate defined during experimental tests, as illustrated in Chapter 5.

The final step of the algorithm concerned the modification of block contact surface geometry, updating the nodal coordinates of worn element with the wear depth values defined before. The nodal coordinate modification process was performed with the aim to maintain the

mesh with a low magnitude of deformation. This assumption guaranteed a good accuracy of results obtained from numerical simulations.

Once the geometry was updated, the iterative process could start again, defining new pressure distributions and, hence, new wear depth values.

In practical terms, the iterative process described before could be resumed with the block diagram showed in Figure 72.

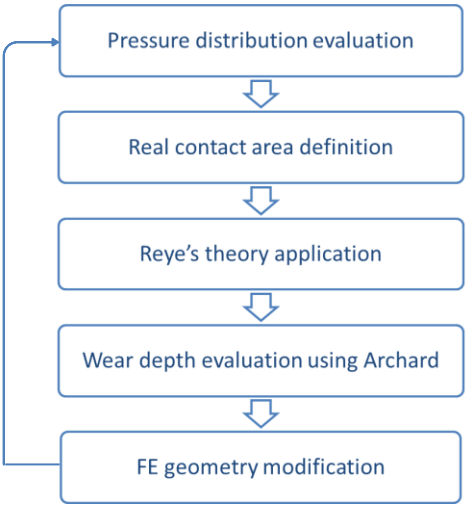

Figure 72 - Block diagram of iterative process

The simulation did not take into account the microstructure of contact surfaces; hence surface roughness or surface texture were not considered. Furthermore, temperature and lubricating oil influences were not considered during simulation steps.

6.3. Results and discussion

Numerical simulations carried out following the iterative process described before outlined, as first result, the pressure distribution progress according to time and obtained after the wear depth values implementation in the FE model. These pressure arrangements defined the real contact areas occurred during the wear process, outlined the evolution of worn interface.

Figure 73 shows pressure distributions obtained at the end of each simulation sub-step. These arrangements were defined on the block contact surface, as described in previous paragraph. All the pressure distributions were considered as expressed in [MPa].

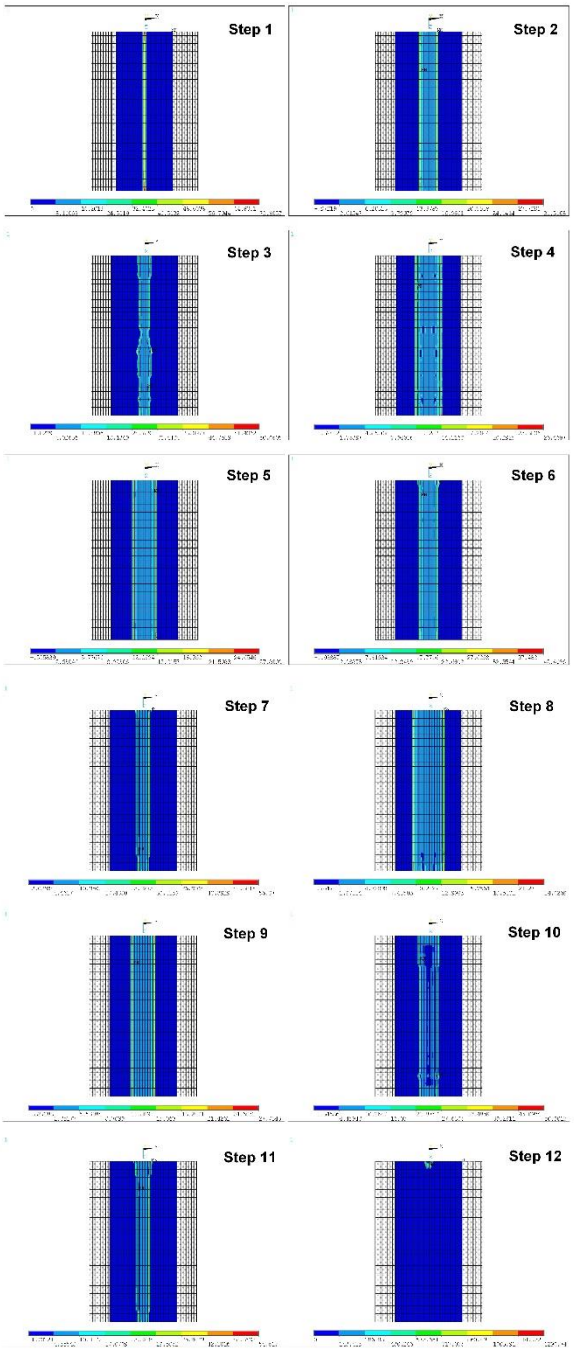

Figure 73 - Pressure distribution evolution on contact surface

As one can see, the first step outlined a pressure distribution that influenced only few elements, defining a narrow contact area. Indeed, the first step described the initial contact between block and ring characterized by a value of wear equal to zero.

The consequent steps defined a variation in pressure distribution occurred on the contact interface. Pressure evolutions described the real contact surfaces generated during the interaction between block and ring and, hence, the evolution of worn zones.

As described in Paragraph 6.2.2, pressure distribution values were implemented in the custom algorithm defined in MatLab domain in order to define wear depth generated after a 5-minutes rotation of the ring. Following the approach outlined in the experimental analysis, wear increments were evaluated every 15 minutes in order to correlate them with the values obtained from experimental tests. The wear values obtained from numerical analysis were illustrated in Table 22.

Table 22 - Average wear values - Numerical analysis

Step [minute]	Average wear value [mm]
15	**1.44**
30	**1.91**
45	**2.18**
60	**3.20**

As for experimental campaign, wear values were reported in a graph in order to define an evolution according to time. Figure 74 illustrates the wear value trend according to time obtained from numerical analysis.

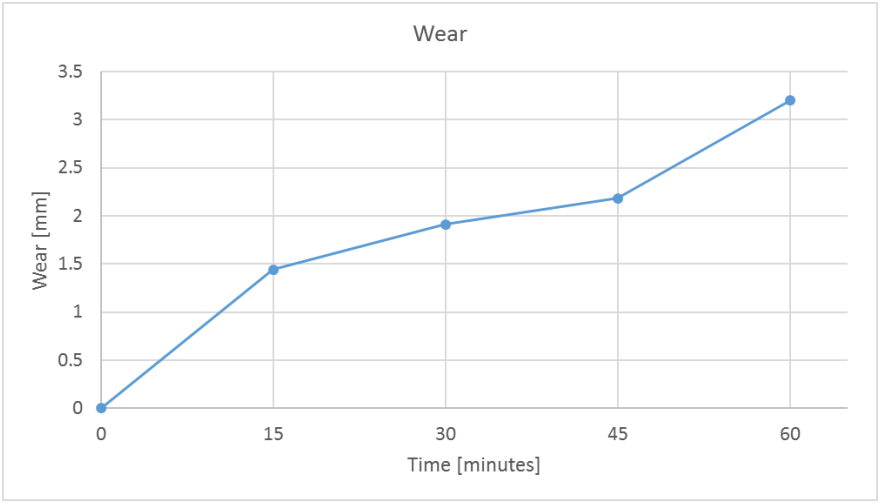

Figure 74 - Wear value trend

As one can expect, the wear trend shows the typical increasing evolution according to time. For a better comprehension of results obtained from wear model defined in the finite element domain, a comparison between experimental wear trend and numerical wear evolution was made. Figure 75 shows both the experimental wear measure and the numerical one.

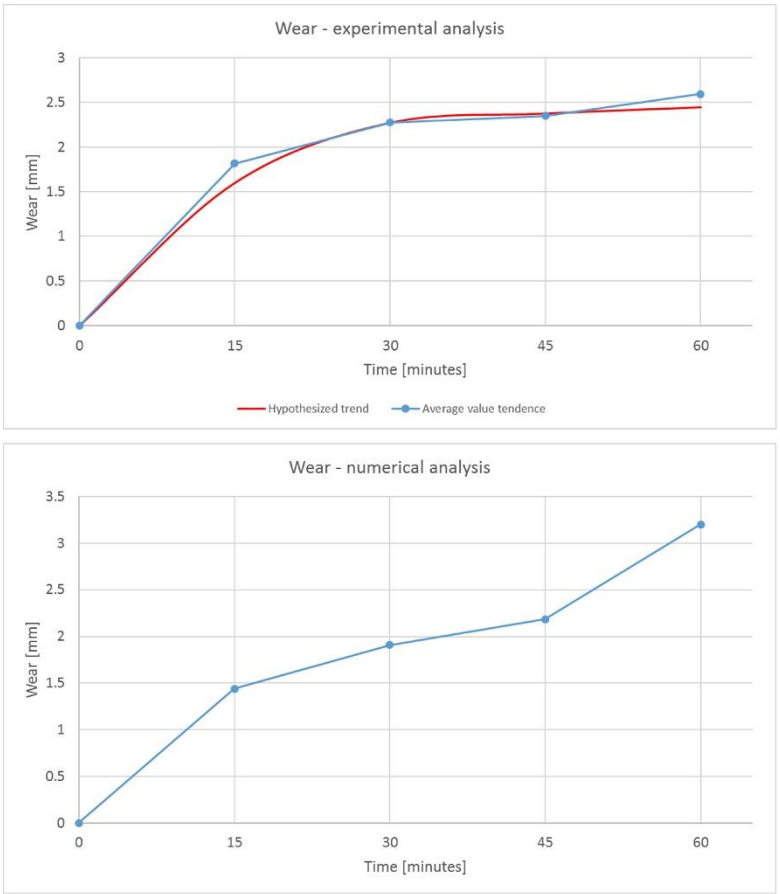

Figure 75 - Wear trend value - comparison between experimental and numerical results

As one can see, the trends are comparable in terms of evolution according to time. Furthermore, the average error between the values of trends described turns out to be about 18%, a good result for a complex phenomenon as the wear process.

Following graphs shown in Figure 75, some considerations could be outlined. Numerical wear trend illustrates an initial increase with a lower slope compared to the experimental one. Furthermore, in the central part of wear evolution the experimental trend describes a quasi-constant tendency, while numerical values define a continuous increase. Moreover, the final value achieved in the numerical analysis results higher than the average value obtained from experimental tests. All phenomena described could be due to the assumptions made before starting numerical simulations. Indeed, as described in previous paragraph, lubricating oil and surface characteristics were not considered in numerical simulations. Furthermore, actual wear process and correlated phenomena generated during experimental tests were not inserted in numerical analysis due to their difficult modeling.

However, results obtained from numerical analysis could be considered as a good starting point for an evaluation of wear process. The model defined describes the evolution of

wear occurring in a contact with a good accuracy, outlining results comparable with experimental tests.

The model obtained using a mixed approach (numerical and experimental) could be a good instrument for wear prediction during the design phase of components, defining the lifetime of contact pair. Furthermore, an application of the wear model in such components characterized by high performances (e.g. automotive and motorsport fields) could lead to an estimation of performance decay according to time and, hence, optimize the design of those components in relative contact.

7. Electronic-LSD internal clutch – wear model application

Wear model described in the previous chapter concerns the evaluation of wear process and its evolution in a generalized contact configuration. Thanks to its features, the model defined could be applied in specific domains, evaluating the wear evolution of such components in reciprocal contact.

Lots of studies were carried out in finite element domain trying to describe the wear phenomenon and its influence on the lifetime of contact pairs. In [172] Flodin and Andersson simulated the wear occurred on spur gears using Winkler model and later they extended their methodology on helical gears [173]. Brauer and Andersson [174] performed wear simulations using a combination of analytical approach based on Hertz theory and finite element method. Hugnell et al. [175] simulated wear values in a cam-follower contact configuration and, in another paper, they studied mild wear process considering a rotation of the follower [176]. Biomedical researches were performed by Fregly et al. [177] on the mild wear process occurred on a tibial insert. On the same topic, Maxian [178] and Bevill [179] carried out studies on wear predictions of hip arthroplasty.

Following the process carried out and described in Chapter 5 and Chapter 6, the wear model was applied in the internal clutch pack of an Electronic-Limited Slip Differential (e-LSD), a technical evolution of the LSD depicted in Chapter 5. The internal clutch pack of this apparatus is similar to those illustrated before and it is composed by a sequence of molybdenum coated and uncoated disks.

In this chapter it is highlighted a study on the contact behavior between treated and untreated disks of a differential clutch aimed to obtain a better knowledge of the relationship between the material properties and the performance of the clutch system during its lifetime.

The generalized wear model described in previous chapter was implemented in a finite element model of the clutch pack while materials properties were obtained from experimental campaigns depicted in Chapter 5.

Following the process outlined in the numerical wear model, the use of Archard's law and Reye's theory allowed the estimation of wear depth and pressure distribution on the disks surfaces. The results obtained permitted the definition of the clutch characteristics reduction, ensuring the evaluation of the service life of the clutch according to a minimum value reachable by the torque.

7.1. Clutch packs tribology

The dynamics of clutch pack installed inside electro-actuated differentials are highly influenced by the disks engagement behavior and their material properties. Torque transmission in differential clutch pack is guarantee by friction surfaces; lots of applications in motorsport field use commercial treated disks, typically treated with molybdenum-based coating or other treatments, with the aim to control as well is possible the vehicle dynamics. To keep a high performance level of the differential during its lifetime it is important to know how each component works, especially the internal clutch.

Tribologic studies on clutch apparatus were made in last years by Lingsten et al. [180] developing an apparatus for continuous wear measurement with the aim to obtain more information about clutch characteristics. Another example of tribologic study has been made by Marklund et al. [181], where wet clutch characteristics have been described to obtain a friction coefficient trend in relation with the temperature and with the implementation of oil characteristics.

The influence of surface topography on the friction characteristics of a sintered-treated clutch pack has been outlined by Nyman et al. [182]. A large number of studies were carried out with the aim to evaluate the progressive wear trend in some contact, as it is possible to see in [183]. In this work, Thompson et al. calculated wear strain in order to modify the elastic strain in an element using the Archard equation.

Another Archard application could be found in Garleanu et al. work [184]; the Archard's law was used to define wearing phenomenon in a FE domain, obtaining a medium level of prediction of wear. Andersson et al. [185] and Liu et al. [186] studied the application of Archard equation to define a modified pressure distribution. In Liu's work the method was applied only on linear systems where full contact is maintained at all times, while in Andersson's study the application of Archard's wear equation outlined some important factors as roughness, temperature and lubricant additive-surface interaction.

Adhesive wear was studied by [187] using an accurate FE model of asperity contact. A detailed study on the tribological and mechanical characteristics of a brake disc using a FE approach was performed by [188] and later by [189].

On the friction characteristics definition, an important study was made by [190], evaluating the characteristics of brake pads material with the aim to provide improved manufacturing process.

An optimization in the design of contact pairs production using a Taguchi approach was developed by [191]. Taguchi method was also followed by [192] in order to define a statistical model and analysis of SiC reinforced aluminum MMCs. The same approach was used by [193] and [194] with the aim to define optimized tribological relationship in different contact pairs.

Other important studies on clutch pack tribologic characteristics definition were made, as outlined in [195] where the engagement of wet clutches were simulated using the most influencing parameters as roughness, fluid viscosity, friction characteristics and groove area ratio of the friction surfaces.

An interesting comparison between experimental and numerical analyses was described in [196] where a test rig was designed to quantify the torque transmission characteristics of wet clutches. The friction-velocity relationship of wet clutches was examined in [197] outlining how different parameters influence anti-shudder properties. The authors carried out

a large study on the characterization of wet clutches for automotive differential application, showing the influence of several operating parameters on the frictional behavior of the clutch.

The entire design of a test bench to define frictional characteristics of transmission fluids was described in [198], outlining the high influence of temperature in transmission fluid properties. The lifetime of clutch pack was evaluated by [199] using SAE#II and a pin-on disk test rigs; the friction coefficient and wear rate trends were defined according to materials properties and operating conditions.

In [200] the contact units formed between a paper based friction material and a glass counterface have been investigated under different pressures and during rubbing in order to evaluate the conditions present in a wet clutch contact.

7.2. e-LSD structure

The mechatronic device object of this chapter is an automotive differential, electrically controlled by an ECU – Electronic Control Unit, which belongs to the semi-active differential's family. Its design originates from a classic self-locking, and therefore passive, mechanism known as LSD – Limited Slip Differential.

The structure can be divided in three main parts: the right cartridge, the left cartridge and the housing. The latter, which is the central element, receives the engine torque by the outer crown fixed to this, and transfers it to the two solar gears; this is possible thanks to four planet bevel gears, which are connected to the central housing through the differential cross. The two bevel wheels, each one fixed to a half shaft and belonging to a different cartridge, generate an axial load due to their geometry; hence, in addition to radial bearings, each cartridge is equipped with an axial bearing to sustain this thrust. The structure of the right cartridge is more complicate as it contains the actuation system and the internal clutch. The actuation is composed by a main piston, placed in a suitable chamber, which is pushed by the oil in pressure; in detail, an external actuator increases the pressure using another piston activated by a ball screw mechanism and a servomotor. The main piston is constituted by two parts: one in contact with the friction disks and the other with the oil chamber. Thus, in order to allow a relative movement, an angular contact bearing is necessary. The internal clutch is formed by a disks' pack (oil immersed) it is composed by 12 disks: 6 friction disks treated with molybdenum coating and 6 untreated separator disks. All these disks are alternatively coupled with the differential cage and the half shaft through a splined coupling: this means that they are constrained for the revolution but free for the axial movements.

The goal of the clutch is the generation of a friction torque that contrasts the relative rotation of the two half shafts: more torque is always delivered towards the slowest wheel, with the purpose to reduce the speed difference and to avoid a wheel spin. In addition to this, an unbalanced distribution of force on the same axis inevitably generates a yaw torque on the vehicle that modifies its attitude: the idea is to operate properly on the torque distribution to control the yaw angle of the vehicle, as well as the traction level [201].

A representation of the e-LSD is shown in Figure 76.

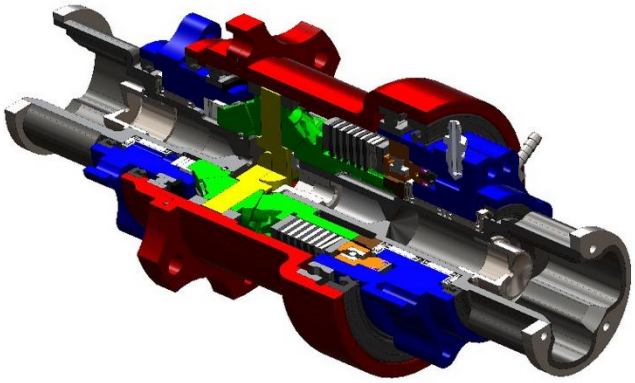

Figure 76 - Cutaway view of e-LSD

7.3. Clutch pack FE modeling and wear depth estimation

As illustrated in Chapter 6, FE method guarantees the possibility to evaluate contact characteristics in terms of pressure distribution and real contact area definition. Following the approach developed in the previous chapter, the same process was chased in the modeling procedure of the clutch pack. According to this, a wear depth estimation was conducted using the same tribological laws choose for the Bloc-on-Ring FE model.

As defined before, to define a wear trend among two components, Archard's law puts in a relationship the wear depth δ, the applied pressure p and the macroscopic displacement occurred during the contact s. These physical quantities were described and implemented in Equation 14, considering also the specific wear rate K and the hardness H of the softer material.

Archard's law is usually used with the assumption of consider a constant pressure trend applied on the contact surfaces. A shown in Figure 77, in this analysis the presence of a Belleville spring entails a variable distribution of the pressure on the disk's surfaces.

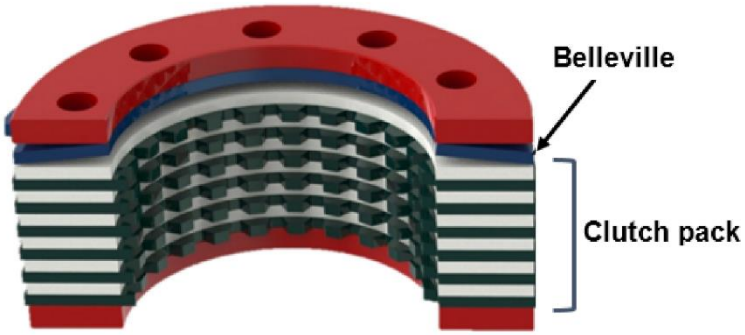

Figure 77 - Detail of the internal clutch's axial section.

A two-dimensional finite element modelling of the clutch was made thanks to the axisymmetric geometry of the assembly, with the advantage of a good trade-off between simulation accuracy and processing speed. During the simulation process all the disks were considered, in order to appreciate their contribution to the evaluation of the elasticity of the clutch pack. Using this FE model it was possible to define a radius dependent pressure distribution acting between the disks in static conditions; the contact area between the spring and the first disk and also between all the other friction surfaces can be considered as circular crown areas. During the simulation, the normal load was fixed on a value that replicates the real load acting in the differential. The first step of FE simulation was performed following these conditions, obtaining a pressure distribution on each contact surface. Figure 78 illustrates the results from the first step of the analysis obtained on the axisymmetric geometry of the clutch pack.

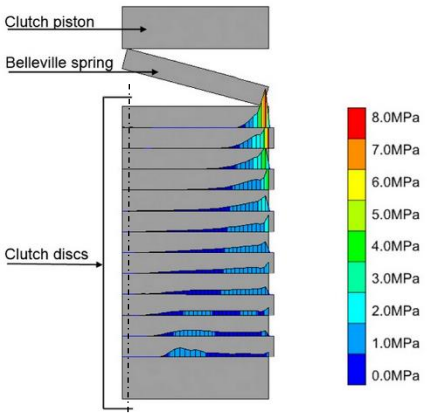

Figure 78 - Pressure distribution on a disk's surface (internal side on the left)

The radius dependent pressure vector obtained on each surface was used to determine contact areas on which a pressure gradient was defined. Reye's hypothesis could be applied on each circular crown area outlined through the previous step. Since the determination of pressure distribution is a process not feasible through a FE modelling, Reye's hypothesis application is essential in this kind of analysis. On the other hand, FE method provides the evaluation of the areas where the Reye's theory could be applied, defining the elements of the model with a pressure gradient. The equation that governs this hypothesis concerns a relationship among the work generated by friction load and the volume removed during the motion of the parts in contact, as expressed in Chapter 6. On each circular crown the worn volume can be estimate as indicated in Equation 16:

$$dV_{wear} = 2\pi \cdot R_c \cdot dR_c \cdot \delta \tag{16}$$

where R_c is the mean radius of the considered circular crown and δ is the wear depth achieved in the same area. On each area interested by the initial pressure, it may be possible

to define the pressure trend as defined in Equation 17:

$$P_{Reye} = \frac{C}{\mu \cdot 2\pi \cdot R_c} \tag{17}$$

where μ is the friction coefficient, C is a constant definable for the vertical translation equilibrium of the normal load acting on the clutch and R_c is the mean radius. The results from this equation defines an exponential law, obtaining a relation between pressure and radius. The application of Equation 14 with few differences allowed the definition of wear depth; compared to the original Archard's law, the displacement achieved during the contact is related to a predefined time (based on previous experiences), the pressure is that obtained from Reye's theory application (defined by Equation 17) while H and K are the same values defined above.

Following this procedure, it was possible to obtain a wear depth trend; this vector was used to update the initial FE model to simulate the new clutch configuration including the estimated wear depth of each contact surface. The iterative process can be resume following the block diagram illustrated in Figure 72.

The application of this approach allowed the estimation of the pressure distribution modification due to the wear increase. At the end of each FE simulation, a modified pressure vector was obtained. The iterative process was applied for the entire clutch pack outlining a relationship between pressure distribution evolution and wear depth increase in each contact surface.

7.4. Results and discussion

The main result of this process was the definition of a torque transmissible trend according to the wear depth increase and, hence, to the number of cycles. This objective was achieved through the use of experimental results in terms of tribologic data depicted in Chapter 5. Furthermore, a numerical approach was followed to estimate the pressure distribution on the contact surfaces and hence the wear evolution.

Figures 79, 80 and 81 show the pressure distribution evolution on the contact surfaces. The first one, Figure 79, shows the distribution after 5000 cycles, while Figure 80 illustrates the pressure status after 15000 cycles. The third image, Figure 81, shows the pressure distribution after 35000. To confirm expected behavior, one can see how the contact surface, and hence the pressure, achieved a uniform distribution according to the increase of cycles number.

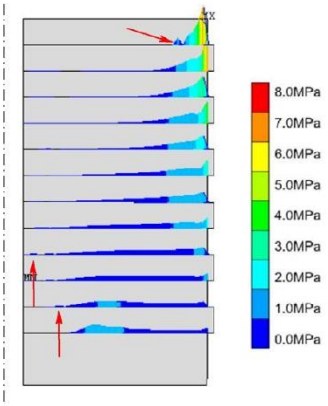

Figure 79 - Pressure distribution (after 5000 cycles)

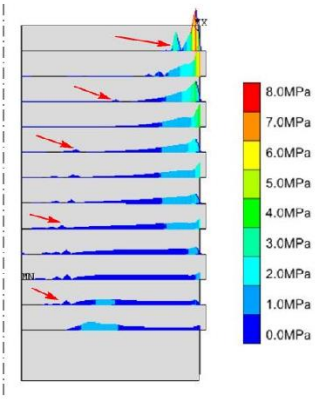

Figure 80 - Pressure distribution (after 15000 cycles)

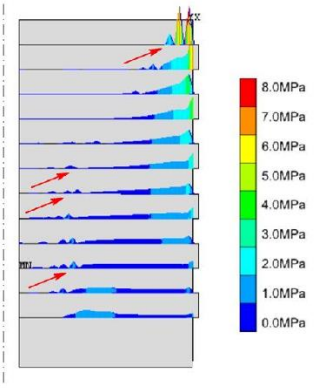

Figure 81 - Pressure distribution (after 35000 cycles)

As expected, the transmissible torque obtained following this process shows a negative exponential trend according to time. As one can see, Figure 82 outlines the torque evolution respect to the number of cycles; a running-in process occurred until the first 15000 cycles, easily visible from the trend evolution. On the right end, the torque has an asymptote mainly due to the wear stabilization achieved on the friction surfaces. Considering a torque variation between the starting point and the end of the process of about 3.5% of the maximum value, it is possible to use the asymptotic value in some future studies.

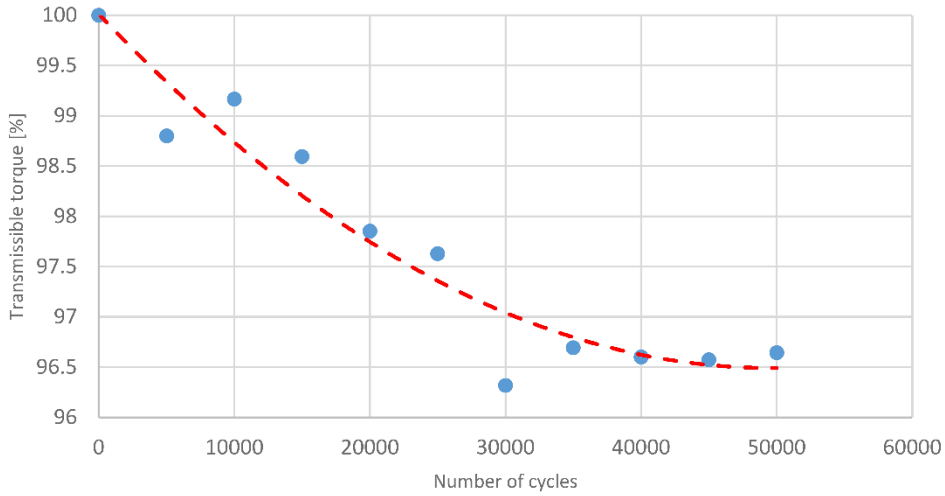

Figure 82 - Transmissible torque trend

The definition of a torque trend could lead to some interesting applications, as the definition of the lifetime of the clutch pack, and it could be used as input for a design methodology used in the e-LSD design. The lifetime estimation could be important to define some interesting parameters change in the e-LSD design, achieving an optimization of the geometry and a different choice of the materials in contact.

Considering a typical automotive application, some considerations were outlined: during a corner, the fully-engaged phases of the internal clutch could keep for an average time of 3 seconds. Envisaging about 20 clutch engagement cycles during a complete lap and an average duration of 50 laps for each competition, the value concerning the total engagement time will be 300 seconds.

Taking into account graphs in Figures 50 and 51, it is possible to see how this total engagement time is a fraction compared to the total experimental tests duration. This results highlights how, at the end of each competition, disks' wear is very low, maintaining the same functionality of the entire clutch.

In addition to the analysis concerning the tribologic characteristics of molybdenum surface treatment, an evaluation of the lifetime of disks pack was made. The possibility to know the lifetime of each component present inside the differential permits a more accurate design of the e-LSD, allowing a disk number reduction and an optimization in the surface treatment.

Thanks to data obtained from experimental analyses, it was possible to define the hypothetical worn thickness occurred in the real disks installed in the differential. Results obtained from this evaluation are shown in the Table 23 and in Table 24.

Table 23 - Supposed worn thickness (friction disks)

Average worn volume (experimental results) [m^3]	**Contact area (differential disk) [m^2]**	**Average worn thickness (differential disk) [m]**
$1.72 \cdot 10^{-9}$	$2.68 \cdot 10^{-3}$	$6.40 \cdot 10^{-7}$

Table 24 - Supposed worn thickness (separator disks)

Average worn volume (experimental results) [m^3]	**Contact area (differential disk) [m^2]**	**Average worn thickness (differential disk) [m]**
$1.05 \cdot 10^{-7}$	$2.68 \cdot 10^{-3}$	$3.90 \cdot 10^{-5}$

The average value of worn thickness of the surface treatment would be $6.40 \cdot 10^{-7}$m, considering a lifetime of the clutch pack of about 3600km (value obtained from the evaluation made before on a motorsport application). For what concerns separators disks, the wear would interest a higher thickness than the friction disks due to the untreated contact surfaces. The average value of the worn thickness would be in this case of about $3.9 \cdot 10^{-5}$m, acceptable for the separator disks.

From wear rate outcome data, the choice of molybdenum as surface treatment allowed to achieve a very low wear rate, mainly due to its high hardness, with an advantage in durability of the treated disks. On the other hand, AISI 1042 steel alloy used for the blocks highlighted a higher level of wear rate than the molybdenum. The use of a less hard material as counter surface allows the substitution of half the number of disk at the end lifetime, permitting a reduction in the cost of the whole clutch pack.

These outcomes could be good starting points for some future actions, mainly addressed to an optimization of the differential design in terms of number of clutch disks and type of surface treatments. Results obtained from this work could be matched with the algorithm and processes defined by [202] and [203] in order to obtain a design optimization of the whole differential. Automotive and motorsport applications need a constant performances and design enhancement of the installed devices; in this way, a knowledge of the decrease of clutch performances during its lifetime is a key point for an adequate design of the differential itself.

Conclusions and final remarks

The work described in this Ph. D. dissertation was conducted with the aim to define a predictive wear model using a mixed experimental and numerical approach.

In practical terms the wear model was developed and defined in a finite element domain using ANSYS software and thanks to the implementation of results obtained from experimental analyses.

The first phase of the research activities concerned an analysis of the state of the art of tribology domain, aimed to perform an evaluation and a description about the fundamental characteristics of friction coefficient and wear phenomenon.

An accurate bibliographic research about tribological tests was carried out in order to obtain an evaluation and characterization of the tribological test bench used for the experimental campaign discussed in this work. This apparatus – a Block-on-Ring test bench – was characterized through preliminary tests with the aim to guarantee a high results accuracy, fundamental process in a tribological definition of materials in contact.

Experimental campaigns performed on two different classes of surface treatments allowed the appreciation of tribological features of materials in contact, outlining a friction coefficient reduction and a poor wear resistance of treatments themselves. These features described a narrow range of application, mainly due to the quick worn process occurring directly on the coatings studied. As before, for each treatment studied, a state of the art analysis on the based material of the coating and its implementation with tribological aims was conducted.

The focalization of experimental analysis on a molybdenum based coating permitted the definition of friction coefficient and specific wear rate, replicating on the test bench the working conditions of a Limited Slip Differential (LSD) clutch pack. A dedicated and accurate bibliography research outlined this application as an innovation in tribological field and, hence, it permitted the appreciation of such characteristics difficult to evaluate in particular working conditions.

The accurate examination of experimental results obtained from tribological analysis concerning molybdenum-steel contact allowed the definition of Block-on-Ring configuration in a finite element domain. Key point of the numerical analysis was the implementation of experimental results in a custom algorithm, aimed to evaluate the wear depth evolution during the Block-on-ring contact. The tool defined following this process allowed the definition of contact pressure evolution and, hence, the wear progression on contact surfaces, replicating the conditions present in the contact between molybdenum and steel described in the experimental campaign. The comparison between experimental and numerical results in terms

of wear evolution according to time highlighted a good accuracy of numerical wear model described and defined in finite element domain.

The consequent implementation, using a finite element modeling approach, of the wear model in the clutch pack of the LSD led to the definition of wear evolution on disks contact surfaces installed inside the differential. The wear evolution estimation allowed the definition of performance decay occurring on the clutch pack in terms of transmissible torque, describing a torque trend according to time.

Practical application of wear model on actual systems allowed to highlight the ability of this model in the wear prediction occurring between two or more components. This feature guarantees a direct implementation inside the design process of such mechanical components in relative contact. The use of this model in engineering practice allows to outline critical issues in designed systems, helping engineers to define parameters for a proper design procedure.

Predictive wear model defined in this work allowed to implement into tribological domain a tool for wear evaluation innovative compared to the current literature.

Future developments of this study can be outlined implementing lubricating oil characteristics and considering temperature and heat generated during the contact directly in the numerical domain. These assumptions may allow the creation of a parametric wear model able to define every wear process using only the characteristics of materials in relative contact.

The consequent application of a parametric wear model during the design process of mechanical components may allow the evaluation of input parameters as better as possible, guaranteeing at the same time the lifetime of the components themselves.

Acknowledgements

The present thesis work was carried out in the Department of Industrial Engineering of the University of Florence.

Foremost, I would like to express my sincere gratitude to my supervisors Prof. Renzo Capitani and Ph. D. Eng. Claudio Annicchiarico for the continuous support of my Ph. D. study and related research, for their patience, motivation, and immense knowledge. Their guidance helped me in all the time of research and writing of this thesis. I could not have imagined having a better advisors and mentors for my Ph. D. study.

I would like to express my sincere gratitude to Prof. Emanuele Galvanetto for his suggestions and insightful comments during the preparation and examination of experimental campaign.

I would like to express my sincere gratitude to all the staff of SPIN-PET srl for their professionalism demonstrated during our collaboration and for the suggestions during the preparation of the research activities.

I would like to thank all the member of the internal Ph. D. Committee for the interest they outcome on my work, to the students that prepared their degree thesis collaborating with me, and to my labmates for the friendship and the stimulating discussion and for all the fun we have had in the last three years. A special thanks to Lorenzo, Tommaso and Francesco.

Last but not the least, I would like to thank my family and my friend for supporting me spiritually throughout my life in general and Martina for giving a lovely support during the writing of this thesis.

Bibliography

[1] P. H. Jost, “Lubrication (Tribology) - A Report on the Present Positions and Industry’s Needs.,” 1966.

[2] D. Dowson, *History of Tribology. 2nd ed.* Professional Engineering Publishing., 1998.

[3] B. Bhushan, *Principles and Applications of Tribology*. John Wiley & Sons, 1999.

[4] E. Rabinowicz, *Friction and Wear of Materials*. John Wiley & Sons, 1965.

[5] G. W. Stachowiak and A. W. Batchelor, *Engineering Tribology*. Butterworth-Heinemann, 1993.

[6] D. H. Buckley, *Surface effects in adhesion, friction, wear, and lubrication*. Elsevier, 1981.

[7] M. Nosonovsky, “Modelling size, load and velocity effect on friction at micro/nanoscale,” *Int. J. Surf. Sci. Eng.*, vol. 1, no. 1, pp. 22–37, 2007.

[8] B. Bhushan and M. Nosonovsky, “Scale effects in friction using strain gradient plasticity and dislocation-assisted sliding (microslip),” *Acta Mater.*, vol. 51, no. 14, pp. 4331–4345, Aug. 2003.

[9] A. Carpinteri and M. Paggi, “Size-scale effects on the friction coefficient,” *Int. J. Solids Struct.*, vol. 42, no. 9–10, pp. 2901–2910, May 2005.

[10] S. Niederberger, D. H. Gracias, K. Komvopoulos, and G. A. Somorjai, “Transitions from nanoscale to microscale dynamic friction mechanisms on polyethylene and silicon surfaces,” *J. Appl. Phys.*, vol. 87, no. 6, p. 3143, 2000.

[11] L. C. Zhang, K. L. Johnson, and W. C. D. Cheong, “A molecular dynamics study of scale effects on the friction of single-asperity contacts,” *Tribol. Lett.*, vol. 10, no. 1–2, pp. 23–28, 2001.

[12] L. Wenning and M. H. Müser, “Friction laws for elastic nanoscale contacts,” *EPL Europhys. Lett.*, vol. 54, no. 5, p. 693, 2001.

[13] N. P. Suh, *Tribophysics*. Prentice-Hall, 1986.

[14] E. Rabinowicz, *Friction and Wear of Materials*, 2nd ed. Wiley, 1995.

[15] H. Kudo, “A note on the role of microscopically trapped lubricant at the tool-work interface,” *Int. J. Mech. Sci.*, vol. 7, no. 5, pp. 383–388, May 1965.

[16] H. E. Staph, P. M. Ku, and H. J. Carper, “Effect of surface roughness and surface texture on scuffing,” *Mech. Mach. Theory*, vol. 8, no. 2, pp. 197–208, Jun. 1973.

[17] M. M. Koura, “The effect of surface texture on friction mechanisms,” *Wear*, vol. 63, no. 1, pp. 1–12, Aug. 1980.

[18] R. Lakshmipathy and R. Sagar, “Effect of die surface topography on die-work interfacial friction in open die forging,” *Int. J. Mach. Tools Manuf.*, vol. 32, no. 5, pp. 685–693, Oct. 1992.

[19] P. K. Saha, W. R. D. Wilson, and R. S. Timsit, "Influence of surface topography on the frictional characteristics of 3104 aluminum alloy sheet," *Wear*, vol. 197, no. 1, pp. 123–129, Sep. 1996.
[20] Z. M. Hu and T. A. Dean, "A study of surface topography, friction and lubricants in metalforming," *Int. J. Mach. Tools Manuf.*, vol. 40, no. 11, pp. 1637–1649, Sep. 2000.
[21] W. Rasp and C. M. Wichern, "Effects of surface-topography directionality and lubrication condition on frictional behaviour during plastic deformation," *J. Mater. Process. Technol.*, vol. 125–126, pp. 379–386, Sep. 2002.
[22] P. L. Menezes, Kishore, and S. V. Kailas, "Studies on friction and transfer layer: role of surface texture," *Tribol. Lett.*, vol. 24, no. 3, pp. 265–273, Nov. 2006.
[23] P. L. Menezes, Kishore, S. V. Kailas, and M. R. Lovell, "Studies on Friction and Formation of Transfer Layer in HCP Metals," *J. Tribol.*, vol. 131, no. 3, pp. 031604–031604, Jun. 2009.
[24] P. L. Menezes, Kishore, S. V. Kailas, and M. S. Bobji, "Influence of tilt angle of plate on friction and transfer layer—A study of aluminium pin sliding against steel plate," *Tribol. Int.*, vol. 43, no. 5–6, pp. 897–905, May 2010.
[25] P. L. Menezes, Kishore, S. V. Kailas, and M. R. Lovell, "Analysis of Strain Rates and Microstructural Evaluation during Metal Forming: Role of Surface Texture and Friction," *Tribol. Trans.*, vol. 55, no. 5, pp. 582–589, Sep. 2012.
[26] C. Pradeep Kumar, P. L. Menezes, and S. V. Kailas, "Role of Surface Texture on Friction under Boundary Lubricated Conditions," *Tribol. Online*, vol. 3, no. 1, pp. 12–18, 2008.
[27] E. S. Gadelmawla, M. M. Koura, T. M. A. Maksoud, I. M. Elewa, and H. H. Soliman, "Roughness parameters," *J. Mater. Process. Technol.*, vol. 123, no. 1, pp. 133–145, Apr. 2002.
[28] P. L. Menezes, Kishore, and S. V. Kailas, "Influence of surface texture on coefficient of friction and transfer layer formation during sliding of pure magnesium pin on 080 M40 (EN8) steel plate," *Wear*, vol. 261, no. 5–6, pp. 578–591, Sep. 2006.
[29] P. L. Menezes, Kishore, and S. V. Kailas, "Effect of surface roughness parameters and surface texture on friction and transfer layer formation in tin–steel tribo-system," *J. Mater. Process. Technol.*, vol. 208, no. 1–3, pp. 372–382, Nov. 2008.
[30] P. L. Menezes, Kishore, and S. V. Kailas, "Effect of Roughness Parameter and Grinding Angle on Coefficient of Friction When Sliding of Al–Mg Alloy Over EN8 Steel," *J. Tribol.*, vol. 128, no. 4, p. 697, 2006.
[31] P. L. Menezes, Kishore, and S. V. Kailas, "Influence of roughness parameters and surface texture on friction during sliding of pure lead over 080 M40 steel," *Int. J. Adv. Manuf. Technol.*, vol. 43, no. 7–8, p. 731, Sep. 2008.
[32] P. L. Menezes, Kishore, and S. V. Kailas, "Influence of surface texture and roughness parameters on friction and transfer layer formation during sliding of aluminium pin on steel plate," *Wear*, vol. 267, no. 9–10, pp. 1534–1549, Sep. 2009.
[33] P. L. Menezes, Kishore, S. V. Kailas, and M. R. Lovell, "Influence of Inclination Angle and Machining Direction on Friction and Transfer Layer Formation," *J. Tribol.*, vol. 133, no. 1, pp. 014501–014501, Dec. 2010.
[34] P. L. Menezes, Kishore, S. V. Kailas, and M. R. Lovell, "Friction and transfer layer formation in polymer–steel tribo-system: Role of surface texture and roughness parameters," *Wear*, vol. 271, no. 9–10, pp. 2213–2221, Jul. 2011.

[35] A. Pottirayil, P. L. Menezes, and S. V. Kailas, "A parameter characterizing plowing nature of surfaces close to Gaussian," *Tribol. Int.*, vol. 43, no. 1–2, pp. 370–380, Jan. 2010.
[36] A. Pottirayil, P. L. Menezes, and S. V. Kailas, "Correlating the Features of Topography to Friction by Sliding Experiments," pp. 361–364, Jan. 2008.
[37] P. L. Menezes, Kishore, and S. V. Kailas, "Study of Friction and Transfer Layer Formation in Copper-Steel Tribo-System: Role of Surface Texture and Roughness Parameters," *Tribol. Trans.*, vol. 52, no. 5, pp. 611–622, Sep. 2009.
[38] P. L. Menezes, K. S. Kishore, and M. R. Lovell, "Role of surface texture on friction and transfer layer formation during sliding of PVC pin on steel plate," in *Proceedings of the 2010 STLE annual meeting & exhibition, Las Vegas, USA*, 2010.
[39] P. L. Menezes, Kishore, and S. V. Kailas, "Subsurface deformation and the role of surface texture—A study with Cu pins and steel plates," *Sadhana*, vol. 33, no. 3, p. 191, Jul. 2008.
[40] P. L. Menezes, Kishore, and S. V. Kailas, "Role of surface texture of harder surface on subsurface deformation," *Wear*, vol. 266, no. 1–2, pp. 103–109, Jan. 2009.
[41] M. A. Moore and F. S. King, "Abrasive wear of brittle solids," *Wear*, vol. 60, no. 1, pp. 123–140, Apr. 1980.
[42] P. L. Menezes, Kishore, and S. V. Kailas, "Effect of Surface Topography on Friction and Transfer Layer during Sliding," *Tribol. Online*, vol. 3, no. 1, pp. 25–30, 2008.
[43] P. L. Menezes, Kishore, S. V. Kailas, and M. R. Lovell, "The Role of Strain Rate Response on Tribological Behavior of Metals," *J. Tribol.*, vol. 135, no. 1, pp. 011601–011601, Dec. 2012.
[44] G. Bregliozzi, A. Di Schino, J. M. Kenny, and H. Haefke, "The influence of atmospheric humidity and grain size on the friction and wear of AISI 304 austenitic stainless steel," *Mater. Lett.*, vol. 57, no. 29, pp. 4505–4508, Nov. 2003.
[45] Z. B. Wang *et al.*, "Effect of surface nanocrystallization on friction and wear properties in low carbon steel," *Mater. Sci. Eng. A*, vol. 352, no. 1–2, pp. 144–149, Jul. 2003.
[46] R. Mishra, B. Basu, and R. Balasubramaniam, "Effect of grain size on the tribological behavior of nanocrystalline nickel," *Mater. Sci. Eng. A*, vol. 373, no. 1–2, pp. 370–373, May 2004.
[47] Z. N. Farhat, Y. Ding, D. O. Northwood, and A. T. Alpas, "Effect of grain size on friction and wear of nanocrystalline aluminum," *Mater. Sci. Eng. A*, vol. 206, no. 2, pp. 302–313, Feb. 1996.
[48] Y. Tsuya, *Microstructure of Wear, Friction and Solid Lubrication*. publisher not identified, 1975.
[49] F. P. Bowden and J. E. Young, "Friction of Clean Metals and the Influence of Adsorbed Films," *Proc. R. Soc. Lond. Math. Phys. Eng. Sci.*, vol. 208, no. 1094, pp. 311–325, Sep. 1951.
[50] G. Straffelini, *Attrito e usura*. Tecniche Nuove.
[51] P. L. Menezes, Kishore, S. V. Kailas, and M. R. Lovell, "Response of Metals and Polymers During Sliding: Role of Surface Texture," pp. 267–269, Jan. 2010.
[52] S. C. Lim and M. F. Ashby, "Overview no. 55 Wear-Mechanism maps," *Acta Metall.*, vol. 35, no. 1, pp. 1–24, Jan. 1987.
[53] J. F. Archard, "Contact and Rubbing of Flat Surfaces," *J. Appl. Phys.*, vol. 24, no. 8, pp. 981–988, Aug. 1953.
[54] N. Saka, A. M. Eleiche, and N. P. Suh, "Wear of metals at high sliding speeds," *Wear*, vol. 44, no. 1, pp. 109 – 125, 1977.

[55] M. M. Khruschov, “Principles of abrasive wear,” *Wear*, vol. 28, no. 1, pp. 69–88, Apr. 1974.
[56] D. H. Buckley, “The use of analytical surface tools in the fundamental study of wear,” *Wear*, vol. 46, no. 1, pp. 19–53, Jan. 1978.
[57] “ASTM G133: standard test method for linearly reciprocating ball-on-flat sliding wear.” .
[58] “ASTM G99: standard test method for wear testing with a pin-on-disk apparatus.” .
[59] F. P. Bowden and D. Tabor, *The Friction and Lubrication of Solids*. Clarendon Press, 2001.
[60] F. F. Ling and C. H. T. Pan, *Approaches to modeling of friction and wear*. Springer.
[61] D. A. Rigney, A. S. for M. M. S. Division, and M. S. of AIME, *Fundamentals of friction and wear of materials.* American Society for Metals, 1981.
[62] I. L. Singer and H. M. Pollock, Eds., *Fundamentals of Friction: Macroscopic and Microscopic Processes*. Dordrecht: Springer Netherlands, 1992.
[63] “ASTM G77: Standard Test Method for Ranking Resistance of Materials to Sliding Wear Using Block-on-Ring Wear Test.” .
[64] “ASTM D5183: standard test method for determination of the coefficient of friction of lubricants using the four-ball wear test machine.” .
[65] “ASTM D4172: standard test method for wear preventive characteristics of lubricating fluid (four-ball method).” .
[66] “ASTM D2266: standard test method for wear preventive characteristics of lubricating grease (four-ball method).” .
[67] “ASTM G132-96 - Standard Test Method for Pin Abrasion Testing.” .
[68] “ASTM G65: Standard Test Method for Measuring Abrasion Using the Dry Sand/Rubber Wheel Apparatus.” .
[69] METROCOM Engineering, “Istruzioni per uso e manutenzione di macchine prova materiali.” .
[70] ePCB, “Datasheet Datalogger USB ADC 20-20bit eT.B.” .
[71] ASM International, Ed., *ASM handbook*, 10th editon. Materials Park, Ohio: ASM International, 1990.
[72] E. Wallner *et al.*, “Nanotechnology applications in future automobiles,” SAE Technical Paper, 2010.
[73] H. Rauscher *et al., Towards a review of the EC Recommendation for a definition of the term “nanomaterial” Part 3, Part 3,*. Luxembourg: Publications Office, 2015.
[74] X. Pang and I. Zhitomirsky, “Electrodeposition of nanocomposite organic–inorganic coatings for biomedical applications,” *Int. J. Nanosci.*, vol. 4, no. 03, pp. 409–418, 2005.
[75] R. A. Vaia and H. D. Wagner, “Framework for nanocomposites,” *Mater. Today*, vol. 7, no. 11, pp. 32–37, Nov. 2004.
[76] J. Yang, T. S. Wang, B. Zhang, and F. C. Zhang, “Sliding wear resistance and worn surface microstructure of nanostructured bainitic steel,” *Wear*, vol. 282–283, pp. 81–84, Apr. 2012.
[77] N. Jin and P. Clayton, “Effect of microstructure on rolling/sliding wear of low carbon bainitic steels,” *Wear*, vol. 202, no. 2, pp. 202–207, Jan. 1997.
[78] P. Clayton and N. Jin, “Unlubricated sliding and rolling/sliding wear behavior of continuously cooled, low/medium carbon bainitic steels,” *Wear*, vol. 200, no. 1, pp. 74–82, Dec. 1996.
[79] D. Crolla, *Encyclopedia of Automotive Engineering*. John Wiley & Sons, 2015.

[80] P. Panek, K. Drabczyk, A. Focsa, and A. Slaoui, "A comparative study of SiO2 deposited by PECVD and thermal method as passivation for multicrystalline silicon solar cells," *Mater. Sci. Eng. B*, vol. 165, no. 1–2, pp. 64–66, Nov. 2009.
[81] D. Basset, "Nanotecnologie e nuove prospettive applicative per i materiali metallici," *Metall. Ital.*, no. 1, 2003.
[82] S. C. Tung and M. L. McMillan, "Automotive tribology overview of current advances and challenges for the future," *Tribol. Int.*, vol. 37, no. 7, pp. 517–536, Jul. 2004.
[83] J. A. Spearot, "Friction, wear, health, and environmental impacts—tribology in the new millennium," presented at the A keynote lecture at the STLE Annual Meeting, Nashville, Tennessee, 2000.
[84] Y. Kim, S. J. Kim, J. Lee, and D. Lim, "Nanodiamond Reinforced PTFE Composite Coatings," *MTZ Worldw.*, vol. 76, no. 2, pp. 32–35, Jan. 2015.
[85] Z. ur Rehman, S. A. Qasim, and M. A. Malik, "DLC Coated Piston Skirts Behavior at Initial IC Engine Start Up," in *Transactions on Engineering Technologies*, G.-C. Yang, S.-I. Ao, and L. Gelman, Eds. Springer Netherlands, 2014, pp. 195–212.
[86] Zahid-Ur-Rehman, S. Adnan Qasim, and M. Afzaal Malik, "Modeling Dry DLC Coated Piston Skirts Elastic Behavior at Low-Speed Initial Engine Start Up," in *Proceedings of the World Congress on Engineering 2013 Vol III*, London, U.K, 2013.
[87] J. Ka\lużny, A. Iskra, M. Babiak, P. Krzymień, M. Giersig, and K. Kempa, "Selected applications of carbon nanotubes in construction of internal combustion engine," *J. Pol. CIMAC*, vol. 9, no. 2, pp. 105–116, 2014.
[88] Y. Wang, *Introduction to Engine Valvetrains*. SAE International, 2007.
[89] G. A. Pignone and U. R. Vercelli, *Motori ad alta potenza specifica*. .
[90] S. V. Johnston and S. V. Hainsworth, "Effect of DLC coatings on wear in automotive applications," *Surf. Eng.*, vol. 21, no. 1, pp. 67–71, Feb. 2005.
[91] A. A. Cerit, F. Nair, and M. B. Karamis, "Wear behaviour of aluminum matrix SiC particle reinforced composite cam profile under dry sliding condition," *J. Balk. Tribol. Assoc. Vol*, vol. 21, no. 1, pp. 186–194, 2015.
[92] J. A. Dicarlo, H. M. Yun, G. N. Morscher, and L. U. Thomas-Ogbuji, "Progress in SiC/SiC Composites for Engine Applications," in *High Temperature Ceramic Matrix Composites*, W. Krenkel, R. Naslain, and H. Schneider, Eds. Wiley-VCH Verlag GmbH & Co. KGaA, 2001, pp. 777–782.
[93] H. Lee and K. Neville, *Handbook of epoxy resins*. New York: McGraw-Hill, 1967.
[94] W. Brostow, S. H. Goodman, and J. Wahrmund, "8 - Epoxies," in *Handbook of Thermoset Plastics (Third Edition)*, Boston: William Andrew Publishing, 2014, pp. 191–252.
[95] J. A. Brydson, *Plastics Materials*. Butterworth-Heinemann, 1999.
[96] W. G. Sawyer, N. Argibay, D. L. Burris, and B. A. Krick, "Mechanistic Studies in Friction and Wear of Bulk Materials," *Annu. Rev. Mater. Res.*, vol. 44, no. 1, pp. 395–427, 2014.
[97] R. Nandan, T. DebRoy, and H. K. D. H. Bhadeshia, "Recent advances in friction-stir welding – Process, weldment structure and properties," *Prog. Mater. Sci.*, vol. 53, no. 6, pp. 980–1023, Aug. 2008.
[98] D. L. Burris, B. Boesl, G. R. Bourne, and W. G. Sawyer, "Polymeric Nanocomposites for Tribological Applications," *Macromol. Mater. Eng.*, vol. 292, no. 4, pp. 387–402, Apr. 2007.
[99] M. Mohseni, H. Yahyaei, H. Yari, and B. Ramezanzadeh, "Nanotribological Characterization of Polymeric Nanocoatings: From Fundamental to Application," in

Nanomechanical Analysis of High Performance Materials, A. Tiwari, Ed. Springer Netherlands, 2014, pp. 3–27.

[100] B. Bhushan, J. N. Israelachvili, and U. Landman, "Nanotribology: friction, wear and lubrication at the atomic scale," *Nature*, vol. 374, no. 6523, pp. 607–616, Apr. 1995.

[101] P. M. Ajayan, L. S. Schadler, C. Giannaris, and A. Rubio, "Single-Walled Carbon Nanotube–Polymer Composites: Strength and Weakness," *Adv. Mater.*, vol. 12, no. 10, pp. 750–753, May 2000.

[102] N. W. Khun, B. C. R. Troconis, and G. S. Frankel, "Effects of carbon nanotube content on adhesion strength and wear and corrosion resistance of epoxy composite coatings on AA2024-T3," *Prog. Org. Coat.*, vol. 77, no. 1, pp. 72–80, Jan. 2014.

[103] N. W. Khun, H. Zhang, J. Yang, and E. Liu, "Mechanical and tribological properties of epoxy matrix composites modified with microencapsulated mixture of wax lubricant and multi-walled carbon nanotubes," *Friction*, vol. 1, no. 4, pp. 341–349, Nov. 2013.

[104] N. W. Khun, H. Zhang, L. H. Lim, C. Y. Yue, X. Hu, and J. Yang, "Tribological properties of short carbon fibers reinforced epoxy composites," *Friction*, vol. 2, no. 3, pp. 226–239, Apr. 2014.

[105] E. T. Thostenson, Z. Ren, and T.-W. Chou, "Advances in the science and technology of carbon nanotubes and their composites: a review," *Compos. Sci. Technol.*, vol. 61, no. 13, pp. 1899–1912, Oct. 2001.

[106] H. Quan, B. Zhang, Q. Zhao, R. K. K. Yuen, and R. K. Y. Li, "Facile preparation and thermal degradation studies of graphite nanoplatelets (GNPs) filled thermoplastic polyurethane (TPU) nanocomposites," *Compos. Part Appl. Sci. Manuf.*, vol. 40, no. 9, pp. 1506–1513, Sep. 2009.

[107] B. Pan, G. Xu, B. Zhang, X. Ma, H. Li, and Y. Zhang, "Preparation and Tribological Properties of Polyamide 11/Graphene Coatings," *Polym.-Plast. Technol. Eng.*, vol. 51, no. 11, pp. 1163–1166, Jul. 2012.

[108] T. Ramanathan *et al.*, "Functionalized graphene sheets for polymer nanocomposites," *Nat. Nanotechnol.*, vol. 3, no. 6, pp. 327–331, Jun. 2008.

[109] A. V. Sumant *et al.*, "Toward the Ultimate Tribological Interface: Surface Chemistry and Nanotribology of Ultrananocrystalline Diamond," *Adv. Mater.*, vol. 17, no. 8, pp. 1039–1045, Apr. 2005.

[110] R. Han, T. Shimamoto, T. Hirose, J.-H. Ree, and J. Ando, "Ultralow Friction of Carbonate Faults Caused by Thermal Decomposition," *Science*, vol. 316, no. 5826, pp. 878–881, May 2007.

[111] J. Cumings and A. Zettl, "Low-Friction Nanoscale Linear Bearing Realized from Multiwall Carbon Nanotubes," *Science*, vol. 289, no. 5479, pp. 602–604, Jul. 2000.

[112] Y. Liao, R. Pourzal, M. A. Wimmer, J. J. Jacobs, A. Fischer, and L. D. Marks, "Graphitic Tribological Layers in Metal-on-Metal Hip Replacements," *Science*, vol. 334, no. 6063, pp. 1687–1690, Dec. 2011.

[113] K. S. Novoselov, V. I. Fal′ko, L. Colombo, P. R. Gellert, M. G. Schwab, and K. Kim, "A roadmap for graphene," *Nature*, vol. 490, no. 7419, pp. 192–200, Oct. 2012.

[114] F. Kirschvink, M. Stürzel, Y. Thomann, and R. Mülhaupt, "Gas phase mineralized graphene as core/shell nanosheet supports for single-site olefin polymerization catalysts and in-situ formation of graphene/polyolefin nanocomposites," *Polymer*, vol. 55, no. 18, pp. 4547–4550, Sep. 2014.

[115] M. J. Allen, V. C. Tung, and R. B. Kaner, "Honeycomb Carbon: A Review of Graphene," *Chem. Rev.*, vol. 110, no. 1, pp. 132–145, Jan. 2010.

[116] R. Gu, W. Z. Xu, and P. A. Charpentier, "Synthesis of graphene-polystyrene nanocomposites via RAFT polymerization," *Polymer*, vol. 55, no. 21, pp. 5322–5331, Oct. 2014.
[117] M. Khajehpour, S. Sadeghi, A. Zehtab Yazdi, and U. Sundararaj, "Tuning the curing behavior of fluoroelastomer (FKM) by incorporation of nitrogen doped graphene nanoribbons (CNx-GNRs)," *Polymer*, vol. 55, no. 24, pp. 6293–6302, Nov. 2014.
[118] T. Kuilla, S. Bhadra, D. Yao, N. H. Kim, S. Bose, and J. H. Lee, "Recent advances in graphene based polymer composites," *Prog. Polym. Sci.*, vol. 35, no. 11, pp. 1350–1375, Nov. 2010.
[119] Y. Zhang, Y. Wang, J. Yu, L. Chen, J. Zhu, and Z. Hu, "Tuning the interface of graphene platelets/epoxy composites by the covalent grafting of polybenzimidazole," *Polymer*, vol. 55, no. 19, pp. 4990–5000, Sep. 2014.
[120] N. Chand, P. Sharma, and M. Fahim, "Correlation of mechanical and tribological properties of organosilane modified cenosphere filled high density polyethylene," *Mater. Sci. Eng. A*, vol. 527, no. 21–22, pp. 5873–5878, Aug. 2010.
[121] X.-J. Shen, X.-Q. Pei, S.-Y. Fu, and K. Friedrich, "Significantly modified tribological performance of epoxy nanocomposites at very low graphene oxide content," *Polymer*, vol. 54, no. 3, pp. 1234–1242, Feb. 2013.
[122] D. R. Lide, *CRC Handbook of Chemistry and Physics, 85th Edition*. CRC Press, 2004.
[123] "It's Elemental - The Element Molybdenum." [Online]. Available: http://education.jlab.org/itselemental/ele042.html. [Accessed: 07-Nov-2016].
[124] C. W. K. Scheele, *Der Königl. Schwedischen Akademie der Wissenschaften Abhandlungen, aus der Naturlehre, Haushaltungskunst und Mechanik, auf die Jahre 1778: Vierzigster Band*. bey Johann Samuel Heinsius, 1783.
[125] J. Emsley, *Nature's Building Blocks*. .
[126] S. L. Hoyt, *Metallography: The metals and common alloys*. McGraw-Hill Book Company Incorporated, 1921.
[127] W. T. (William T. Brannt, A. Krupp, and A. Wildberger, *The metallic alloys : A practical guide for the manufacture of all kinds of alloys, amalgams, and solders, used by metal-workers ... with an appendix on the coloring of alloys*. Philadelphia : H.C. Baird & Co, 1889.
[128] C. K. Gupta, *Extractive Metallurgy of Molybdenum*. CRC Press, 1992.
[129] F. L. Hess, "Molybdenum deposits," *Short Rev. U. S. Geol. Surv. Bull*, no. 761, p. 34, 1924.
[130] "Molybdenum (Mo) - Chemical properties, Health and Environmental effects." [Online]. Available: http://www.lenntech.com/periodic/elements/mo.htm. [Accessed: 07-Nov-2016].
[131] "www.lme.com: London Metal Exchange: Home." [Online]. Available: http://archive.is/www.lme.com. [Accessed: 07-Nov-2016].
[132] W. O. Winer, "Molybdenum disulfide as a lubricant: a review of the fundamental knowledge," *Wear*, vol. 10, no. 6, pp. 422–452, 1967.
[133] "New transistors: An alternative to silicon and better than graphene," *EurekAlert!* [Online]. Available: http://www.eurekalert.org/pub_releases/2011-01/epfd-nta012811.php. [Accessed: 07-Nov-2016].
[134] H. Topsøe, B. S. Clausen, and F. E. Massoth, "Hydrotreating Catalysis," in *Catalysis*, P. D. J. R. Anderson and P. D. M. Boudart, Eds. Springer Berlin Heidelberg, 1996, pp. 1–269.
[135] "Lubricant."

[136] M. E. Bell and J. H. Findlay, “Molybdenite as a New Lubricant,” in *Phys. Rev.*, vol. 59, 11 vols., 1941, p. 922.
[137] T. Spalvins, J. S. Przybyszewski, and L. R. Center, *Deposition of sputtered molybdenum disulfide films and friction characteristics of such films in vacuum*. National Aeronautics and Space Administration, 1967.
[138] S. Wan, A. K. Tieu, Y. Xia, H. Zhu, B. H. Tran, and S. Cui, “An overview of inorganic polymer as potential lubricant additive for high temperature tribology,” *Tribol. Int.*, vol. 102, pp. 620–635, Oct. 2016.
[139] L. Liu, Z. Huang, and P. Huang, “Fabrication of coral-like MoS2 and its application in improving the tribological performance of liquid paraffin,” *Tribol. Int.*, vol. 104, pp. 303–308, Dec. 2016.
[140] P. Zhang *et al.*, “Preparation and characterization of MoS2-TiL/MoS2-TiH nano multilayer coating with excellent wear properties,” *Mater. Lett.*, vol. 173, pp. 35–38, Jun. 2016.
[141] Y. He, S. C. Wang, F. C. Walsh, Y.-L. Chiu, and P. A. S. Reed, “Self-lubricating Ni-P-MoS2 composite coatings,” *Surf. Coat. Technol.*
[142] S.-C. Shi, J.-Y. Wu, T.-F. Huang, and Y.-Q. Peng, “Improving the tribological performance of biopolymer coating with MoS2 additive,” *Surf. Coat. Technol.*, vol. 303, Part A, pp. 250–255, Oct. 2016.
[143] A. Banerji, S. Bhowmick, and A. T. Alpas, “Role of temperature on tribological behaviour of Ti containing MoS2 coating against aluminum alloys,” *Surf. Coat. Technol.*
[144] “ASM Handbook, Volume 4A: Steel Heat Treating Fundamentals and Processes - ASM International.” [Online]. Available: http://www.asminternational.org/bestsellers/-/journal_content/56/10192/05344G/PUBLICATION. [Accessed: 08-Nov-2016].
[145] T. Novi, “FEM thermal analysis of a semi-active differential,” Università degli Studi di Firenze, 2015.
[146] W. U. Ritz, “Eine Neue Metode zur Lösung gewisser Variationsprobleme der Matematischen Physik,” *Math.*, vol. 135, pp. 1–61, 1909.
[147] R. Courant, “Variational methods for the solution of problems of equilibrium and vibrations,” *Bull. Am. Math. Soc.*, vol. 49, no. 1, pp. 1–23, Jan. 1943.
[148] R. W. Clough, *The Finite Element Method in Plane Stress Analysis*. American Society of Civil Engineers, 1960.
[149] M. J. Turner, “Stiffness and Deflection Analysis of Complex Structures,” *J. Aeronaut. Sci.*, vol. 23, no. 9, pp. 805–823, Sep. 1956.
[150] A. Hrennikov, “Solution of problems in elasticity by the frame work method,” vol. 8, pp. 169–175, 1941.
[151] O. C. Zienkiewicz and Y. K. Cheung, “The Finite Element Method in Structural and Continuum Mechanics. Numerical solution of problems in structural and continuum mechanics.” [Online]. Available: https://www.abebooks.com/Finite-Element-Method-Structural-Continuum-Mechanics/14381771621/bd. [Accessed: 15-Nov-2016].
[152] G. Strang and G. Fix, *An Analysis of the Finite Element Method*. Wellesley-Cambridge Press, 2008.
[153] K.-J. Bathe, *Finite element method*. Wiley Online Library, 2008.
[154] J. N. Reddy, *An Introduction to the Finite Element Method*. McGraw-Hill, 2006.
[155] P. Ŝolín, *Partial Differential Equations and the Finite Element Method*. John Wiley & Sons, 2005.

[156] J. K. Hastings, M. A. Juds, and J. R. Brauer, “Accuracy and Economy of Finite Element Magnetic Analysis,” presented at the 33rd Annual National Relay Conference, 1985.
[157] P. Long, W. Jinliang, and Z. Qiding, “Methods with high accuracy for finite element probability computing,” *J. Comput. Appl. Math.*, vol. 59, no. 2, pp. 181–189, May 1995.
[158] A. Haldar and S. Mahadevan, *Reliability Assessment Using Stochastic Finite Element Analysis*, 1 edition. New York: Wiley, 2000.
[159] P. Podra and S. Andersson, “Simulating sliding wear with finite element method,” *Tribol. Int.*, vol. 32, no. 2, pp. 71–81, 1999.
[160] N. H. Kim *et al.*, “Finite element analysis and experiments of metal/metal wear in oscillatory contacts,” *Wear*, vol. 258, no. 11–12, pp. 1787–1793, Jun. 2005.
[161] W.-M. Zhang and G. Meng, “Numerical simulation of sliding wear between the rotor bushing and ground plane in micromotors,” *Sens. Actuators Phys.*, vol. 126, no. 1, pp. 15–24, Jan. 2006.
[162] V. Hegadekatte, N. Huber, and O. Kraft, “Finite element based simulation of dry sliding wear,” *Model. Simul. Mater. Sci. Eng.*, vol. 13, no. 1, p. 57, 2005.
[163] V. Hegadekatte, N. Huber, and O. Kraft, “A finite element based technique for simulating sliding wear,” in *World Tribology Congress III*, 2005, pp. 731–732.
[164] V. Hegadekatte, N. Huber, and O. Kraft, “Modeling and simulation of wear in a pin on disc tribometer,” *Tribol. Lett.*, vol. 24, no. 1, pp. 51–60, Oct. 2006.
[165] V. Hegadekatte, S. Kurzenhäuser, N. Huber, and O. Kraft, “A predictive modeling scheme for wear in tribometers,” *Tribol. Int.*, vol. 41, no. 11, pp. 1020–1031, Nov. 2008.
[166] I. R. McColl, J. Ding, and S. B. Leen, “Finite element simulation and experimental validation of fretting wear,” *Wear*, vol. 256, no. 11–12, pp. 1114–1127, Jun. 2004.
[167] A. Attanasio and D. Umbrello, “Abrasive and diffusive tool wear FEM simulation,” *Int. J. Mater. Form.*, vol. 2, no. S1, pp. 543–546, Aug. 2009.
[168] C. González *et al.*, “Numerical analysis of pin on disc tests on Al–Li/SiC composites,” *Wear*, vol. 259, no. 1–6, pp. 609–612, Jul. 2005.
[169] T. Telliskivi, “Simulation of wear in a rolling–sliding contact by a semi-Winkler model and the Archard’s wear law,” *Wear*, vol. 256, no. 7–8, pp. 817–831, Apr. 2004.
[170] D. J. Dickrell and W. G. Sawyer, “Evolution of Wear in a Two-Dimensional Bushing,” *Tribol. Trans.*, vol. 47, no. 2, pp. 257–262, Apr. 2004.
[171] T. Reye, “Zur Theorie Zapfenreibung,” *Civil.*, vol. 4, pp. 235–255, 1860.
[172] A. Flodin and S. Andersson, “Simulation of mild wear in spur gears,” *Wear*, vol. 207, no. 1–2, pp. 16–23, Jun. 1997.
[173] A. Flodin and S. Andersson, “A simplified model for wear prediction in helical gears,” *Wear*, vol. 249, no. 3–4, pp. 285–292, May 2001.
[174] J. Brauer and S. Andersson, “Simulation of wear in gears with flank interference—a mixed FE and analytical approach,” *Wear*, vol. 254, no. 11, pp. 1216–1232, Oct. 2003.
[175] A. Hugnell and S. Andersson, “Simulating follower wear in a cam—follower contact,” *Wear*, vol. 179, no. 1, pp. 101–107, Dec. 1994.
[176] A. B.-J. Hugnell, S. Björklund, and S. Andersson, “Simulation of the mild wear in a cam-follower contact with follower rotation,” *Wear*, vol. 199, no. 2, pp. 202–210, Nov. 1996.
[177] B. J. Fregly, W. G. Sawyer, M. K. Harman, and S. A. Banks, “Computational wear prediction of a total knee replacement from in vivo kinematics,” *J. Biomech.*, vol. 38, no. 2, pp. 305–314, Feb. 2005.

[178] T. A. Maxian, T. D. Brown, D. R. Pedersen, and J. J. Callaghan, "A sliding-distance-coupled finite element formulation for polyethylene wear in total hip arthroplasty," *J. Biomech.*, vol. 29, no. 5, pp. 687–692, May 1996.
[179] S. L. Bevill, G. R. Bevill, J. R. Penmetsa, A. J. Petrella, and P. J. Rullkoetter, "Finite element simulation of early creep and wear in total hip arthroplasty," *J. Biomech.*, vol. 38, no. 12, pp. 2365–2374, Dec. 2005.
[180] N. Lingesten, P. Marklund, E. Höglund, M. Lund, J. Lundin, and R. Mäki, "Apparatus for continuous wear measurements during wet clutch durability tests," *Wear*, vol. 288, pp. 54–61, May 2012.
[181] P. Marklund and R. Larsson, "Wet clutch friction characteristics obtained from simplified pin on disc test," *Tribol. Int.*, vol. 41, no. 9–10, pp. 824–830, Sep. 2008.
[182] P. Nyman, R. Mäki, R. Olsson, and B. Ganemi, "Influence of surface topography on friction characteristics in wet clutch applications," *Wear*, vol. 261, no. 1, pp. 46–52, Jul. 2006.
[183] J. M. Thompson and M. K. Thompson, "A Proposal for the Calculation of Wear," in *Proceedings Of The 2006 International Ansys Users Conference & Exhibition, Pittsburgh, Pa*, 2006.
[184] D. Garleanu, V. Popovici, G. Garleanu, and M. Costoiu, "Finite Element Analysis Used for Determination the Endurance of Surfaces," in *Proceedings of the 1st WSEAS International Conference on Visualization, Imaging and Simulation*, Stevens Point, Wisconsin, USA, 2008, pp. 151–154.
[185] J. Andersson, A. Almqvist, and R. Larsson, "Numerical simulation of a wear experiment," *Wear*, vol. 271, no. 11–12, pp. 2947–2952, Sep. 2011.
[186] Y. Liu, Y. Hoon Jang, and J. R. Barber, "Finite element implementation of an eigenfunction solution for the contact pressure variation due to wear," *Wear*, vol. 309, no. 1–2, pp. 134–138, Jan. 2014.
[187] A. K. Waghmare and P. Sahoo, "Adhesive Wear Based on Accurate FEA Study of Asperity Contact and n-Point Asperity Model," *Int. J. Surf. Eng. Interdiscip. Mater. Sci. IJSEIMS*, vol. 4, no. 1, pp. 1–24, Jan. 2016.
[188] B. Ali, "Finite Element Analysis of Automotive Disk Brake and Pad in Frictional Model Contact," *Int. J. Manuf. Mater. Mech. Eng. IJMMME*, vol. 5, no. 4, pp. 32–62, Oct. 2015.
[189] A. Belhocine and W. Z. W. Omar, "Modeling and Analysis of the Mechanical Behavior of Dry Contracts Slipping Between the Disc and the Brake Pads," *Int. J. Surf. Eng. Interdiscip. Mater. Sci. IJSEIMS*, vol. 4, no. 2, pp. 34–62, Jul. 2016.
[190] M. Asif, K. Chandra, and P. S. Misra, "Characterization of Iron Based Hot Powder Brake Pads for Heavy Duty Applications," *Int. J. Mech. Mater. Eng.*, vol. 8, no. 2, 2014.
[191] A. M. Zaharudin, R. J. Talib, M. N. Berhan, S. Budin, and M. S. Aziurah, "Taguchi method for optimizing the manufacturing parameters of friction materials," *Int. J. Mech. Mater. Eng.*, vol. 7, no. 1, pp. 83–88, 2012.
[192] S. Rajesh, A. G. Krishna, P. R. M. Raju, and M. Duraiselvam, "Statistical Modeling and Analysis of Dry Sliding Wear of SiC Reinforced Aluminum MMCs," *Int. J. Surf. Eng. Interdiscip. Mater. Sci. IJSEIMS*, vol. 1, no. 1, pp. 57–70, Jan. 2013.
[193] P. Sahoo and P. Gadhari, "Optimization of Friction and Wear Properties of Electroless Ni-P-Al2O3 Composite Coatings," *Int. J. Surf. Eng. Interdiscip. Mater. Sci. IJSEIMS*, vol. 2, no. 2, pp. 34–52, Jul. 2014.

[194] P. S. Gajjal, G. Lathkar, and H. Bagchi, “Tribological Relationship for Sintered Bearing Using Taguchi Technique,” *Int. J. Surf. Eng. Interdiscip. Mater. Sci. IJSEIMS*, vol. 3, no. 1, pp. 48–57, Jan. 2015.
[195] H. Gao and G. C. Barber, “Engagement of a Rough, Lubricated and Grooved Disk Clutch ith a Porous Deformable Paper-Based Friction Material,” *Tribol. Trans.*, vol. 45, no. 4, pp. 464–470, Jan. 2002.
[196] E. J. Berger, F. Sadeghi, and C. M. Krousgrill, “Torque Transmission Characteristics of Automatic Transmission Wet Clutches: Experimental Results and Numerical Comparison,” *Tribol. Trans.*, vol. 40, no. 4, pp. 539–548, Jan. 1997.
[197] R. Mäki, P. Nyman, R. Olsson, and B. Ganemi, “Measurement and Characterization of Anti-shudder Properties in Wet Clutch Applications.” [Online]. Available: http://papers.sae.org/2005-01-0878/. [Accessed: 18-Nov-2016].
[198] R. Mäki, “Wet clutch tribology: friction characteristics in all-wheel drive differentials,” 07-May-2003. [Online]. Available: http://epubl.ltu.se/1402-1757/2003/28/index-en.html. [Accessed: 18-Nov-2016].
[199] W. Ost, P. De Baets, and J. Degrieck, “The tribological behaviour of paper friction plates for wet clutch application investigated on SAE#II and pin-on-disk test rigs,” *Wear*, vol. 249, no. 5–6, pp. 361–371, Jun. 2001.
[200] M. Ingram, H. Spikes, J. Noles, and R. Watts, “Contact properties of a wet clutch friction material,” *Tribol. Int.*, vol. 43, no. 4, pp. 815–821, Apr. 2010.
[201] C. Annicchiarico, S. Cappelli, L. Gasperini, T. Innocenti, and R. Capitani, “Design of an Active Vehicle System for a Hybrid Race Car.” [Online]. Available: http://papers.sae.org/2011-24-0167/. [Accessed: 18-Nov-2016].
[202] G. Ferrari, “A New Calculation Method for Belleville Disc Springs with Contact Flats and Reduced Thickness,” *Int. J. Manuf. Mater. Mech. Eng. IJMMME*, vol. 3, no. 2, pp. 63–73, Apr. 2013.
[203] A. Andrade-Campos, “Development of an Optimization Framework for Parameter Identification and Shape Optimization Problems in Engineering,” *Int. J. Manuf. Mater. Mech. Eng. IJMMME*, vol. 1, no. 1, pp. 57–79, Jan. 2011.